POLITECNICO DI TORINO

Department of Mechanical and Aerospace Engineering

Master degree course in Aerospace Engineering

Master Degree Thesis

Aerodynamic study of a racing car

Supervisor
Prof. Gaetano Iuso

Candidate
Alessandro Marcato
Matricola: 239353

Academic Year 2017 – 2018

Acknowledgements

I would like to mention all those who helped me in the preparation of the thesis with suggestions, criticisms and observations: to them my gratitude and my gratitude goes. A special thanks to my family, in particular to my mother and father: it is thanks to their support and their encouragement if today I managed to reach this goal. I would like to thank Prof. Gaetano Iuso, supervisor of this work and an inexhaustible source of knowledge. In addition to having guided me in the redaction, he passed on the passion with valuable lessons and advice during his university course.

I would also like to acknowledge J.A.S. Motorsport for hosting me in its headquarters and allowing me to produce this work. The professionalism, the competence, the kindness and the friendliness of all his collaborators have allowed me to face these 6 months with a strong motivation and a constant desire to learn and improve but always in serenity and harmony, making me feel one of them, part of the team. A special thanks goes to Nicola De Val, who followed me throughout my journey with extreme patience giving me many teachings and constant support, to Fabrizio Grieco and Matteo Santià, excellent travel companions.

A special dedication to my friends, to my fellow classmates and to Maria Luciana and Angelo, who shared with me every day anxieties, sacrifices, joys and successes. The affection and the support that have shown me make this goal even more precious.

Contents

List of Figures

List of Tables

Chapter 1

Introduction

This thesis work aims to analyze the aerodynamic aspects of a competition car. In particular, we considered here the Honda Civic 2018, a 5-door sedan of the Japanese house, which competes in the TCR championship, built by J.A.S. Motorsport of Arluno (MI). Thanks to the internship at this company, I was able to observe all the construction phases of the car and understand how a car championship is dealt with in many ways, from the logistic one to the preparation of the setup for the different tracks, to the continuous refinements on the mechanics, on the chassis and on the aerodynamic part. In this thesis, we will examine initially the aerodynamic aspects that involve the design phase of the car, starting from the shape of the standard one leading to the construction of the track car, and then those that accompany the teams during all competitions, linked to the definition of the setup and development of the car. Concretely, we will analyze the CFD maps that the company TotalSim was commissioned to perform on the Honda Civic in different configurations created in the design period of the car and, once chosen the final configuration, we will build aerodynamic maps, easily usable by track engineers, which will make it possible to take full advantage of the characteristics of the car on each track. Finally, an improvement will be described which, studied during this year, can be implemented in the next season.

In May I started a stage at J.A.S. Motorsport, an Italian car racing team founded in 1995 and known for its long activity with Honda. J.A.S. Motorsport builds Honda cars with TCR-specifics for different customers in the world and is directly involved in the TCR series, the car championship of touring cars, as customer support.

Therefore, its work differs mainly in these two aspects [**8**]:

- **Engineering and Manifacturing:**

  J.A.S. Motorsport was born as an independent racing team and over the years has become a center of design and production of racing cars, specialized in all the categories of Touring and GT cars. It is currently divided into two sections: one of which produces the Honda Civic (for the Touring category) and the other deals with the production of the Honda NSX (for the GT category). Within the company there is a sector entirely dedicated to the production of highly sophisticated chassis for racing cars. Starting from bare shells from the Honda factories, the chassis is welded and

equipped with additional reinforcements and roll bars. This production process is a very long and precise job that can take up to 1000 hours.
J.A.S. includes a design team that is composed of engineers who design every single component of the race car; all this thanks to the intensive use of 3D CAD modeling. The whole vehicle, in its smallest part, is designed and represented on the PC, through which it is possible to carry out many analyzes before the car is made, including finite element analysis, virtual dynamics, CFD and rapid prototyping. This allows, from the beginning, a construction of a car designed in the smallest detail. Furthermore, CAD modeling enables accurate and fast solutions as well as significant savings in money.

These production facilities have the capacity to produce a considerable number of race cars that are then directed to the internal assembly department where the cars are set up and configured according to customer needs. For the production and maintenance of engines, J.A.S. works in close collaboration with Autotecnica Motori, a very recognized company in the world of motorsport and a manufacturer of high performance components.

- **Customer Support:**

  The second aspect of the work that characterizes J.A.S. Motorsport is the customers assistance. The company follows customers even after the sale of the car. Thanks to a well-structured organization formed by highly professional staff, the Customer Support features a wide variety of tasks, including:

  - Race/Rally cars engineering/development/production;
  - Spare parts;
  - Hot line technical consulting (trouble-shooting, set-ups, instructions of use);
  - Technical assistance on site (race/rally engineering, qualified mechanics and technicians);
  - Engineering of components and special installations upon request (custom made solutions);
  - Information and clarifications about technical regulations and homologation forms.

Once we have have briefly illustrated the organization of the Company and all the activities that are carried out daily, we focus on the description of the laws that regulated the championship to approach to the aerodynamic analysis that is made out on its cars. This thesis work aims to analyze the aerodynamic aspects of a competition car. In particular, we considered here the Honda Civic 2018, a 5-door sedan of the Japanese car company, which competes in the TCR championship.

1.1 TCR championships

To understand the studies and changes made in the car that we will address in the following chapters, we need to be aware of the championship in which we participate and its rules. We will concentrate mainly on describing the aerodynamic aspects that are bound by the Motorsport Federation and then highlight and analyze the aspects in which, instead, it is possible to "play with".

The study in the smallest details of the regulation that prevails in the championship in which we will compete is a fundamental work that a team must necessarily carry out before the car's design phase. Having clear the limits within which one can act is essential to be able to concentrate on the aspects in which the regulation has left free expression, so as to better develop all the components - mechanical and otherwise - and maximize the performance of the car. It is precisely in these "unregulated" aspects that a team can make the difference with the other ones.

On the basis of the reasons given, we provide a brief description of the TCR championships, followed by hints about the technical and sports regulations.
TCR Championships are essentially championships where cars with TCR approval can run. The existing championships are regional (Asia, Europe, Middle East), national (Italy, Germany, UK ...) and there is also the world championship called WTCR. We describe this last championship and its format as an example, however the lower TCR championships are united by the same principles of the latter one.

The FIA World Touring Cup (FIA World Touring Car Cup), shortened to WTCR, is an international automotive championship promoted by Eurosport Events Limited (EEL) and WSC, owner of the TCR concept and trademark and approved by the FIA (Fédération Internationale de'Automobile), born in 2017 from the fusion between the WTCC world tourism championship and the TCR International Series. [**10**] The championship has lost the name of "world championship" due to the new regulation that prohibits manufacturers from taking part officially.
Producers have to develop cars for the competition that will be sold to private teams and they will also be authorized to provide continued technical support and development for these teams.

1.1.1 WTCR calendar

Subject to FIA, the inaugural WTCR calendar will visit 10 race tracks across three continents in 2018 for a total of 30 races. The provisional calendar is as follows:

Table 1.1: WTCR calendar for 2018

Marrakech (Morocco): 7-8 April
Hungaroring (Hungary): 28-29 April
Nürburgring Nordschleife (Germany): 10-12 May
Zandvoort (Netherlands): 19-21 May
Vila Real (Portugal): 23-24 June
Slovakia Ring (Slovakia): 13-15 July
Ningbo (China): 29-30 September
Wuhan (China): 5-7 October
Suzuka (Japan): 27-28 October
Macau (Macau): 15-18 November

1.1.2 WTCR weekend format

Each event will consist of three races – an increase from the previous two of WTCC. One qualifying session and one race will take place on the opening day: on the second day there will be a three-phase qualifying session and two races with the first race utilizing a reverse grid.

Table 1.2: Weekend format

Day one:
Free Practice 1 (30 minutes)
Free Practice 2 (30 minutes)
Qualifying (30 minutes)
Race 1
Day two:
Qualifying Q1 (25 minutes)
Qualifying Q2 (10 minutes)
Qualifying Q3 (top-five shootout)
Race 2
Race 3

In *Race 1* top 10 classified finishers score points as follows: 27-20-17-14-12-10-8-6-4-2, in *Race 2* top 10 positions reversed after Q2, top 10 classified finishers score points as follows: 25-18-15-12-10-8-6-4-2-1 and in *Race 3* grid as per combined order after Q3, top 10 classified finishers score points as follows: 30-23-19-16-13-10-7-4-2-1. [**9**]
TCR Europe, for example, has a different weekend format with only one qualifying and two races.

1.2 The Sporting Regulation

The regulations that characterize a championship are essentially the sporting and technical ones; the first lists the rules from the point of view of the competition and the course of the championship (mainly used by the teams), the second describes in every detail every technical aspect a car that must have to participate in the championship and for this reason is mainly studied by manufacturers.

In sporting regulation are discussed topics such as: incidents and sanctions, safety cars, fuel, grid and many others, among which the one that most involves us is the Balance of Performance.

Balance of Performance, or BoP for short, is a regression in motorsport in order to bring different vehicles to the same level or at least a similar level of performance. This concept was defined in the late 1980*s* as a "classless society". [**11**]

In race cars based on standard vehicles, the sports performance of vehicles can be very different, as standard vehicles are not designed exclusively for dynamic driving characteristics. In the development of a production vehicle, requirements for comfort, use of indoor space, economy, consumption reduction or production costs are also required. These can have a counterproductive effect on the use in motorsport. In order to keep race cars close to mass production and to contain development costs, performance balancing was introduced to bring the different vehicle concepts to a single level of performance.

In principle, for the prototypes and formula cars there is no need for a performance balancing as these vehicles are not based on the technical bases of a production vehicle and therefore there are no restrictions in that way. In those regulations, all teams and manufacturers have the same technical requirements for building this race car.

1.2.1 Balance of performance and technical specification

We quote the article concerning this weight balance, as described in the Sporting Regulations [**6**]:

> The balance of Performance (BoP) will be defined by WSC before the start of the season and will be adjusted by the BoP Compensation Weight Automatic Formula as defined by WSC Technical Bulletin. The BoP and the adjustments to the technical specifications of the cars are carried out by WSC. In order to optimize the BoP WSC reserves the right to adjust the following items for each competitor:
>
> - Minimum weight of the car
> - Engine performance level implemented by monitored electronic components
> - Any other technical restriction it may deem necessary
>
> In order to establish and maintain the BoP, WSC will make use of following actions:
>
> - BoP by numbers;

  - For this purpose WSC will define Cars' Numerical Models and will define the BoP cars' parameters on the Series' Circuits.
  - All full-season entrants will communicate all requested technical information.
  - WSC may request any reasonable surveyed measurements (e.g. engine dyno, wind tunnel, etc.) in order to determine or verify the communicated values.
  - The Cars' Numerical Models will be steadily updated during the season using the logged data.
- BoP sessions of the TCR models may be held before the start of the season. All models of car will be tested. Failure to attend may entail a penalty to be decided by WSC.
  - One or more official testing sessions may be organized by WSC. All full-season entrants are obliged to be present with at least one of the cars they intend to enter in the season.
- BoP corrections during the season following the demonstrated performance level in the previous events. Any breaches of these rules will be reported to the Stewards. Penalties may go as far as disqualification from the Competition.

Therefore, in our discussion, the BoP is important for two different aspects: as regards weight balancing in case of "minimum weight of the car" and in aerodynamic terms of downforce and drag in the case of minimum ride height that can be an "other technical restriction".

1.3 The Technical Regulation

We now approach the second regulation between the two previously mentioned. This, as alluded, is the one that involves us most as it is addressed directly to the constructors of racing cars. It is the base from which we start to define the car in every aspect. It defines the geometric limits of the body, the characteristics of the engine, gear and transmission, places restrictions on the suspension, wheels and tires, and establishes the accessories (such as safety equipment, cockpit...).

From the aerodynamic point of view the laws that most interest us concern the geometry that the vehicle must assume: from the most general as maximum width or height to the most specific as can be the restrictions on splitter, rear wing, diffusor... By making full use of the boundaries defined by the technical regulation it is possible to make a difference in the race.

Licensed by WSC to EEL/FIA as the FIA WTCR regulations, the TCR technical regulations will be frozen until the end of 2019. Only TCR cars homologated by WSC and assigned with the FIA WTCR passport issued by the FIA are eligible. The FIA is responsible for technical management in consultation with TCR representatives.

No fewer than 19 TCR-based championships or series exist around the world while several manufacturers have, or are in the process, of homologating TCR cars including Alfa Romeo, Audi, Ford, Honda, Hyundai, Kia, Lada, Opel, Peugeot, Renault, Seat, Subaru and Volkswagen brands. To date, more than 600 TCR racing cars have been built and sold to customer teams.

We quote and comment on some important articles that most characterize the championship and that later will allow us to analyze the aerodynamic aspects of the car, aware of the possibilities of movement within the laws in force on the championship. These laws are divided into sections according to the topic they deal with: [**7**]

1.3.1 Definition

Model of car [2.13] All the identical cars belonging to a family and to a production series distinguishable by an identical conception and identical external general lines of the bodywork, and by an identical mechanical conception of the engine and the transmission to the wheels.

1.3.2 Regulations

Eligible cars [3.2] Eligibility criteria for TCR Touring Car:

- The model of car is on the list of TCR eligible cars for 2018 published by the WSC (only front-wheel drive cars).
- The cars correspond to FIA Homologation Criteria for Touring Cars (FIA Group A).
- The model of car is produced by an OEM and belongs to a mass-produced family.
- 4/5 doors
- Minimum length $4.2\,m$
- Mono turbo charged 4-stroke petrol mass production Engines with cylinder capacity from $1750\,cm^3$ to maximum $2000\,cm^3$ and with a maximum power output of $350\,bhp$.
- Hybrid propulsion is not allowed.

WSC reserves the right to accept other cars, when the general characteristics match with the TCR concept. WSC reserves also the right to approve or to refuse applications which might not be in compliance with the above criteria.

Material [3.5]
Titanium or magnesium alloys, ceramic or exotic materials and sophisticated coatings are not permitted unless used for the production part or explicitly

authorized by these regulations. All flexible supports (engine, transmission, sub frames, etc.) may be replaced by stiffer brackets with same functional dimensions. If not otherwise defined by the present regulations the aggregate's position may not be modified. (Certification) External bodywork parts may be repaired by adding material respecting the certified properties (minimum weight, functional shape, etc.). Such operation needs the approval of the technical delegate.

A large part of these rules serves to reduce the costs of the championship. Indeed the use as faithful as possible of the standard car greatly reduces the freedom of design; moreover the experimentation or the simple use of precious alloys and materials would significantly increase the cost of the car, making the championship elitist, as happened in the past for the WTCC, where only a few wealthy teams they could compete. The stewards consent to the use of exotic materials if they are already present in the standard vehicle, therefore at "zero cost" for the construction teams. In the next section, about the bodywork, the interesting articles from the aerodynamic point of view emerge: the WSC technicians have regulated the fundamental geometries of the car, the dimensions of the maximum openings for ventilation, fixed devices like splitter and rear wing, etc...

1.3.3 Bodywork

Width of bodywork: Maximum $1950\,mm$

Bonnet and boot lids [4.1.1]
It must be possible to open them without use of tools. The retaining springs (not the hinges) may be removed, but the car must have supports to hold the bonnet and the boot lid in open position. (Certification) Openings in the engine bay bonnet are allowed up to a maximum total surface of $1050\,cm^2$, including any original opening(s) but must be covered by wire netting with maximum mesh surface of $500\,mm^2$ (Certification). Trims on the openings can be added to the bonnet provided that they do not protrude from the outer surface more than $15\,mm$ outwards and $50\,mm$ inwards (Certification). Cut-outs in the original production bonnet for the trims are allowed up to a total surface of maximum $2350\,cm^2$ including any original cut outs. The production internal reinforcements may be removed in the opening zone. (Certification)

Exterior [4.3]
The only body parts that can be replaced and changed in shape are:

- Front bumper; Shape resemble the original must be approved by WSC prior to production; no dive planes allowed.
- Front fenders' lower edge behind the wheel may not be higher than front door's bottom border. Shape must be approved by WSC prior to production (no louvres allowed)

- Side sills (these may be added if not present in the production car)
- Rear wheel arch extensions
- Rear door bulge compatible with the rear arch extensions
- Rear bumper; Shape resemble the original must be approved by WSC prior to production.
- Wheel arch liners

No flat floor behind the vertical plane tangent to the back side of the front wheels and the foremost point of the rear bumper. Engine bay protection panel between the frame rails are permitted. (Certification) It is not allowed to tape the joints between bodywork panels. The hood's and boot lid's original position may not be changed.

Aerodynamic devices [4.4]

Rear wing with brackets (Certification)

The original car's devices must be removed and must be replaced with one compulsory rear wing made up of:

- One aluminium extruded wing profile (WSC delivery corresponding to the profile defined below)
- Specific part produced following exactly the WSC rear wing dimensions and functions
- Material: aluminium or fibre reinforced plastic
- Production drawings corresponding to the WSC 3D model will be delivered for certification.

Rear wing definition & Dimensions:

- Straight, adjustable, single piece with no flap -Type BE 183-176 $+/-0.5\,mm$
- Chord $= 250 + / - 1\,mm$
- Width $= 1380 + 0/ - 1\,mm$
- Trailing edge thickness $= 2 + / - 0.5\,mm$

Table 1.3: Airfoil coordinates

$x\%$	0	1.25	2.5	5	7.5	10	15	20
$-Y_v$	2.79	0.53	0.07	0.10	0.62	1.32	2.86	4.35
$-Y_o$	2.79	7.31	9.40	12.52	14.95	16.94	20.05	22.30

$x\%$	30	40	50	60	70	80	90	95	100
$-Y_v$	6.79	8.80	10.02	11.40	11.95	11.80	9.03	5.58	0.10
$-Y_o$	25.01	25.98	25.65	24.39	21.44	17.43	11.43	6.63	0.20

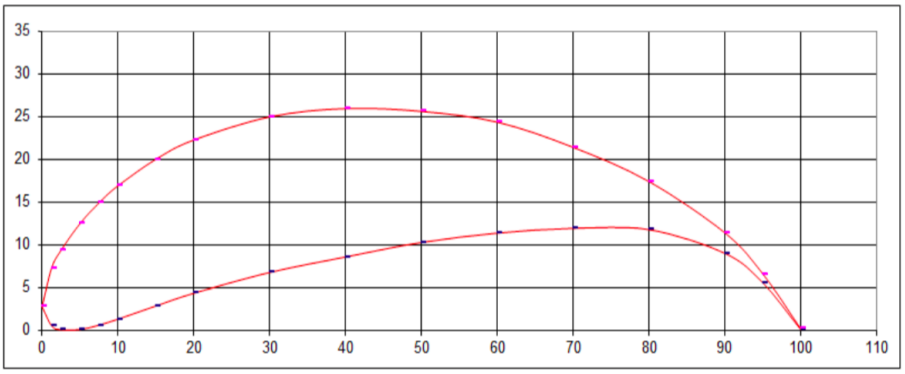

Figure 1.1: Airfoil coordinates

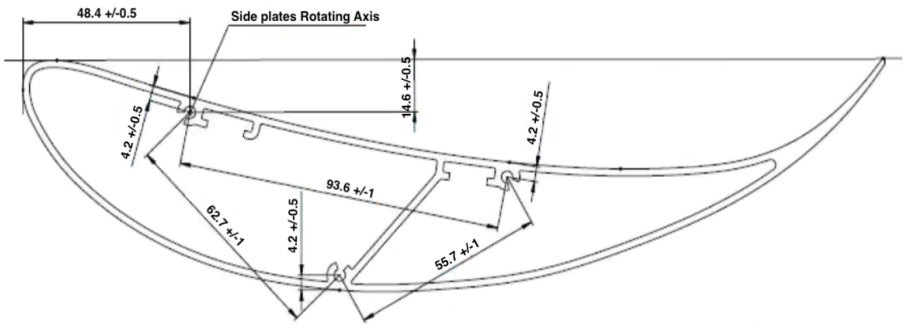

Figure 1.2: Rear wing structure

2 Brackets

Dismountable, flat, plane surface perpendicular to wing profile surface. Mounted on the boot lid or on the rear window and to the lower or to the upper wing profile surface. Min. transversal distance between both supports and between supports and side plates = 100 mm. The leading edge must be rounded with

a constant radius. The trailing edge may be chamfered to a max. of $20\,mm$ (min. thickness at the trailing edge $= 2\,mm$).

2 SIDE PLATES

All edges will be rounded with at least $R = 3\,mm$ (Safety)

- Dismountable, flat, continuous surface perpendicular to profile centreline.
- Side plates may rotate with respect to the wing profile.
- This device must be rigid and offer no possibility for the penetration of air (groove, hole, opening, etc.).
- Material: aluminium, plastic

No element of the rear wing including side plates and brackets may be located beyond the following limits:
X = $1050\,mm$ from rear axle centreline.
Z = Highest point of roof.

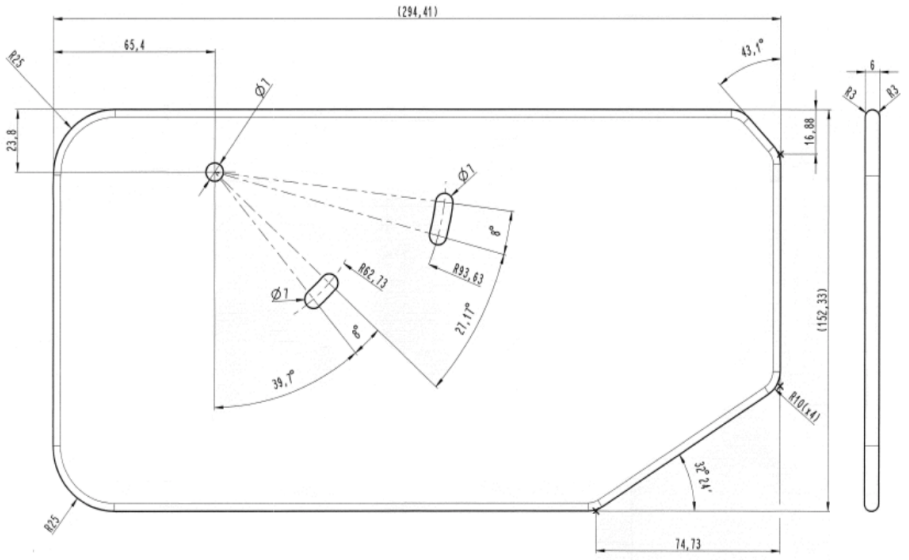

Figure 1.3: Side plate geometry

THE FRONT SPLITTER (Certification):

- WSC delivered and adapted to each car; It will also be possible to reduce the front splitter's protrusion into the wheel arch in case of collision with the front tire's enveloping curve.

- Specific part following exactly the WSC CAD model front splitter's dimensions (length, width and angles, front overhang, vertical projection, sections of areas touched by the airstream) (see Drawings)
  - lateral prolongation in "x" for cars with bigger front overhang is allowed (max. width in "y" 50 mm)
  - The distance between splitter's contour vertical projection and bumper contact area on the front splitter is limited as follows:
    * In the middle area ($y = \pm 400\,mm$) will be between 35 and 85 mm.
    * Outside $y = \pm 400\,mm$ is limited to max. 210 mm.
    * In the transition area to the wheel arches is limited to max. 45 mm.
  - The layout of the areas covered by the bumper is free.
  - The areas next to wheel arches may remain flat.
  - production drawings will be delivered for certification
  - material: fibre reinforced plastic
  - Scrutineering shape jigs for external contour, leading edge and lower face will be delivered on WSC request.
  - WSC may approve justified waiver.
  - Note: in case of doubts, the WSC CAD 3D model overrides the drawings.

The foremost edge of the front splitter at $y = 0$ will protrude the bumper contour by max. 35 mm in vertical projection.

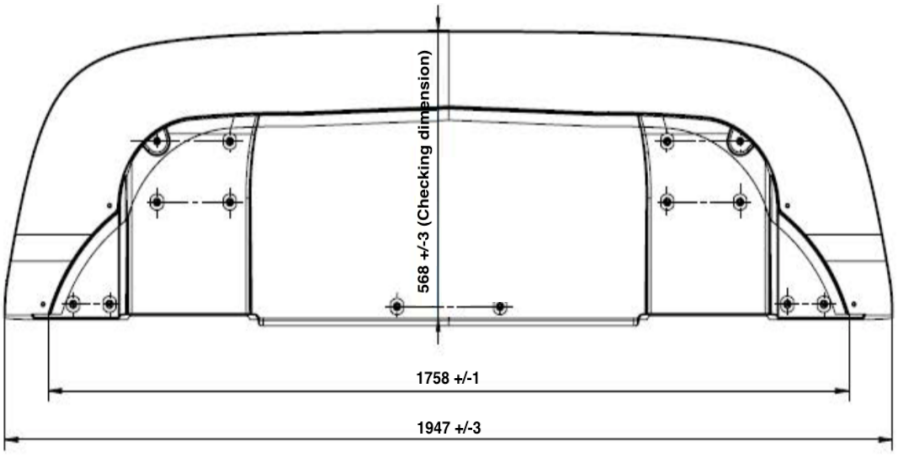

Figure 1.4: Splitter geometry - Upper side

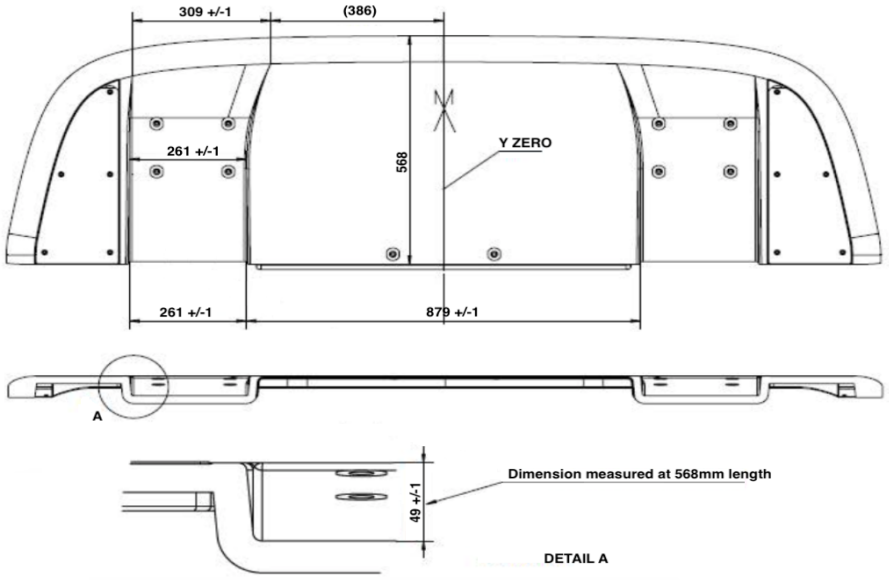

Figure 1.5: Splitter geometry - Down side

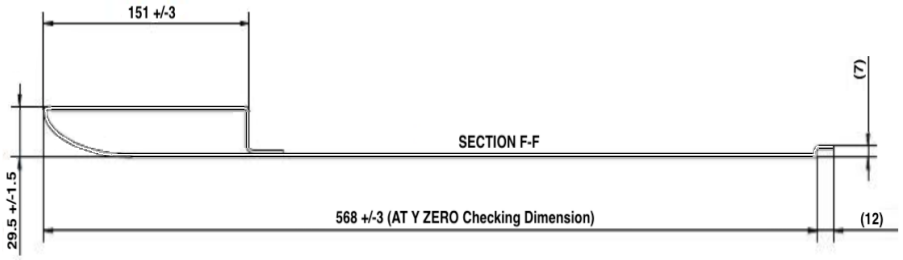

Figure 1.6: Section geometry

Front Splitter Brackets' design is free. (Certification)
Rear diffuser included in the rear bumper: (Certification)

- One single plane between a vertical plan minimum 380 mm behind the rear axle centre line and the bumper's vertical projection
- Hollow area for the exhaust end pipe(s) allowed
- Maximal width: 1650 mm
- Max inclination to the doors' lower edge: 25°
- No air circulation over the diffuser

Mass production flexible skirts reducing the ground clearance may be removed. (Certification) The ground clearance check will consider these parts as bodywork

Having defined these limits, selected among the most interesting as regards the topics we will discuss later, we start the design and construction phase of the car, at the end of which we need to check the performances. For example, while the engine and the suspensions are tested on the test bench, or on the track, the aerodynamic analysis of the car can be performed in a wind tunnel (very expensive, requires longer times and the physical creation of the car) or through a CFD analysis, widely used because, in addition to being much cheaper, it can be carried out during the design phase through 3D CAD drawing, before the actual construction of the car.

Chapter 2

Bibliographic literature

The study of aerodynamics first took hold on aircraft to allow - of course - the flight, and then on land to improve its performance, arriving to the present day to progress "in parallel" in order to identify increasingly effective solutions for speed, maneuverability and, last but not least, the reduction in consumption. Leaving aside the first studies that date back to the Renaissance, experimentation on the resistance of bodies in the air began in the eighteenth century. The development of aviation in the twentieth century has extended the research in this field, first with theoretical experiments, then on models and parts of aircraft, then with tests on stationary bodies in a fluid in motion. This last practical procedure is that of the aerodynamic tunnel, or wind tunnel, which allows to reproduce the conditions of interaction between body and air. In recent years, however, the computer has been able to regulate the phases of research and aerodynamic planning, analyzing with mathematical models every aspect of the pressure distributions determined by the wind on the various components and parts of the aircraft.

Although aircraft and cars in traveling through the air may seem completely different, they both generate the same forces. A competition car is a highly complex aerodynamic device that it is always in proximity to the ground and this complicates the airflow around it. [**1**]

Car has to overcome aerodynamic drag and it has to generate a force that allows it to stay on the ground so that its tires can generate grip and provide tractive forces (accelerative, braking, cornering) - the so famous "downforce". Drag opposes forward motion and it's a dominant factor in determining acceleration and deceleration at higher speeds and maximum speed.

However, in race car design, drag reduction (by streamlining vehicle shapes) is secondary. It is the creation of downforce that is extremely important and leads to the major improvements in race car performance, especially when cornering, where the forces of inertia that cause centrifugal forces tend to make both the trajectory and the grip unstable. Downforce, hence, is the most important single element in the performance of the cars and for that reason in some cases, this has involved drastic changes to rule as lap times have tumbled to the extent that things seemed to be getting unsafe.

The only objective of aerodynamics in competition cars is the increase in performance. The increase in the downforce allows the car to keep itself more adherent to the ground

with a gain of stability in the straight. However, the most common disadvantage is that the more aerodynamic load and grip increases, the greater the drag force increases with decreasing peak speeds in straight sections.

We can understand, through this historical example, the importance that aerodynamics has had over the years, even in a remote past, and that has given impetus to the interest in the study of the interaction between fluids and bodies. In 1588, the English ships had to face an invasion of the powerful Spanish Armada. The Spanish ships were large and heavy, equipped with numerous soldiers and big cannons, while the English ships were smaller and lighter, had no soldiers and possessed small, short-range cannons. It therefore seemed that there were no comparisons between the two naval fleets. However, the heavy, sluggish Spanish ships could not counter the fast and maneuverable English ships that triumphed in the conflict. In turn, naval power was going to depend on the speed and maneuverability of ships. From that moment on, drag on ship became a major problem among the engineers of that time and gave the impulse of the study of fluid dynamics. [**3**]

The history of the means of locomotion, whether aerial or terrestrial, has always shown that the discovery or application of the idea immediately takes over a rapid evolution that leads to subsequent developments and conceptions. From that moment follow new studies aimed at mechanical refinement, often linked to the innovation of materials and construction techniques. At that point the evolution becomes slow and progressive. Only in the '50*s*, with industrial growth and technological progress, important studies are undertaken in the design of objects and in particular of means of transport. The project no longer focuses solely on the technical-mechanical aspect, but looks forward to the form and to the aesthetic concepts. Thanks to aeronautical research applied to Formula 1 cars, there is a strong awareness that aerodynamics is a fundamental component of the project itself, the importance of which increases with the increase of the speeds reached. In fact, for several years, in the context of the programming of any vehicle that has to interact with air or water, aerodynamics is one of the main elements of study, as it is able to influence fuel consumption, performance, noise and its stability at high speeds - obviously the only target of aerodynamics in competition cars is the increase in performance and there are few attentions regarding fuel consumption and noise produced.

The use and knowledge of downforce has come a long way in half a century. The first known attempt to run an airfoil on a racing car was a Swiss engineer, Micheal May, on a Porsche 550 RS in 1956. The car had an airfoil mounted above the cockpit, acting through the centre of gravity of the car.

During the early 1960s designers and engineers made further attempts at gaining an advantage from aerodynamics, other than by reducing the drag. Racers have continually and habitually experimented with ideas that seem to produce benefits to performance and spoilers started appearing on sports cars.

The next mental leap that produced possibly the biggest performance advance of all came in the late 1970 when another clever engineer Peter Wright successfully introduced the concept of ground effect into Formula 1 with the *Lotus Type 78*.

The run-up to maximum aerodynamic vertical load became a priority for the development of the cars in the years to follow and in 1982 the maximum lateral accelerations reached values over $3.5\,g$, thanks to forces deporting equal to twice the weight of the car.

This type of performance, however, were not obtained without problems: the suspensions had to be stiffened to support the very strong vertical loads and to keep the side skirts in the correct position. Moreover, the pilots complained that the cars seemed to run on rails, the deporting force being too high; precisely this problem probably caused the death of Gilles Villeneuve, who was unable to discard the March of Jochen Mass, which continued at a reduced speed, in order to leave the road, during the qualifying session in Zolder - Belgium in 1982. [**2**] Following this fatal season, in which there were also other accidents, in 1983 the skirts were banned and the exploitation of the underbody was limited to the rear diffuser only.

In '90*s* the question of downforce versus drag had to be considered anew, and designers started looking at the underside of the car again as a potential downforce inducer. It was realized that with a small ground clearance and the right amount of nose down attitude, a crude form of wing section could be created beneath the cars in spite of flat bottom and we were back to ground effect. It proved vital to allow the air from the underside to escape as efficiently as possible at the rear of the cars, and diffusers came into being to do just that.

These changes, however, led to a decrease in spectacle, in fact the wake effect becomes almost penalizing, reducing and making turbulent the flow that invests the wings and the bottom of the car. Also to overcome this problem, in 2009, the federation imposed a drastic reduction in the width of the rear wing, with a marked change in the design of the cars. Finally, an important new feature introduced in 2011 in F1, the DRS (Drag Reduction System), adjustable flap on the rear wing controlled by the driver: when activated, it decreases its inclination (angle of attack), reducing momentarily the aerodynamic drag (the drag) of the wing, increasing the top speed on the straights, to facilitate overtaking. The aerodynamics in Formula 1 has always been the driving sector in all motorsport, however, in the smaller leagues, many aerodynamic constraints are imposed in order to reduce the cost of participation as much as possible allowing the access to the competitions to many more teams,.

One of the most interesting advances in aerodynamics over the past 20 years or so, has been the advent of computer modeling and specifically computational fluid dynamics which, as mentioned, has revolutionized the study of the interaction between the air flow and the car.

Chapter 3

CFD analysis and results

The aerodynamic analysis through CFD software allows to simulate in a very short time, the effect of many modifications applied to the car. Once the initial geometry of a part of the body has been defined, before its real creation, it is possible to test its aerodynamic efficiency and, following the results, it is easy and intuitive to understand if this shape (which obviously has to respect the regulations mentioned in Chapter 1.3) is the most appropriate or if it requires a modification of some surfaces. Once the shape has been modified, we can test it again, until you get the result that we consider optimal for that component. All this improvement process would be very complex and expensive in the wind tunnel and would require, as already mentioned above, the material construction of the piece or a scale model for insertion in the test section of the tunnel. It must be taken into account that it is not enough to consider only one piece of the body of the car at a time in the simulation, but the whole vehicle must be considered as each component generates a flow deformation that interferes with the another ones. Therefore, each simulation must be performed on the whole body.

However, the wind tunnels represent a precise instrument of aerodynamic analysis whose most important aspect is their ability to accurately recreate the complexity of the aerodynamic flows.

J.A.S. Motorsport for the aerodynamic analysis of its vehicles apply to TotalSim Ltd, a Brackley company (UK) leader in the CFD sector, which collaborates with many important customers in every sector, from Formula 1 to WRC, from cycling to sailing. We analyze the software and numerical methods used to obtain the aerodynamic results that have been provided to us.

3.1 The matematical modeling tool

Computational Fluid Dynamics (CFD) is a computer based mathematical modeling tool which can be considered the amalgamation of theory and experimentation in the field of fluid flow. The simulation consists in the numerical elaboration of sophisticated mathematical models that describe the temporal evolution of the fluid through its fundamental fluid-dynamic parameters: speed, pressure, temperature, density. CFD simulations provide information on the flow and properties of fluids that can be difficult or expensive to

obtain by measurement and which provide insight and understanding of flow behavior in a specific situation. CFD can recreate real track conditions, such as cornering and braking and its simulations are repeatable, removing almost all the "noise" that afflicts the full-scale tests. The use of numerical simulation in the design phase is necessary where the need to perform forecasts for analysis on a large number of case studies, allows the elimination, at least in the initial stages, of the creation of numerous prototypes. In practice, this virtual simulation tool is able to provide responses consistent with reality, in times and costs decidedly reduced compared to what is necessary to carry out in the physical experimentation and so it will be cheaper and faster than a test in a windtunnel.

In fact, this is one of the main reasons that makes CFD an extremely advantageous tool in design analysis: it allows to perform, in a relatively simple way parameterization for different initial configurations, both for geometries and for boundary conditions, allowing to evaluate the responses of the components under examination to operating conditions close to the physical reality. The process developed by TotalSim (which includes complete car simulation starting from 3D CAD) can generally be completed in less than a week, and once the baseline has been generated, it can turn hundreds of simulations per week.

TotalSim to provide us the aerodynamic performance of the car uses the *OpenFOAM®* software, a free, open source CFD software package licensed and distributed by the OpenFOAM Foundation. This is often enriched with a mesh deformation software package called *Sculptor®* that allows parametric shape deformations to be performed directly onto a CFD model. This vastly reduces the need for costly re-meshing and makes CFD a viable tool for design optimization [**12**].

TotalSim uses a transient DES methodology to run the simulations.

3.1.1 DES

Detached eddy simulation (DES) is a modification of a RANS model in which the model switches to a subgrid scale formulation in regions fine enough for LES calculations. This hybrid model attempts to treat near-wall regions in a RANS-like manner, and treat the rest of the flow in an LES-like manner aiming to alleviate the costly near-wall meshing requirements imposed by LES.

3.1.2 RANS

The Reynolds-averaged Navier–Stokes equations (or RANS equations, for short) are time-averaged equations of motion for fluid flow. The idea behind the equations is Reynolds decomposition, whereby an instantaneous quantity is decomposed into its time-averaged and fluctuating quantities. The RANS equations are primarily used to describe turbulent flows and they can be used with approximations based on knowledge of the properties of flow turbulence to give approximate time-averaged solutions to the Navier–Stokes equations. For a stationary, incompressible Newtonian fluid, these equations can be written as:

$$\rho \bar{u}_j \frac{\partial \bar{u}_i}{\partial x_j} = \rho \bar{f}_i + \frac{\partial}{\partial x_j} \left[-\bar{p}\delta_{ij} + \mu \left(\frac{\partial \bar{u}_i}{\partial x_j} + \frac{\partial \bar{u}_j}{\partial x_i} \right) - \rho \overline{u'_i u'_j} \right] \tag{3.1}$$

The left hand side of this equation represents the change in mean momentum of fluid element owing to the unsteadiness and the convection in the mean flow. This change is balanced by the mean body force, the isotropic stress owing to the mean pressure field, the viscous stresses, and apparent stress:

$$\left(-\rho\overline{u_i' u_j'}\right) \tag{3.2}$$

owing to the fluctuating velocity field, generally referred to as the Reynolds stress. This nonlinear Reynolds stress term requires additional modeling to close the RANS equation for solving, and has led to the creation of many different turbulence models.

3.1.3 LES

Large eddy simulation (LES) is a mathematical model for turbulence initially proposed in 1963 by Joseph Smagorinsky to simulate atmospheric air currents.

The simulation of turbulent flows, by numerically solving the Navier–Stokes equations, requires to resolve a very wide range of time and length scales, all of which affect the flow field. Such a resolution can be achieved with direct numerical simulation (DNS), but DNS is computationally expensive, and its cost prohibits simulation of practical engineering systems with complex geometry or flow configurations, such as turbulent jets, pumps, vehicles, and landing gear.

The principal idea behind LES is to reduce the computational cost by ignoring the smallest length scales, which are the most computationally expensive to resolve, via low-pass filtering of the Navier–Stokes equations. Such a low-pass filtering, which can be viewed as a time and spatial averaging, effectively removes small-scale information from the numerical solution. This information is not irrelevant and its effect on the flow field must be modeled, a task which is an active area of research for problems in which small-scales can play an important role, such as near-wall flows, reacting flows, and multiphase flows.

So, for DES simulations: regions near solid boundaries and where the turbulent length scale is less than the maximum grid dimension are assigned the RANS mode of solution. As the turbulent length scale exceeds the grid dimension, the regions are solved using the LES mode. Therefore, the grid resolution is not as demanding as pure LES, thereby considerably cutting down the cost of the computation. DES behave as a hybrid RANS-LES model. Grid generation is more complicated than for a simple RANS or LES case due to the RANS-LES switch and provides a single smooth velocity field across the RANS and the LES regions of the solution.

3.2 The final configuration of the car

Before analyzing the path that, starting from a "standard" car, led us to the creation of the car in the shape in which it appears today, we analyze this last configuration, describing how the flow interacts with the car. This backward journey allows us to understand more easily the logic behind the car's design phases, to deduce the motivation of some

changes conscious of the final effect they create. Using the data provided by TotalSim Ltd., obtained using the software and methodology described above, the vehicle is analyzed through maps showing the pressure coefficient and the total pressure coefficient of the car.

***NB**: All the results and considerations made in this chapter and in the first section of the next chapter (Chapter 4.1) are based on numerical data and on the maps provided by TotalSim Ltd. So, although we are talking about one of the leading companies in the aerodynamic field, with a lot of experience in the motorsport sector at all levels, I can not guarantee the correctness of the data supplied to me. My analysis and comments are closely related to these data.*

3.2.1 Nomenclature and geometry model

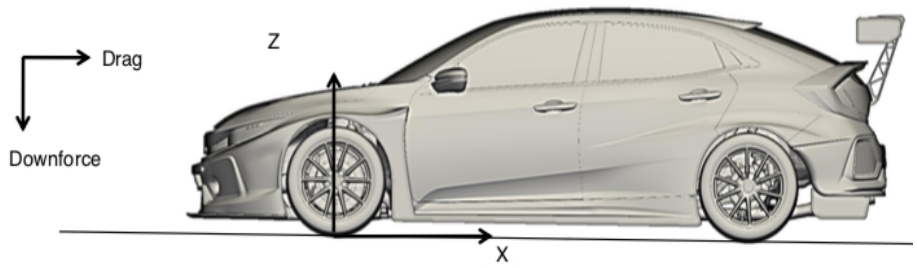

Figure 3.1: Reference system

We define a number of key aerodynamic terms used throughout the report.

- *Drag*: Force resolved parallel to ground in positive x-direction.
- $Downforce$: Force resolved perpendicular to ground in negative z-direction.
- C_p: Pressure coefficient – Non-dimensionalised static pressure.

$$C_p = \frac{p - p_0}{1/2\rho_\infty u_\infty^2} \tag{3.3}$$

- C_{pX}: Pressure coefficient resolved in the x-direction.
- C_{pZ}: Pressure coefficient resolved in the z-direction.
- C_{pT}: Total pressure coefficient – A measure of the energy in the flow.

$$C_{pT} = \frac{p_s + 1/2\rho_\infty u_\infty^2}{p_\infty + 1/2\rho_\infty u_\infty^2} \tag{3.4}$$

- U_w: Near wall velocity – Velocity of flow near the surface of the car, which can be used to identify regions of slow or separated flow.

- *Balance*: The balance gives the % of the vehicle forces transferred through the front contact patch including the wheel and suspension forces.

The 3D CAD model in different views is illustrated in the following figures:

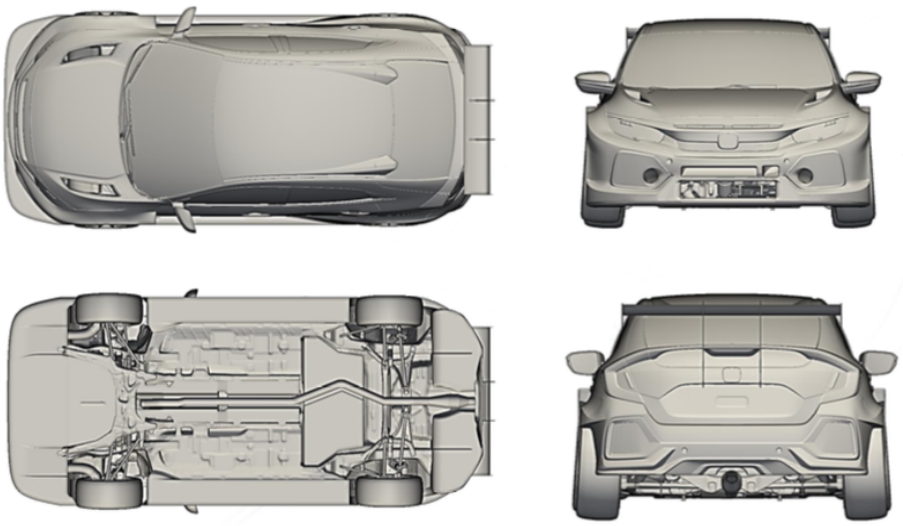

Figure 3.2: Orthogonal view

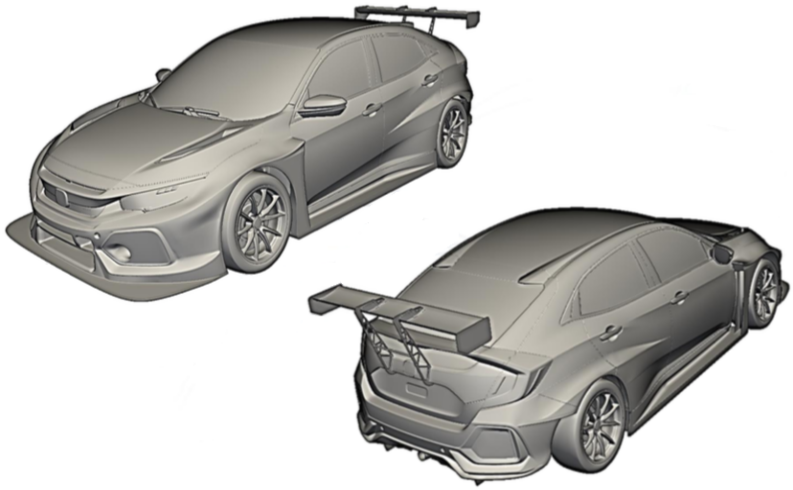

Figure 3.3: 3/4 view - upper side

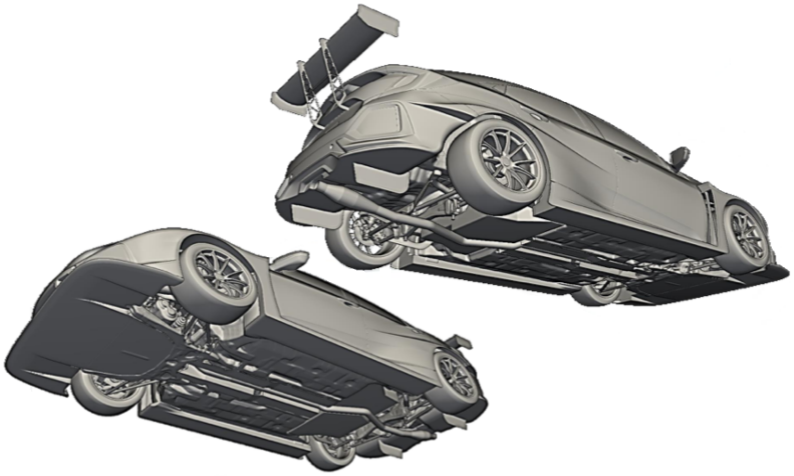

Figure 3.4: 3/4 view - down side

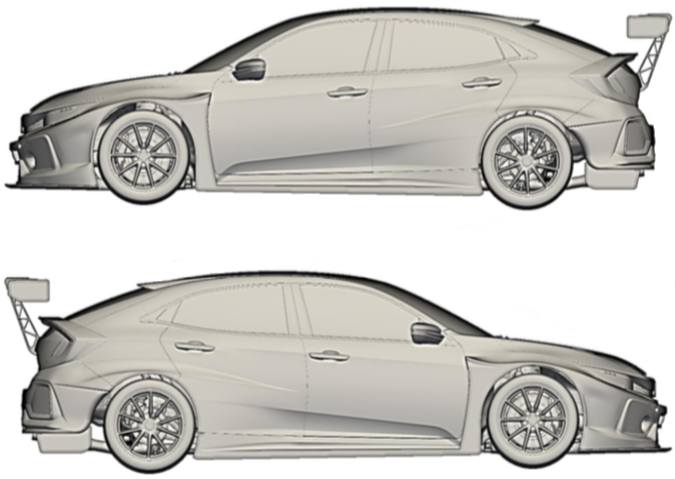

Figure 3.5: Lateral view

We define TotalSim's standard convention for measuring the ride height and aerodynamic balance of the car.

- **Front/Rear Ride Heights (mm)**: Vertical distances between the reference points supplied by JAS (shown in the below images) and the ground.
- **Pitch Balance (% Front)**: Percentage of total downforce acting through the front contact patch (i.e. load transferred to the front tyres).
- **Roll Balance (% Right)**: Percentage of total downforce acting through the RHS contact patch (i.e. load transferred to the RHS tyres).
- **Yaw Balance (% Front)**: Percentage of total side force acting through the front wheel axle line in the lateral direction.

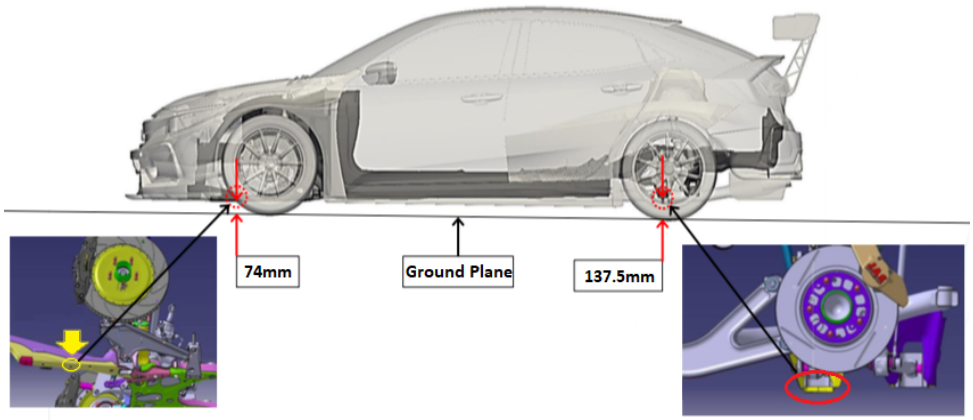

Figure 3.6: Ride heights setting

We can consider four conditions of motion in the track:

Table 3.1: Characteristic parameters at different attitudes

CONDITION	FR-RH (mm)	RR-RH (mm)	YAW (deg)	ROLL (deg)	STEER (deg)	SPEED (m/s)
Static	83	147.5	0.5	0	0	44.444
Straight	74	137.5	0.5	0	0	44.444
Braking	53	151.5	0.5	0	0	44.444
Corner	83	147.5	3	1	6	44.444

TotalSim defines the yaw, steer and roll angles as the following:

- **Positive Yaw**: Flow approaches from drivers right hand side.
- **Positive Steering Angle**: 'Turning left' i.e. wheels points to the drivers left hand side.
- **Positive Roll**: Ground plane slopes downwards on the drivers left hand side.

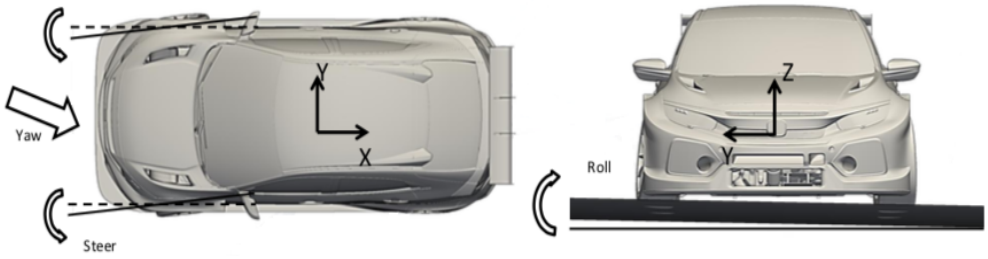

Figure 3.7: Angle conventions

We present a summary of the main boundary conditions applied to the model. A moving wall boundary condition is applied to rotating wheel surfaces with an angular

velocity based on the vehicle speed and rolling radius. The fluid region around the wheel spokes are modeled in a rotating reference frame to simulate the momentum imparted into the flow (note the spokes and CFD mesh do not physically spin). Referring to the radiators, their pressure drop is supplied directly by the manufacturer as the study of the flows would require a too dense mesh. Indeed, the imposition of a too refined grid would make the CFD calculations too long and laborious.
The pressure drop tables are illustrated with varying speed:

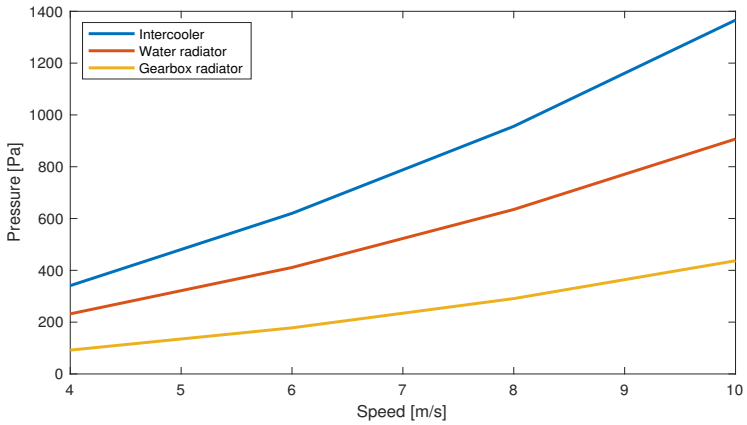

Figure 3.8: Pressure drop of radiators and intercooler

The engine intake and exhaust have been modeled as velocity outlets and inlets respectively.

3.2.2 CFD maps results

We begin to analyze the results obtained from the CFD calculation; the simulations were conducted on the 3D model of the entire car. We will see the values that assume the pressure coefficients, which characterize the flow that circulates around the car, through the four orthogonal projections. Later, for a more accurate analysis, the model will be dissected along all the axes of our reference system.

We study the flow that winds the car longitudinally: starting from the front, we notice how on the bumper there is a large area of stagnation in which the pressure coefficient Cp reaches values close to 1. Subsequently the fluid accelerates above the front hood and the Cp becomes negative, since this surface is generally convex and the flow therefore tends to accelerate. At the entrance of the windscreen, the air slows down again due to the sudden change in slope and the pressure increases. The flow accelerates again on the roof of the vehicle (due to its convex shape) where we observe the lowest pressure (and therefore the highest speed for Bernoulli law) that takes the flow in its path.

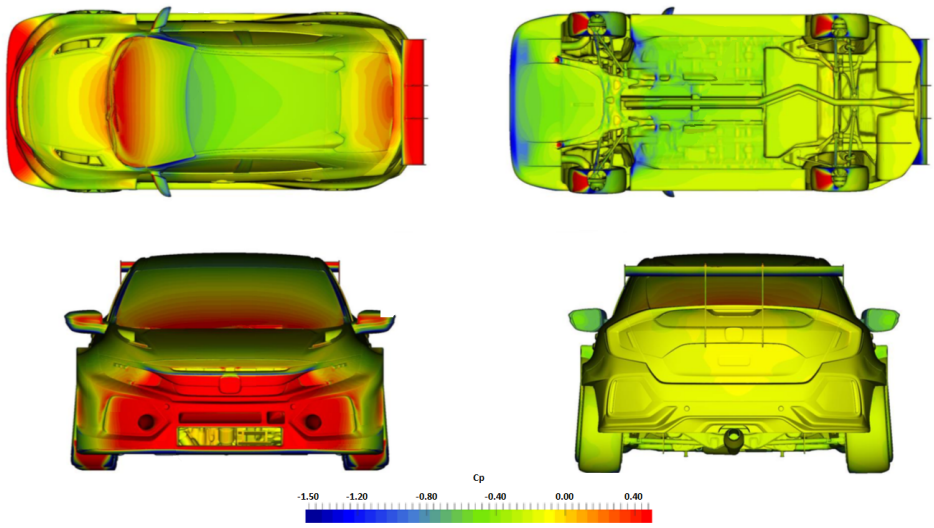

Figure 3.9: C_P **maps**

The trend of the pressure coefficient clearly identifies the components that contribute to the forces acting on the entire vehicle. We study the drag from the front and back views, while from the above and below view the vertical force can be analyzed, the downforce. The color map allows confirmation of what was seen before in every aspect. As seen from the first two images, the body tends to generate lift and therefore to have a negative C_p, especially in the roof and in the side pylons.

All the underbody (characterized by a negative pressure coefficient) tends to generate downforce, especially in the splitter and in the rear wing where we highlight the minimum pressure values. As mentioned, the front of the car is characterized by various points of stagnation of the flow, mainly responsible for drag, but the side bumpers and the roof generate a thrust force that "helps" the car in its travel. Particularly noteworthy is the back area, with an almost homogeneous color. This is due to the separation of the current that generates a stream behind the car that sucks the back of the car contributing significantly to the longitudinal force.

The principle that governs the generation of lift, obtained by exploiting the underbody of the car, is as follows: in the front part the air flow passage section is considerably reduced, thus increasing the speed and decreasing its pressure. Subsequently, at the back, it is necessary to slow down the fluid at the free flow velocity in a gradual and controlled manner so that no vein detachment occurs. This last task is carried out by the diffuser, which therefore has the function of recovering the kinetic energy in the most efficient way possible. The downforce is then generated by the throat zone, where the flow has a high speed and a low pressure; the larger the throat area, the greater the downforce. Also the diffuser creates a certain percentage of downforce, being the average pressure of the fluid that passes through the diffuser lower than the ambient one. However, later on, we will see how the effect of the pressure reduction in the underbody is in some cases completely overturned due to the increase in the speed of the flow over the roof of the car.

The most efficient solution would obviously be to adopt a flat underbody [1], which drastically reduces the produced drag and increases the speed of air flow between the car and the ground. The modeling of the flat bottom allows you to have benefits, such as the ability to create a low pressure area that generates downforce. Given the large surface area of the bottom, even a small pressure decrease can generate a great attractiveness downwards.

A fundamental aerodynamic element that from the first images showed its efficiency is the front splitter. From the images described above, together with the rear wing, it is the component where the greatest color changes occur, both as regards the flow over the car and the underlying one. Together with a substantial increase in downforce at the front, it causes a substantial invariance of drag generated, given the very small front section that this device has. The generated downforce increases with the length of the splitter (i.e. its extension in the direction of the progress of the car), up to a certain value, beyond which there is no longer any increase. The splitter works because it concentrates a high pressure area just above it (where it joins with the spoiler) and simultaneously creates a very marked depression zone immediately below, with the overall result of a strong increase in downforce at the bottom. front axle.

It is essential that the car has a perfect aerodynamic balance: if you only add the front splitter just described, you will have a great aerodynamic load at high speeds and it is therefore necessary something at the rear that balances such failure. A rear spoiler is the easiest way to achieve this effect. The rear wings can have innumerable shapes and can be realized through a simple inclined bulkhead or from a more complex three-dimensional appendix, suitably shaped to make it harmonic with the rest of the car's line.

The inclination and the length of the wing are the determining parameters for the designer, as they influence the increase in drag and downforce. In general, increasing the length of the wing or its angle causes a more or less linear increase in the downforce and at the same time the drag. However, the efficiency increases only with the increase in the angle of the bulkhead. A good compromise is therefore to have a spoiler with a very high angle, for example 60 degrees with respect to the horizontal axis of the vehicle, but having a moderate length. [2]

Looking at the CFD studies, there is a substantial increase in static pressure in a very large area above the tail of the car, as well as a clear reduction in pressure below the car. The spoiler in fact deflects the air flow, providing a strong vertical component and at the same time slows it down. These effects lead to an overall increase in rear downforce.

Unfortunately, the decrease in pressure also affects the area behind the car body, leading to a considerable increase in drag. The area of low pressure that reigns in the air zone behind the car is then increased. Finally, the pressure decrease under the body will lead to a higher flow of air that will lead to a further increase in drag if the car does not have a flat bottom. In conclusion, the effect of a rear spoiler is generally to give greater

[1] Prohibited by the regulation

[2] As we saw in *Section 1.3.3*, regarding the regulation of the TCR car, the rear wing is fixed in all its geometry

stability to the rear wheels at high speeds, but at the same time decrease the maximum speed of the vehicle, as they significantly increase the resisting forces.

It must be remembered that in some cases a small spoiler having a reduced angle of inclination with respect to the horizontal, can even reduce the overall drag of the car; it happens that, in the absence of the spoiler, the detachment of the vein from the surface occurs after the flow has bypassed the edge of the rear bonnet: if this happens, the air acquires considerable speed on the edge of the bonnet and consequently suffers a strong depression that causes a penalizing drag. The use of a small spoiler, anticipating the detachment of the fluid vein, avoids this inconvenience. [**13**]

We continue with the aerodynamic analysis carried out on the results obtained by TotalSim Ltd:

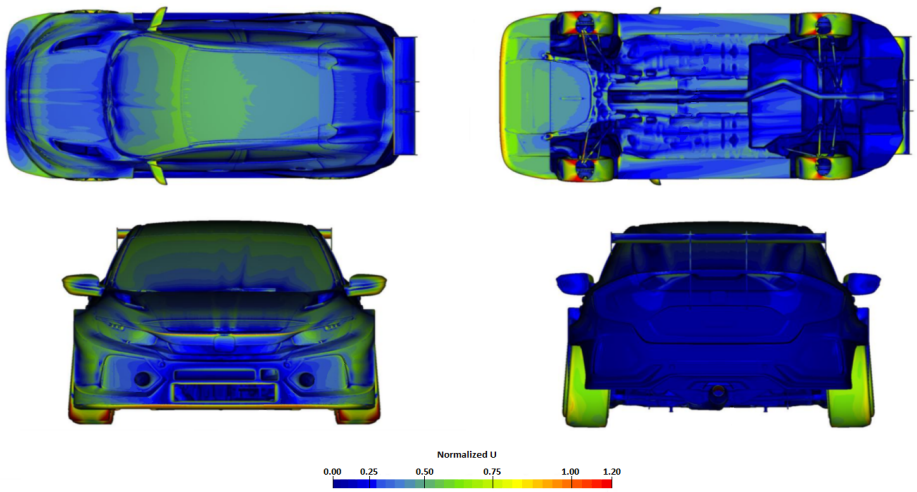

Figure 3.10: Normalized speed maps

The normalized speed allows me an immediate comparison with the speed u_∞ which corresponds to the car's speed of $44.4\,m/s = 160\,km/h$.

$$NormalizedU = \frac{U_{local}}{u_\infty} \tag{3.5}$$

We can distinguish that above the car there is a flow zone that runs at a lower speed than that which flows below the splitter and therefore generates one of the largest downforce. In the underbody of the car runs a flow that generally has a lower speed than the corresponding points above it, and therefore generates a counter lift force as also confirmed by the following figure.

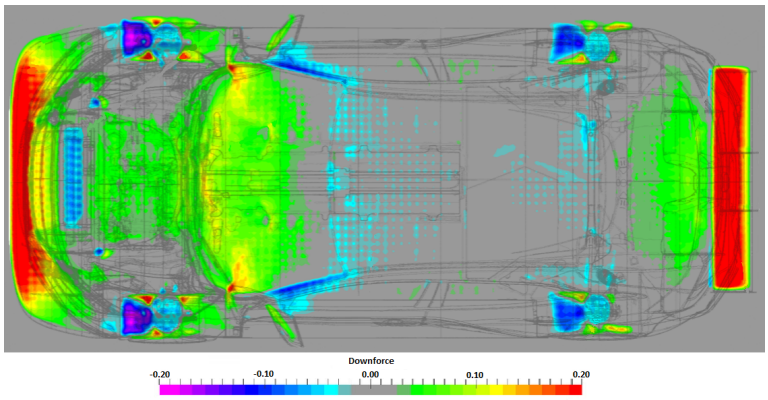

Figure 3.11: Downforce map

This map shows the difference in pressure coefficients along the vertical direction (z-axis) and therefore can be compared to a punctual force. Comparing the pressure coefficients below and above the car is clearly visible the actual downforce that is in the car. Negative values (Purple/Blue) represent a lift force, positive values (Red/Green) represent a downforce force.

We see how fenders, wheels contact patch, the A-pillar, roof and radiators generate a lift force and that there are essentially three large zones that generate downforce: front zone (due to the splitter), middle zone (due to the floor and stagnation on windscreen), rear zone (due to the diffuser/tailgate and the rear wing).

Likewise, it is possible to apply this reasoning along the horizontal axis (x-axis) too, obtaining the drag force. Negative values (Purple/Blue) represent a thrust force, the positive ones (Red/Green) represent a drag force.

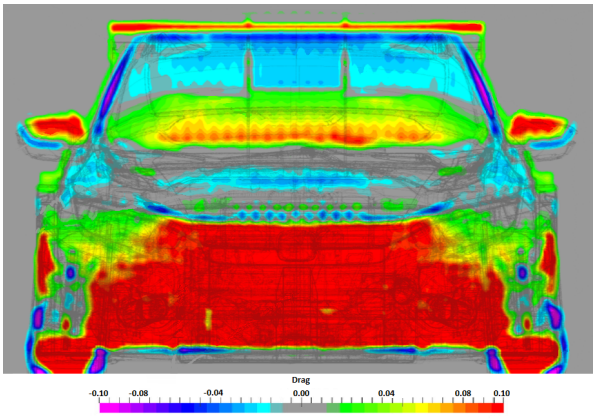

Figure 3.12: Drag map

X-CpT slices show the energy of the flow. Red indicates high energy whilst blue indicates low energy. X-Cp slices show the static pressure around the car. Red indicates high positive static pressure whilst blue indicates low negative static pressure. We now analyze different sections of the car along all three axes of the reference system to study

the flow in detail:

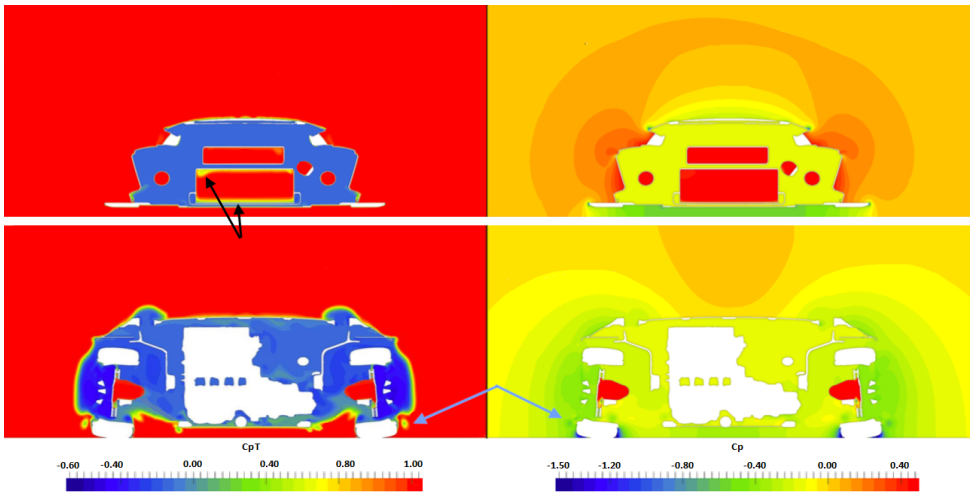

Figure 3.13: C_PT **&** C_P **maps @** $X = -0.7$ **and** $X = -0.1\,m$

We note that the flow is clean, tidy and very energized as wakes and vortices have yet to be developed. There is a large amount of high CpT to the radiator cores (some signs of boundary layer growth - as we see from the black arrows). The flow inside the brake cooling ducts is also kept clean and energized.

Adjacent to the perimeter of the car we see how it began to develop the boundary layer and therefore a loss of energy. High energy flow on the front brakes. The front splitter is responsible for two phenomena: the generation of vortex outboards, responsible for a small drag, and an expansion of the underlying flow into the wheel arches.

In parallel with the energy analysis, we conduct an analysis of the pressure coefficient. The map at the top right allows mainly as under the central splitter there is a strong suction pressure, main responsible for the downforce. The slowing of the lateral flow is due to the geometry of the vehicle that has yet to reach the maximum extension, considering that it is considered a rather advanced section.

The presence of vortices is also confirmed by the pressure coefficient which appear to be characterized by a darker color (as we see from the blue arrows). An important factor to highlight is that the wake is kicked out to reduce the wheel arch pressures to help expand splitter flow.

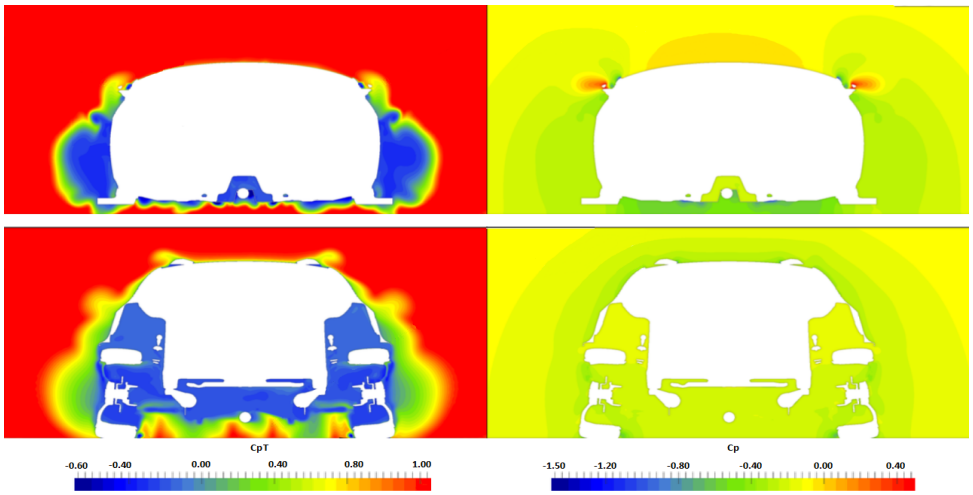

Figure 3.14: C_PT **&** C_P **maps @** $X = 0.64$ **and** $X = 2.70\,m$

It is clear how the trail generated by the wheels expands along the side of the car. It is characterized by energy dissipation and therefore by a blue color. Other separations are evident under the floor two to exposed chassis structures (we remember that the bottom of the car for regulation can not be flat).

Separations grow downstream but still some high CpT available, that is important for the generation of downforce throughout the car. It is also possible to notice the birth of small vortices from the rear tires.

In the figure at the top right emerges the importance of the bonnet cut-outs because, in addition to allowing the flow not to stagnate in the engine compartment and provide for cooling of the latter, they also allow the undisturbed flow to slide more along the side mirrors reducing the coefficients of pressure around them. The pressure coefficient appears high, however, lower than that which characterizes a region of stagnation.

In 3.15, we notice a large loss of energy due to the wake vortexes that have been created within the rear tires that propagate outside the vehicle. In these maps the effect of the rear spoiler and the rear wing is particularly evident.

From these maps and from the following ones, the importance of the rear diffuser is clear. As previously described, the flow passage section is initially restricted, thus increasing its speed and decreasing the pressure, then it is necessary to slow down the fluid at the free flow rate, but gradually and controlled so that it does not occur the detachment of vein. This last task is carried out by the diffuser, which therefore has the function of recovering the kinetic energy in the most efficient way possible. Also the diffuser creates a certain percentage of downforce, being the average pressure of the fluid that passes through the diffuser lower than the ambient one.

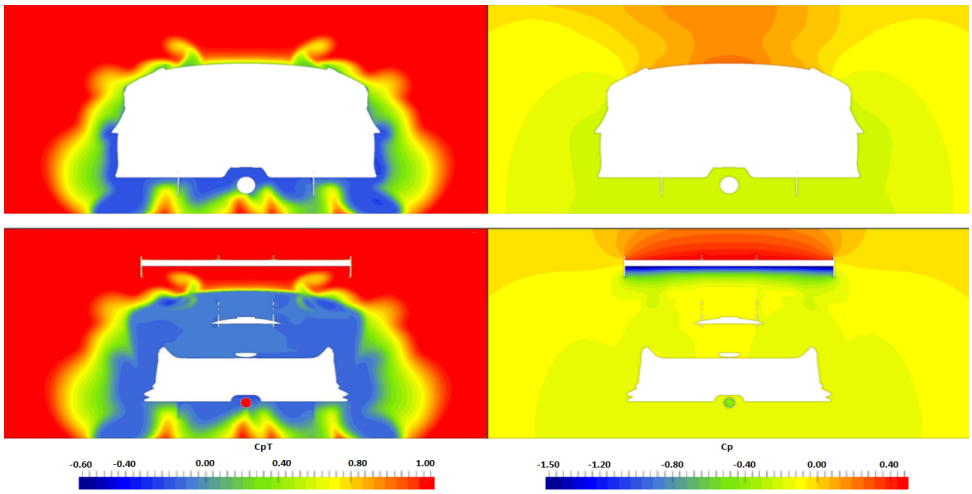

Figure 3.15: C_PT **&** C_P **maps @** $X = 3.22$ **and** $X = 3.50\,m$

It is not possible to establish with certainty what the best ground clearance at the aerodynamic level is. Following the Bernoulli principle it would seem that the closer you get to the ground, the more the generated downforce increases, as the velocity of the fluid in the narrow section increases. But the experimental data show that if you go below a certain height value from the ground, the viscous friction forces become predominant, decreasing the generated downforce; this decrease can also be accentuated by a possible detachment of the vein in the passage of the fluid on the diffuser, due to a too abrupt negative pressure gradient (i.e. from low pressure to high pressure).

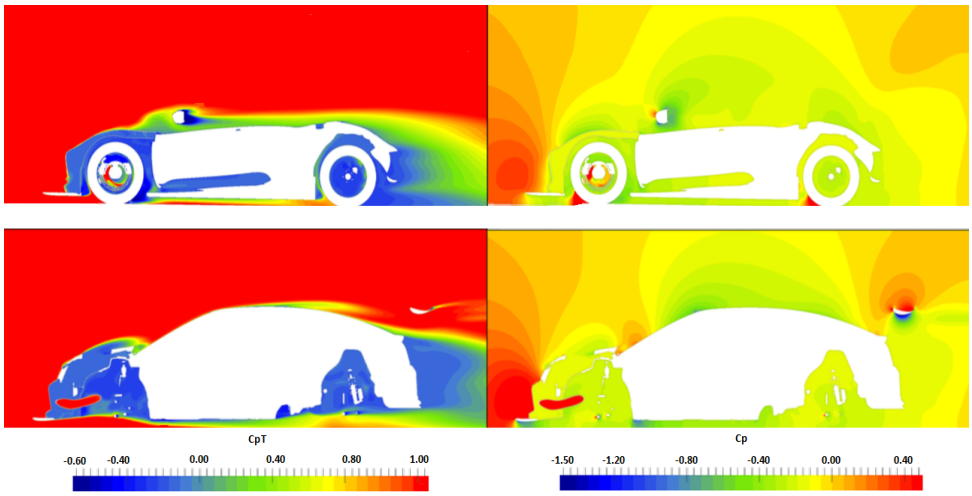

Figure 3.16: C_PT **&** C_P **maps @** $Y = -0.86$ **and** $Y = -0.60\,m$

There is a localized suction pressure due to separation on the underside of the chassis leading edge.
In lateral view we can confirm what we saw previously: the bonnet cut-out wake is directed

towards the mirrors in order to reduce the pressure.

We can confirm this effect also in the following image:

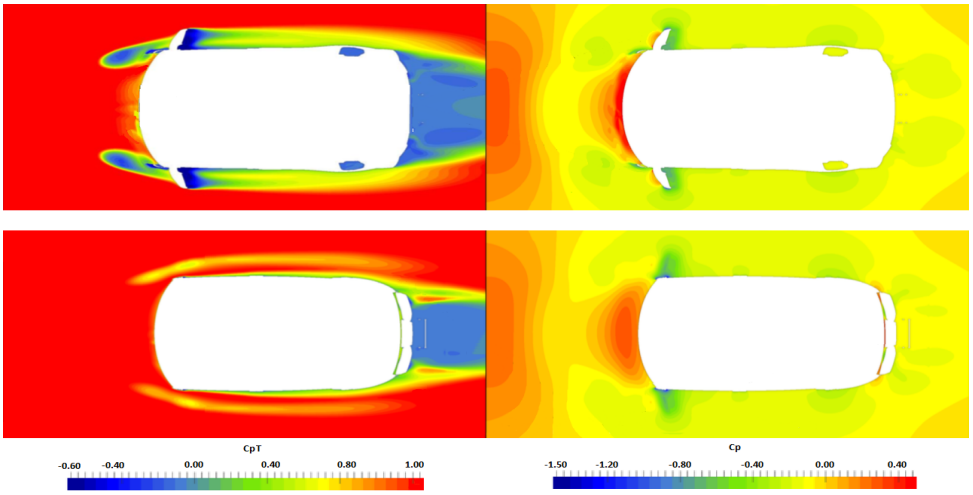

Figure 3.17: C_PT **&** C_P **maps @** $Z = 0.76$ **and** $Z = 0.86\,m$

We also note that the wake is tucked in at rear to minimize drag.

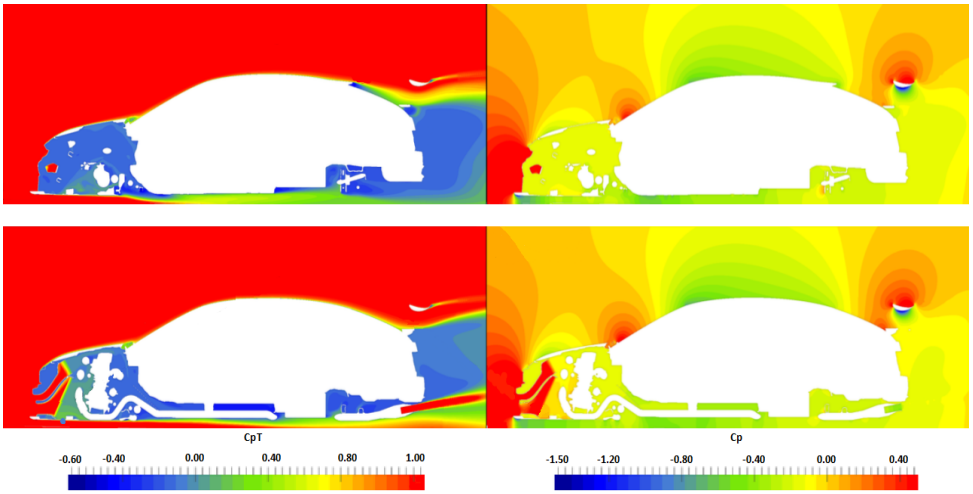

Figure 3.18: C_PT **&** C_P **maps @** $Y = -0.38$ **and** $Y = 0.00\,m$

Very clean flow over the top of the car. But separation from the roof trailing edge spoiler reduces effect from the rear deck spoiler. Engine bay wake exits under the floor and reduces the amount of high CpT flow downstream. We see a tidy flow under the car at centreline.

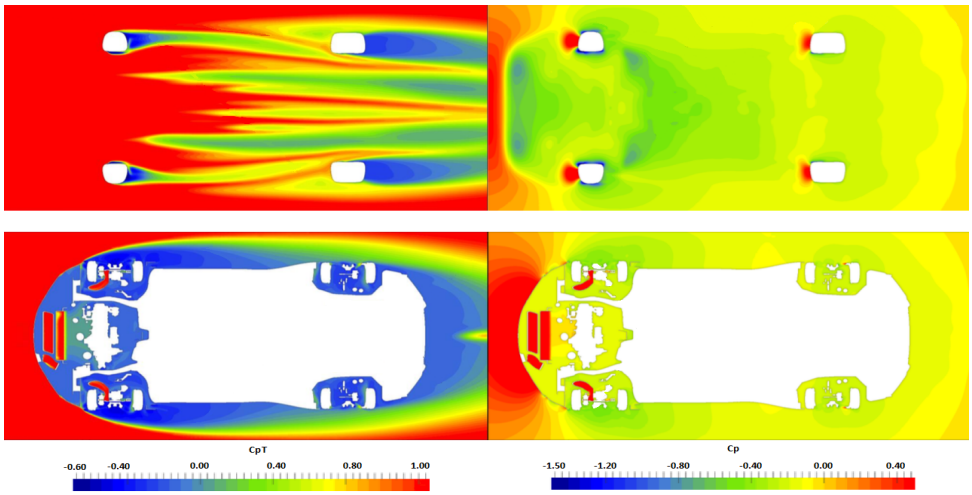

Figure 3.19: C_PT **&** C_P **maps @** $Z = -0.12$ **and** $Z = 0.22\,m$

We notice a relatively narrow wheel wakes which gets pulled inboards due to the low pressure present below the car and a localised low pressure under the front end of chassis There is a relatively large wake kicked out to help improve front downforce; the low pressure outboards of the wheels increases splitter performance.

By modifying the boundary conditions, we can simulate some configurations that the car takes on the track. So far, we have analyzed only the static case, thus assuming the car stationary and the flow that laps at the speed of $44.4\,m/s$. By adjusting suspension heights and rotations as described in 3.1, it is possible to carry out the CFD simulation of the car in conditions that are closer to the real track conditions.

In order not to burden the discussion too much, we briefly describe the most important effects that can be identified by comparing the three conditions:

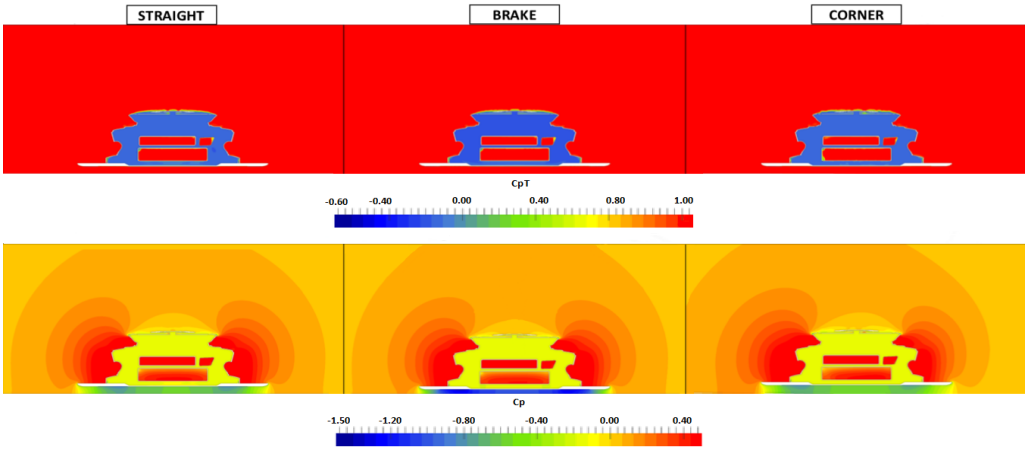

Figure 3.20: C_PT **&** C_P **maps @** $X = -0.80\,m$

- BRAKE: Lower suction pressures observed under the splitter due to the low ride height in breaking condition.
- CORNER: There is a subtle separation on the water radiator duct corners on the RHS due to the yaw and a sower suction on the splitter.

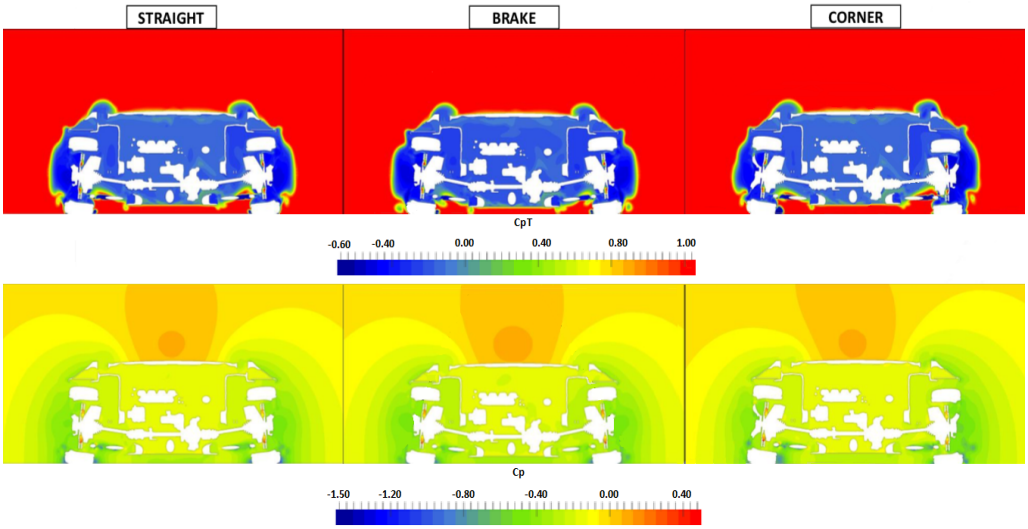

Figure 3.21: C_PT **&** C_P **maps @** $X = 0.00\,m$

- BRAKE: Stronger vortices from the splitter foot.
- CORNER: Stronger tyre squirt vortex on RHS. Increased expansion of splitter flow on LHS.

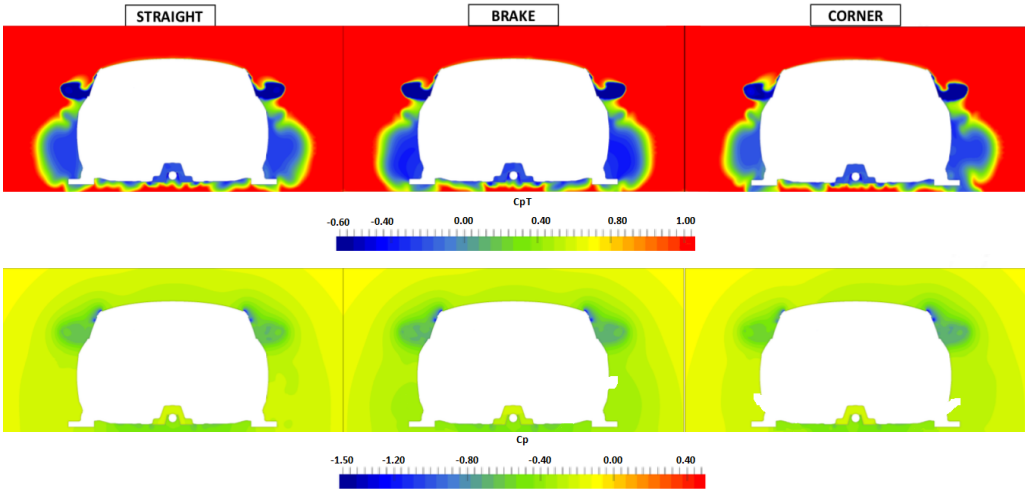

Figure 3.22: C_PT **&** C_P **maps @** $X = 0.86\,m$

- BRAKE: Lower flow energy under the sills due to larger front wheel wakes. Lowered pressures in general than the straight case.
- CORNER: Lower pressure observed on the LHS of the car.

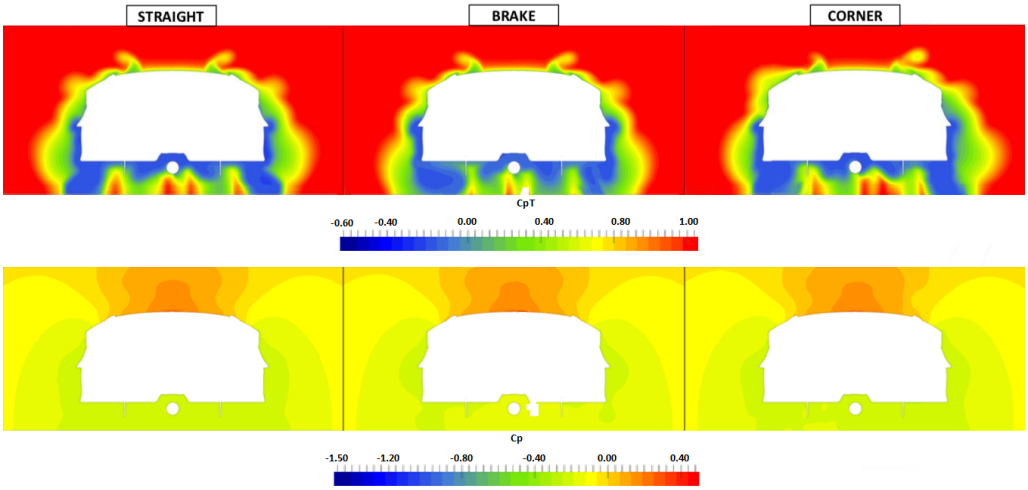

Figure 3.23: C_PT **&** C_P **maps @** $X = 3.20\,m$

- BRAKE: Change in CpT distribution which ultimately results in higher static pressure under the diffuser.

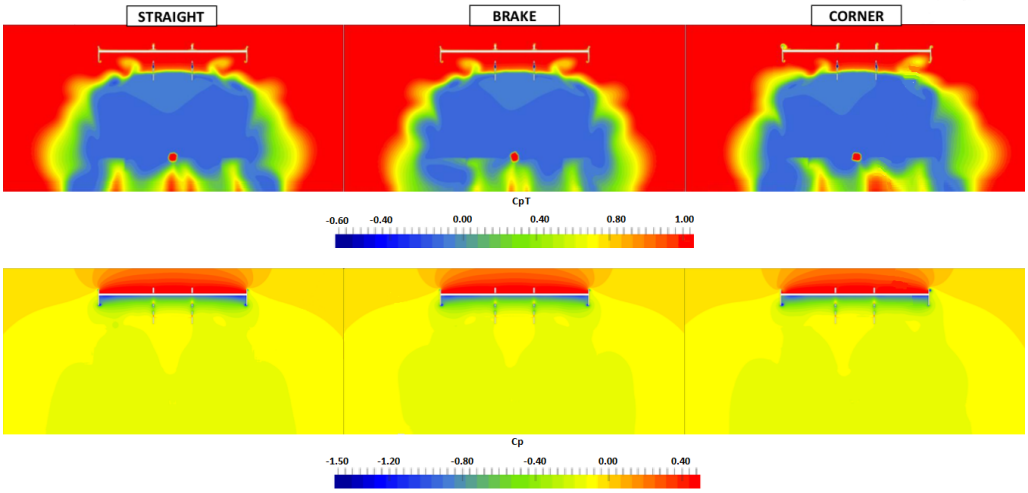

Figure 3.24: C_PT **&** C_P **maps @** $X = 3.60\,m$

- CORNER: Loss in rear wing performance due to larger A-pillar vortex formed.

To analyze the aerodynamic forces acting in the cars it is convenient to distinguish between the components or groups of components that are primarily responsible for these

stresses. This figure presents a breakdown of the individual sub assemblies by which forces can be recorded on.

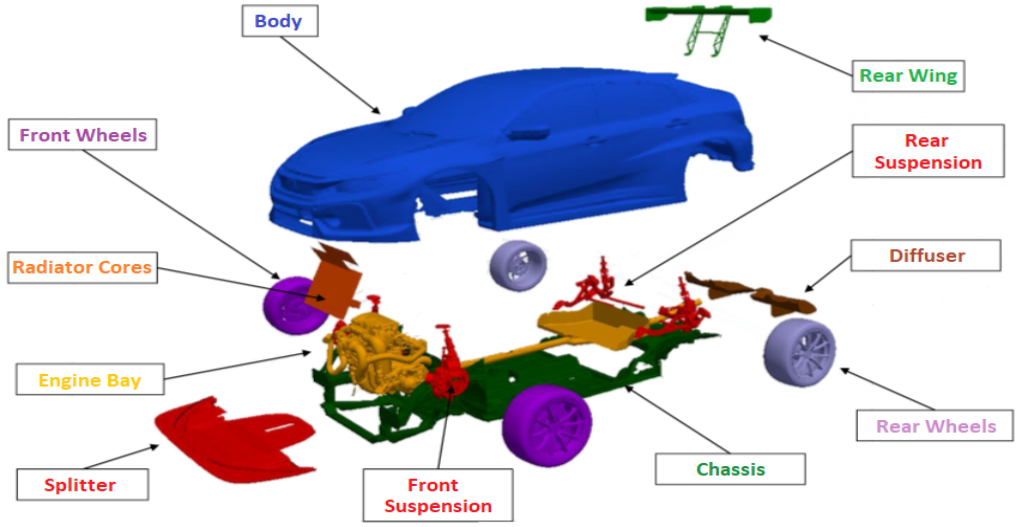

Figure 3.25: Car sub-assemblies

After the analysis of the different CFD maps of the car, we present a summary of the overall results of the CFD simulations for various vehicle attitudes.

		FULL VEHICLE FORCES							RADIATORS		
		DRAG	SIDE	DOWNFORCE			EFFICIENCY	BALANCE	MASS FLOWS		
CONDITION	SPEED (m/s)	TOTAL (N)	TOTAL (N)	TOTAL (N)	FRONT (N)	REAR (N)	L/D (-)	PITCH (% Front)	WATER (kg/s)	IC (kg/s)	GEARBOX (kg/s)
STATIC	44.4	1154	-51	1927	1105	822	1.671	57.4%	3.410	0.975	0.061
STRAIGHT	44.4	1146	-58	2027	1157	869	1.769	57.1%	3.414	0.976	0.060
BRAKE	44.4	1150	-35	2420	1692	728	2.104	69.9%	3.451	0.986	0.061
CORNER	44.4	1157	-373	1851	1071	780	1.600	57.9%	3.380	0.972	0.060

Figure 3.26: CFD results data

If we split these results into different contributions given by the groups of components described above we obtain:

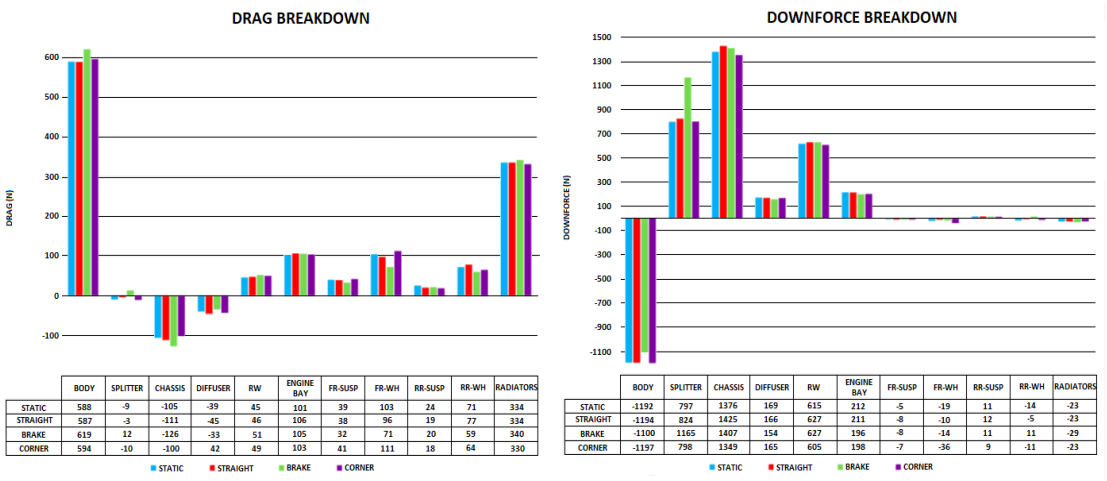

	BODY	SPLITTER	CHASSIS	DIFFUSER	RW	ENGINE BAY	FR-SUSP	FR-WH	RR-SUSP	RR-WH	RADIATORS
STATIC	588	-9	-105	-39	45	101	39	103	24	71	334
STRAIGHT	587	-3	-111	-45	46	106	38	96	19	77	334
BRAKE	619	12	-126	-33	51	105	32	71	20	59	340
CORNER	594	-10	-100	42	49	103	41	111	18	64	330

	BODY	SPLITTER	CHASSIS	DIFFUSER	RW	ENGINE BAY	FR-SUSP	FR-WH	RR-SUSP	RR-WH	RADIATORS
STATIC	-1192	797	1376	169	615	212	-5	-19	11	-14	-23
STRAIGHT	-1194	824	1425	166	627	211	-8	-10	12	-5	-23
BRAKE	-1100	1165	1407	154	627	196	-8	-14	11	11	-29
CORNER	-1197	798	1349	165	605	198	-7	-36	9	-11	-23

Figure 3.27: Drag and downforce breakdown in four different configurations

From the left graph you can see how the main source of drag is from the bodywork. On brake the drag bodywork is greater than the other configurations because the car, lowering at the front and getting up at the rear, tends to have a larger front surface. Thrust is generated on chassis and diffuser due to pressure reflection within the car. Continuing the description of the graph, it is clear that another contribution derives from the wheels and suspensions (obviously a greater contribution is due to the front components compared to the rear ones). In contrast to the body, in the braking phase the front wheels are more covered and therefore their contribution to the resistance is lower than the rear ones. Another significant contribution to the amount of drag derives from the radiators.

Due to the shape, the body is the main lift generator. The contribution of the wheels being symmetrical is negligible and they are practically irrelevant to the formation of vertical aerodynamic forces. To compensate for the effect of the body and generate a positive downforce force requires aerodynamic devices such as the splitter, the rear wing and the diffuser, which are added to the chassis and the engine bay in such a way that the overall force acting on the car is facing down.

The braking attitude shows the largest performance from the two splitter to the low front ride height. In addition to the greater ground effect, the inclinating splitter becomes a real aileron and keeps the car adhering to the track.

The one described above is easily deducible also from the following graphs.
Drag distribution illustrates how the drag varies along the car at a particular x-station while drag accumulation illustrates how the drag accumulates along the length of the car.

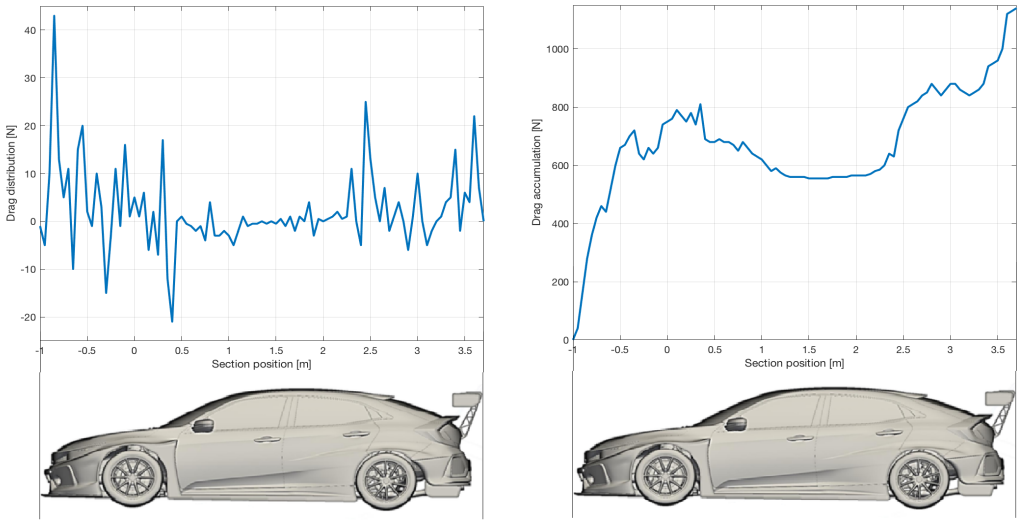

Figure 3.28: Drag distribution

Downforce distribution illustrates how the lift varies along the car at a particular x-station. Downforce accumulation illustrates how the lift accumulates along the length of the car.

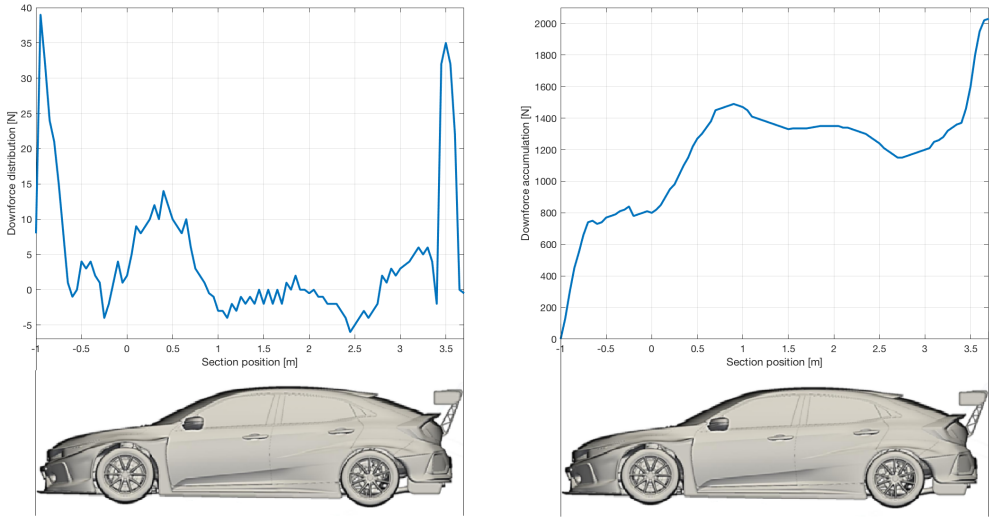

Figure 3.29: Downforce distribution

So we can conclude that:

- At these conditions, the car generates $\approx 1140 \sim 1160\,N$ of drag depending on the car attitude.

- The largest downforce ($2420\,N$) and L/D (≈ 2.1) is seen at the braking attitude. Splitter performance increases significantly due to at the low front ride height.
- At the static, straight and corner conditions, the car shows $\approx 57-58\%$ balanced in front.
- Balance shifts forwards by $\approx 13\%$ at the braking attitude compared with the straight-ahead condition, due to the increase in downforce from the splitter.
- The cooling mass flows through the radiator cores are $\approx 3.4\,kg/s$, $\approx 0.98\,kg/s$ and $0.06\,kg/s$ for the water, intercooler and gearbox radiators respectively.
  Flow visualizations show tidy and good amount of high energy flow going through the radiator ducts.

3.3 Analysis of the changes made

All the following cases are alternatives proposed by J.A.S. Motorsport on the basis of its experience acquired over the years and analyzed by TotalSim in order to choose between the configurations that optimizes the performance of the car that for aerodynamic purposes correspond to the decrease in drag force and the increase in downforce.

In some cases we have not only evaluated the aerodynamic aspect but also the costs, the feasibility, the practicality, all of course in compliance with the regulation. These changes led us to the construction of the final Honda Civic TCR 2018 analyzed in the previous chapter as "Final Configuration". Now, we look at the process that led to the determination of the shape of that final car.

3.3.1 Baseline

Starting from a car called "baseline", the first 3D draft of the car, we describe some of the stages of the route carried out following the CFD analysis conducted by the company TotalSim. Comparing the data obtained from the numerical software of the starting configuration (*baseline*), with those obtained after the installation of new components, we will evaluate whether it is convenient for the change to be implemented or not.

So the procedure follows the steps that will lead to the determination of the "final configuration": it provides that once defined the "base" car are considered the installations of the components one at a time, if the overall performance of the car, from the aerodynamic point of view, they are improved then a new "baseline" is defined considering this last installation and the analysis of another element is continued, otherwise if the performances are not improved the previous baseline is preserved.

The results of the "$Baseline_0$" are shown in the following figures, where the starting baseline is considered with *0*:
[3]

[3] We could compare the 3D geometry of this $Baseline_0$ with the final configuration geometry shown in *Section 3.2.1.*

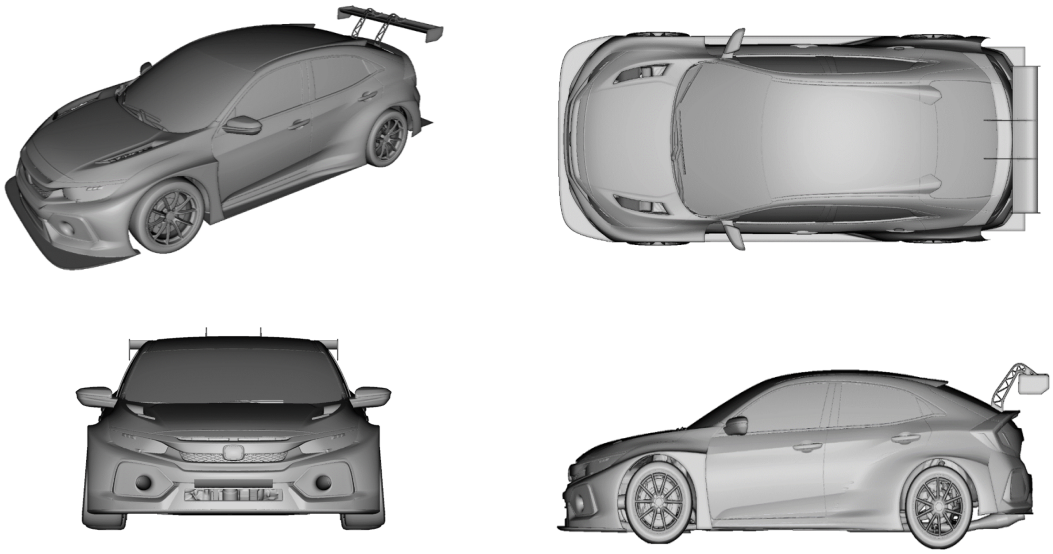

Figure 3.30: 3D Baseline geometry

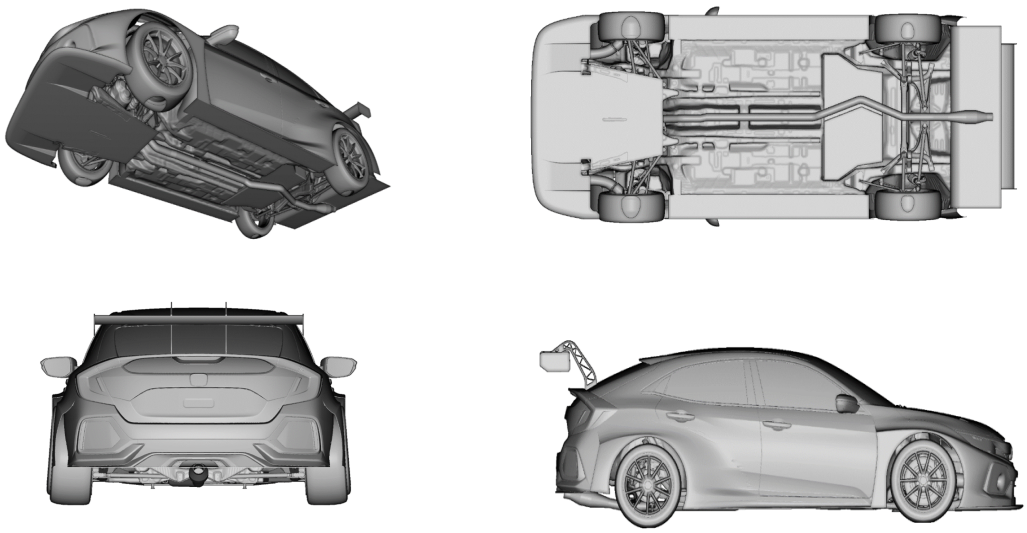

Figure 3.31: 3D Baseline geometry

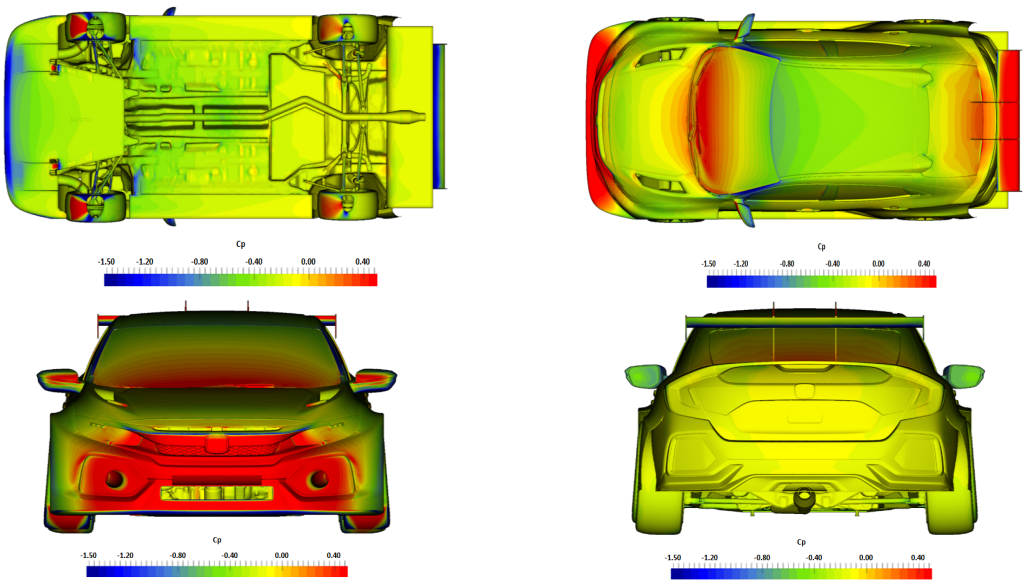

Figure 3.32: C_P **maps**

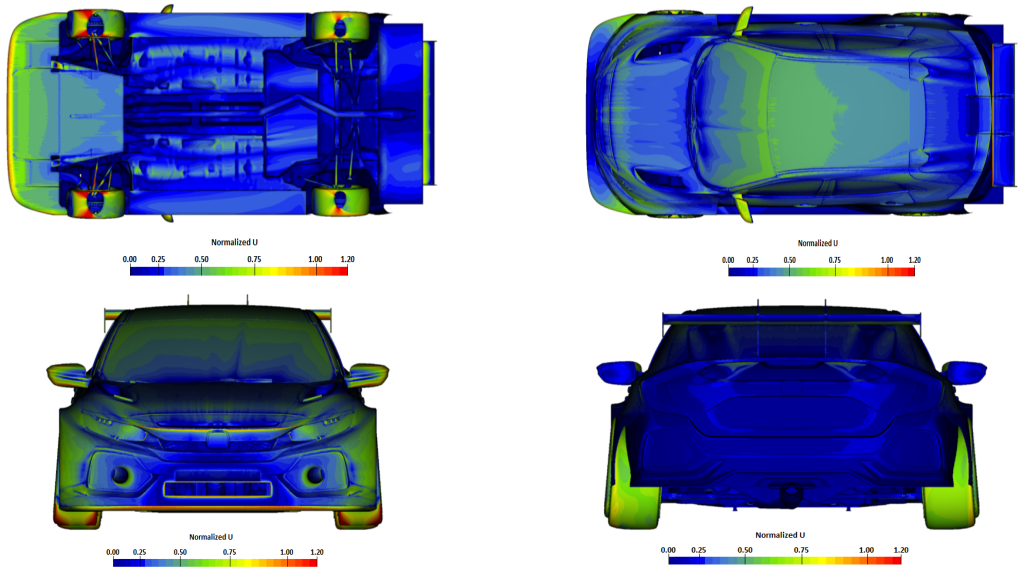

Figure 3.33: Normalized speed maps

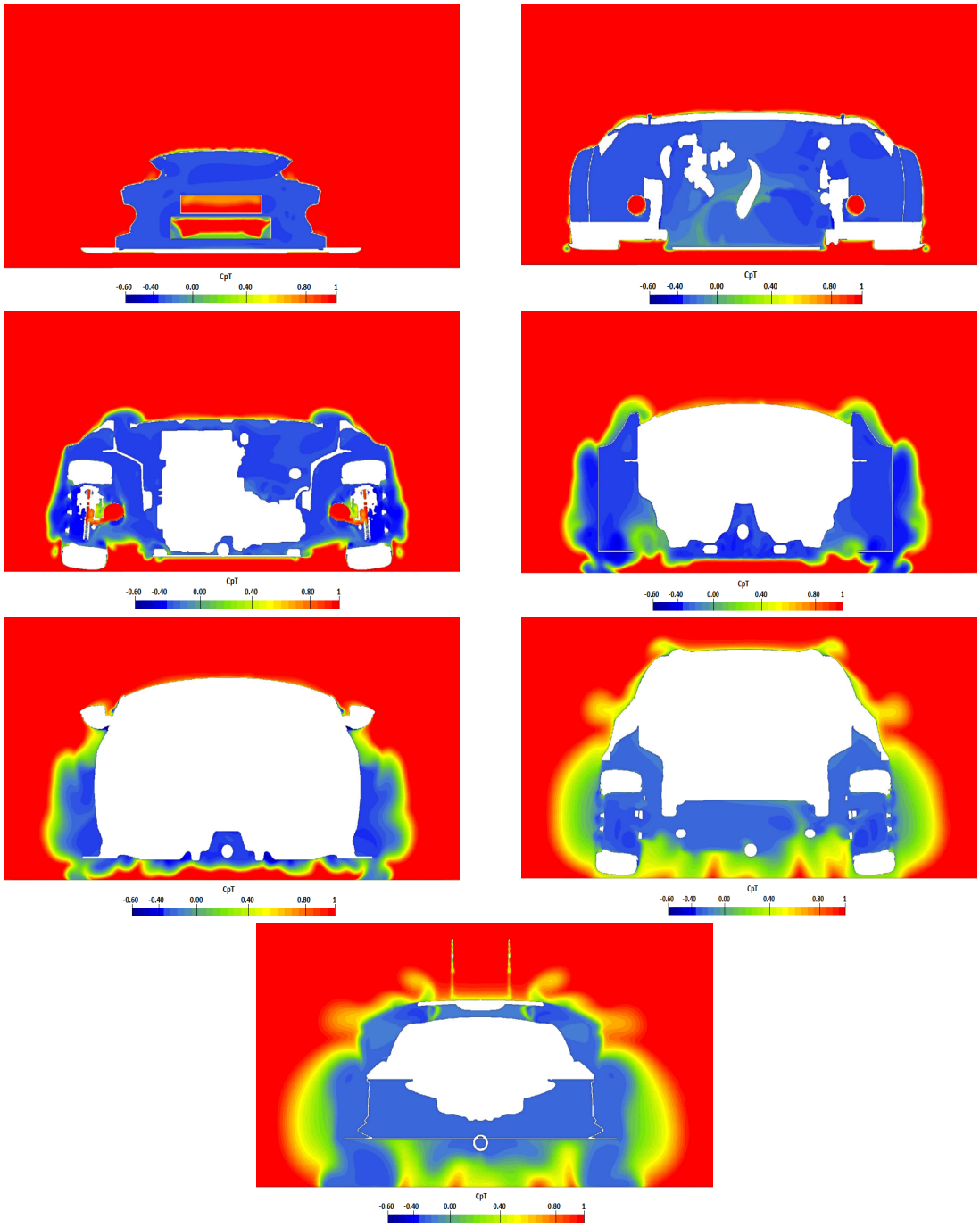

Figure 3.34: C_PT **maps @** $X = -0.76$, $X = -0.44$, $X = -0.14$, $X = 0.36$, $X = 0.72$, $X = 2.56$ **and** $X = 3.42\,m$

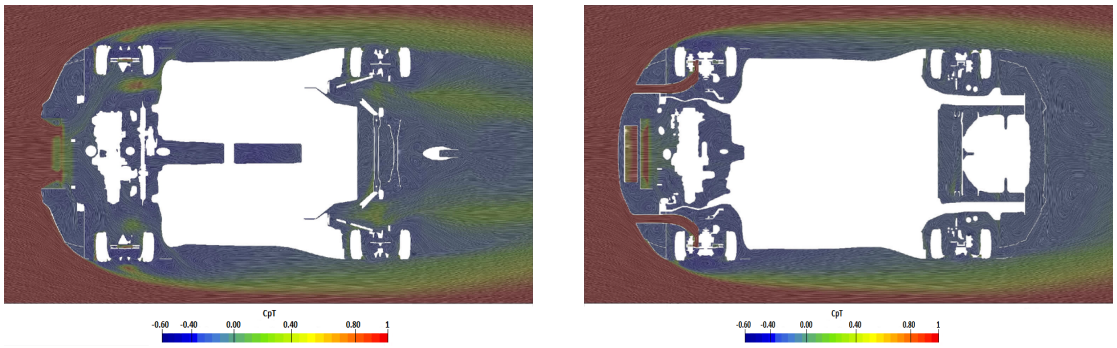

Figure 3.35: C_PT **maps - upper view @** $Z = 0.06$ **and** $Z = 0.20\,m$

Once the results of the CFD simulations have been visualized, it is possible to highlight the most critical areas from the aerodynamic point of view and to experiment with some solutions that improve the flow around the car.

***NB**: As previously mentioned, the aerodynamic analysis carried out through software, like all the simulation methods, has its own degree of accuracy. The typical approach requires to discretize the fluid domain in elementary cells so as to obtain a calculation grid (also called mesh), on which to apply iterative resolution methods in order to solve the Navier-Stokes equations or the Euler equations. The comparison between the numerical simulations of the different configurations allows to cancel some approximations made by the software.*

We go into the analysis of some changes: we initially consider the comparison between two different types of fenders.

3.3.2 Rear and Front Fender

This revised rear fender is wider and it has reduced clearance at the leading edge.

This change slightly affects the drag coefficient as the fender is more connected to the car, giving it a more aerodynamic shape. From the point of view of the vertical aerodynamic forces, no particular effects are noted. The greater width of the fender (in respect of the maximum width imposed by the regulation: width of bodywork: Maximum $1950\,mm$) allows the widening of the wheels, therefore a more stable car.
Similarly, this concept of modification can also be implemented on the front.

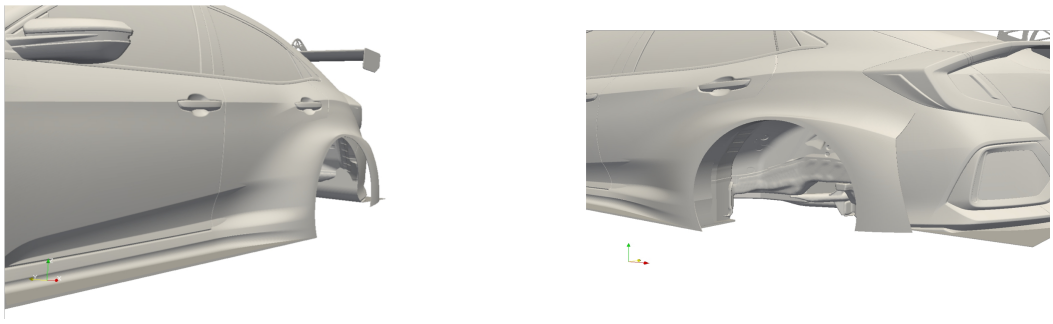

Figure 3.36: Baseline configuration

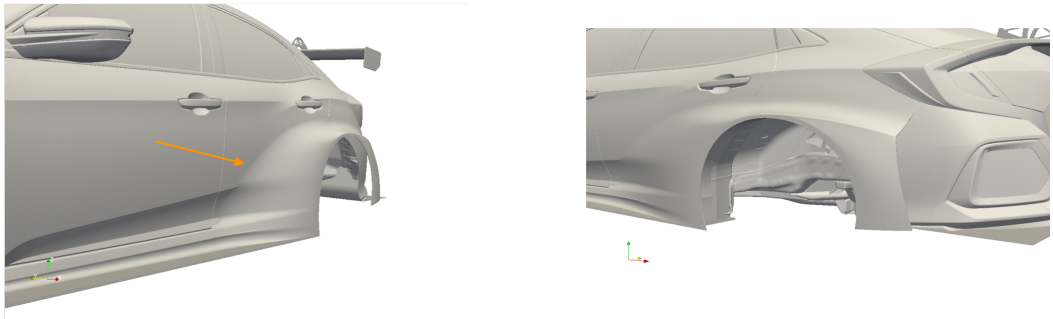

Figure 3.37: New configuration

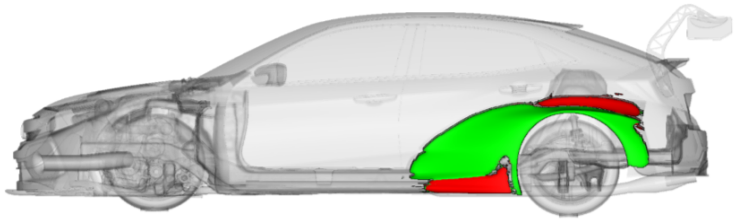

Figure 3.38: Change made on rear fender: RED = old, GREEN = new

We have seen how creating a concave leading edge surface the result has not improved. For this reason we choose the previous solution: we kept the green configuration described before in Figure 3.38. In fact a slightly larger trail is produced from the front edge of the rear fender and the flow passes tangentially to the fender. This larger wake leads to a greater resistance of about $10\,N$, a number not clearly visible from the aerodynamic map. In the previous case, we can guess how the flow passed more gently the posterior fender and remained more attached to the body. A slight decrease in pressure inside the wheel arch generates a slight increase in the aerodynamic load. However, being a downforce at the rear is not of much interest for the performance of the car.

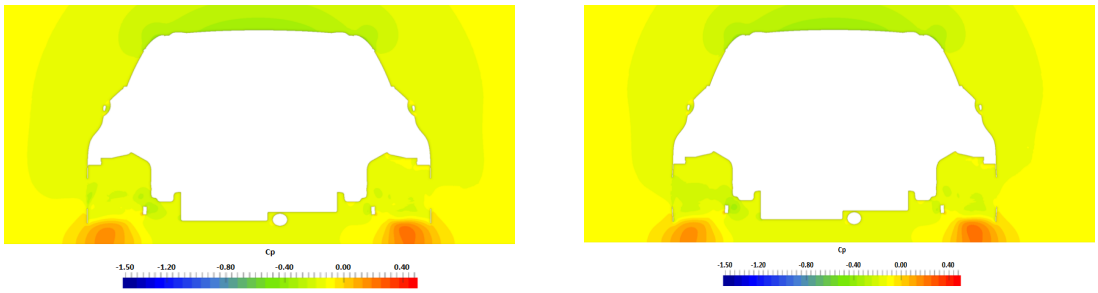

(a) Baseline configuration (b) New configuration

Figure 3.39: Comparison between C_P maps @ $X = 2.36\,m$

Similarly, this concept of modification was also tested in the front fender of the car with the same results. To further improve efficiency we thought about modeling the front fender by impressing the side dimples before the wheels, so as to further divert the flow to the outside of the car by reducing the resistance. We also see a slight increase in downforce, but the decrease in vehicle strength (about $20\,N$) is already a sufficient condition to confirm the fender's intuition. As we can see from the following image, the last front fender had a greater angle.

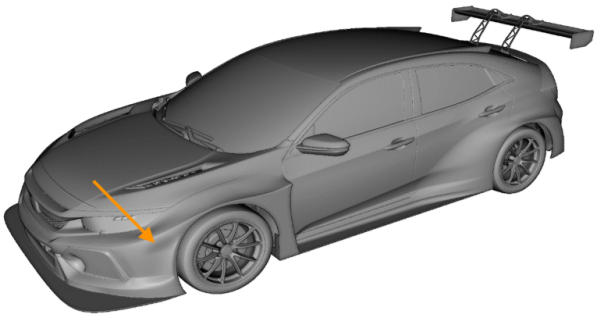

Figure 3.40: Side dimples on front fender

The same idea applied to the rear fender does not have the same effect. In fact, when the flow is diverted to the front, it undergoes an increase in resistance locally, but its overall positive effect is visible along the whole vehicle with the flow that envelops it the most. For the rear fender, on the other hand, the local increase in resistance due to the deviation of the flow is not compensated by any reduction, since the length of the vehicle has been completed and this solution is not advantageous. So this configuration is the best performing with significant downforce and L/D increases. Another fundamental aspect is that the balance is shifted forwards from 58.6 % to 61 %.

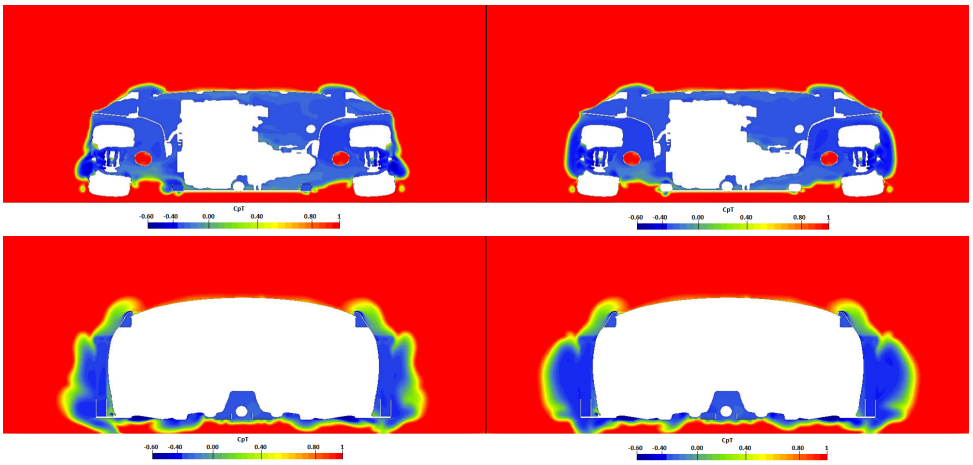

Figure 3.41: Comparison between C_PT maps (baseline vs. new configuration) @ $X = -0.20$ and $X = 0.48\,m$

It is possible to exploit the fenders as "ailerons" so that they generate lift, making the car more stable and adherent to the ground. It is the same principle as the canards, mounted on the front of the bumper. From the numerical simulations we can see how the best results are obtained from the front fenders as they are more invested by the flow. The posterior ones, on the other hand, do not provide a great effect. As shown in the figures below, the ramp (defined Kamm Flick) at the end of the fender allows the creation of a zone with greater pressure that slightly increases the downforce of the car. We show the aerodynamic maps obtained for the front fender: the new configuration shows a $15\,N$ increase in total downforce and a $5\,N$ decrease in total drag. This results in a $1.5\,\%$ increase in efficiency.

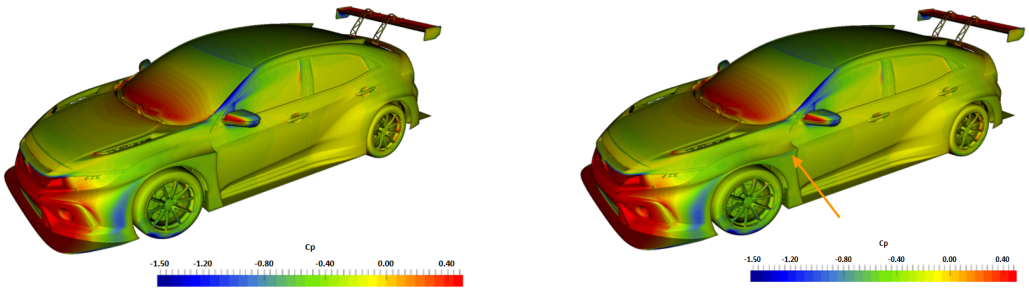

(a) Baseline configuration

(b) New configuration

Figure 3.42: Comparison between C_P maps on 3D view

We see how in the highlighted area there is a "stain" tending to red that shows how there is a more stagnant area that compresses the fender towards the ground.

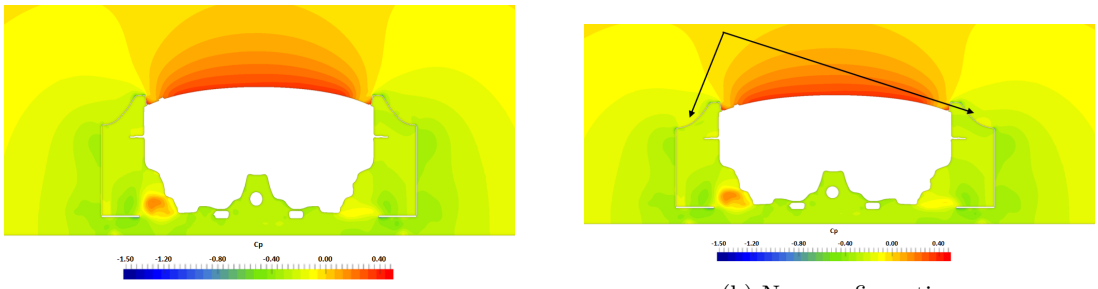

(a) Baseline configuration

(b) New configuration

Figure 3.43: Comparison between C_P maps on section view @ $X = 0.36\,m$

As mentioned previously, the Kamm Flick in the rear fender has no visible effects; we note how the aerodynamic maps are substantially identical.

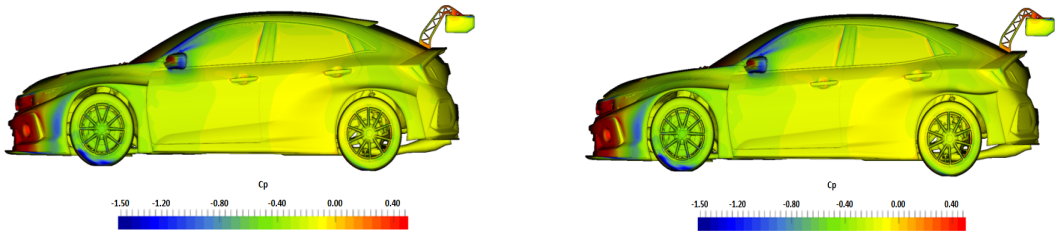

(a) Baseline configuration

(b) New configuration

Figure 3.44: Comparison between C_P maps on lateral view

3.3.3 Arch Exit Modification

We consider different configurations of the arch exit. It is important to allow the turbulence that is created around the wheels to flow so that excessive overpressure does not generate a significant increase in the resistance value. Various solutions are tested, all easily installable and at low costs.

1) Flow exits arch at a steep angle. This configuration does not allow the flow to remain attached to the body of the car, it involves a considerable drag and an increase in thickness of the wake generated by the car. The recirculation behind front tire is also a big drag manager.

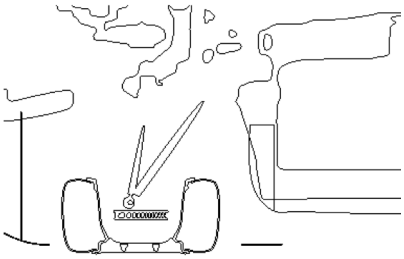

(a) Section geometry

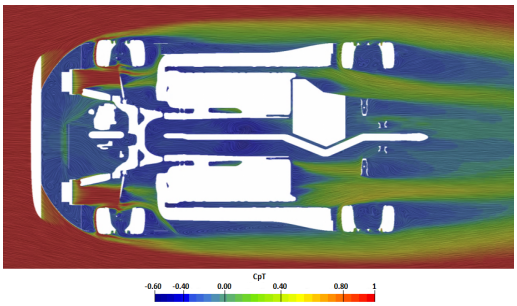

(b) C_PT map @ $Z = -0.02\,m$

Figure 3.45: Baseline configuration FRONT

2) Fender exit separator helps to flow into the bodywork. The recirculation region still present.

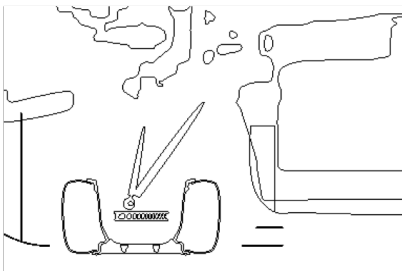

(a) Section geometry

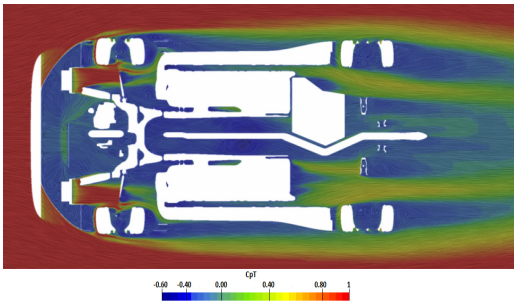

(b) C_PT map @ $Z = -0.02\,m$

Figure 3.46: First configuration FRONT

3) Added gurney is starting to break up recirculation region. This arch exit, according to data obtained by TotalSim, allows to reduce the drag of $22\,N$.

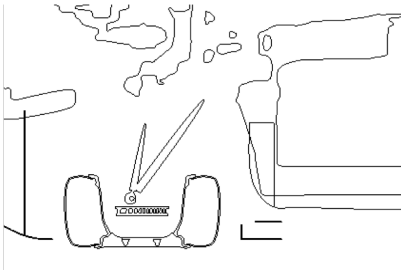

(a) Section geometry

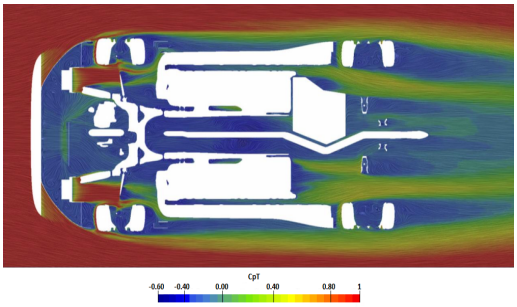

(b) C_PT map @ $Z = -0.02\,m$

Figure 3.47: Second configuration FRONT

4) This configuration allows to accompany the flow along the external body more smoothly, reducing friction also thanks to the breaking of the whirling phenomenon behind

the wheel but it forms a flow exiting through outboard fender channel that eliminates all the improvements of the deviator flap. This contrary flow is due to the depression that is created behind the tire that sucks the air, at greater pressure placed on the outside of the fender.

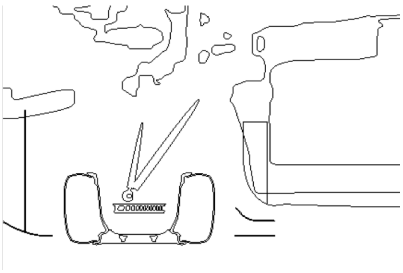

(a) Section geometry

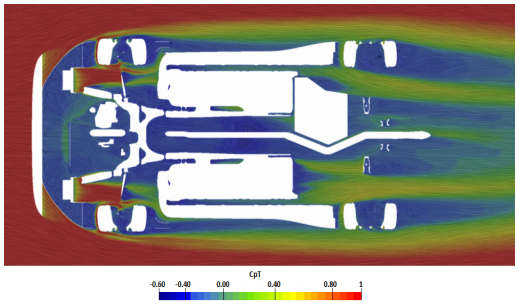

(b) C_PT map @ $Z = -0.02\,m$

Figure 3.48: Third configuration FRONT

5) Even with the addition of the gurney you have a flow exiting through outboard fender channel.

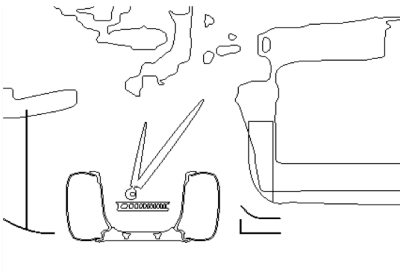

(a) Section geometry

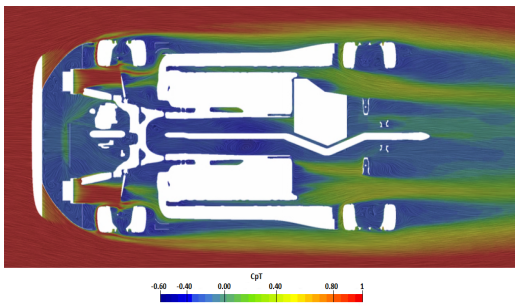

(b) C_PT map @ $Z = -0.02\,m$

Figure 3.49: Fourth configuration FRONT

6) The addition of another wing, without the presence of the gurney, does not positively influence both the generation of recirculation and the birth of the opposite flow.

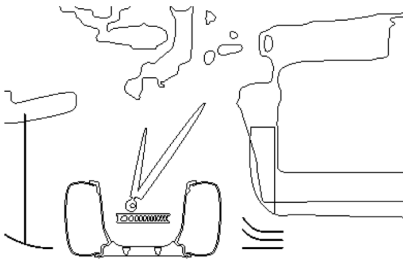

(a) Section geometry

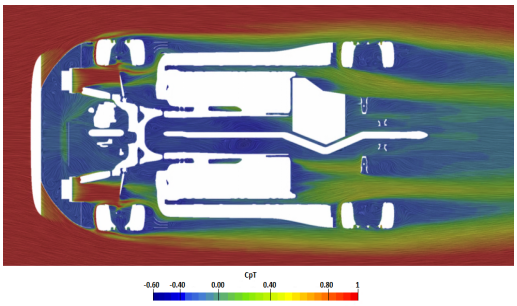

(b) C_PT map @ $Z = -0.02\,m$

Figure 3.50: Fifth configuration FRONT

We have therefore concluded that for this component the presence of the gurney does not help to block such recirculation. Although less effective for the flow in the internal channel, the flat fender exit separator was chosen. Probably the ideal choice would be to consider a fender separator composed of a flat surface to the outside of the car and a curvilinear surface inward, but the advantages would still be reduced to the detriment of achievement and budget.

Similarly to what we saw for the front fender, also for the rear one it is important to analyze the flow coming out from the wheel arches. We consider the following three cases:

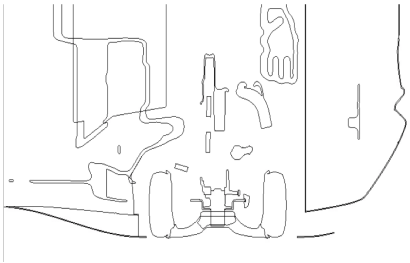

(a) Section geometry

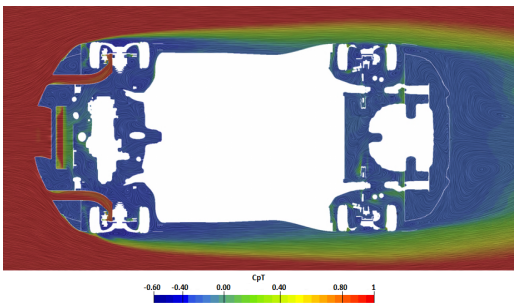

(b) C_PT map @ $Z = 0.18\,m$

Figure 3.51: First configuration REAR

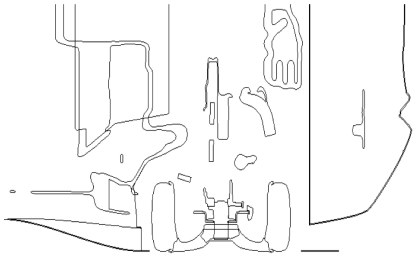

(a) Section geometry

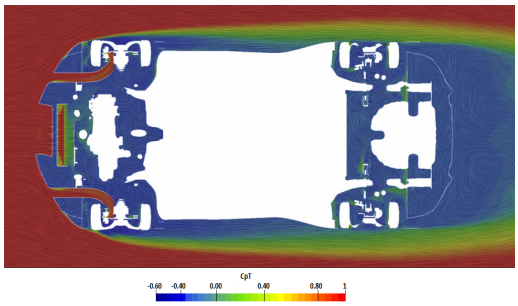

(b) C_PT map @ $Z = 0.18\,m$

Figure 3.52: Second configuration REAR

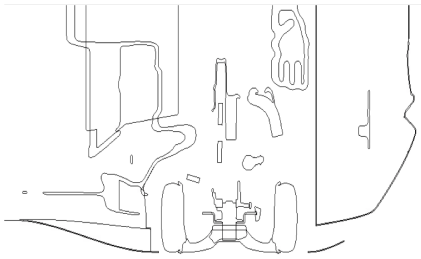

(a) Section geometry

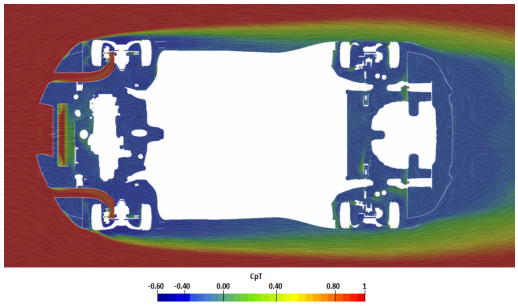

(b) C_PT map @ $Z = 0.18\,m$

Figure 3.53: Third configuration REAR

All these configurations are quite similar from the standpoint of resistance and slightly different from that of the downforce. However, the third case, which is the most performing from the aerodynamic point of view, is not installed in the car because it was responsible for many punctures in previous years' experience during the races. Collisions very often occur in such competitions and this appendix, being fragile and placed in a position of probable contacts, is easily fractured. Often, once broken, it caused the puncture of the tire, irreparably ruining the race. For these reasons it is preferred to use the following configuration in which this appendix is deleted. Despite the very slight aerodynamic losses, there is no longer any risk of running into this damage.

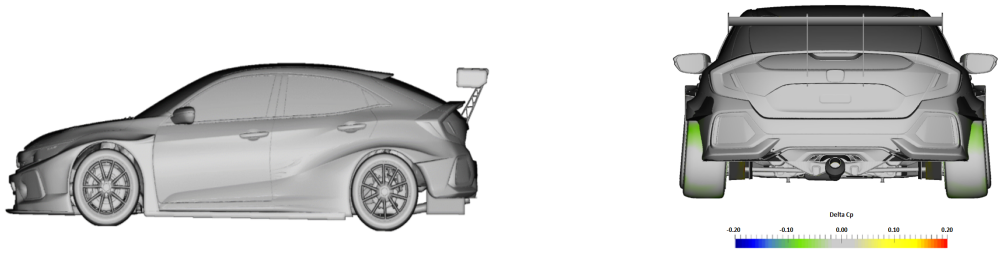

(a) Lateral view

(b) Rear view

Figure 3.54: Final configuration

3.3.4 Trimmed Diffuser and Exhaust Blister

A revised rear diffuser was drawn and the centre section of which extends further forward than before. At the same performance, we use configurations that reduce costs and make the solution practical.

For these reasons we have chosen a rear diffuser that follows the shape of the bumper and allows it to be integrated with the geometry of the latter one in such a way as to make it a single component. In this way the rear bumper also includes the diffuser which otherwise, if they were two separate components would require precise positioning, a particular fixing etc... which would increase costs and decrease practicality. To confirm this, from the map we see very small changes to downforce and drag.

We considered a blister in the diffuser in order to lower the splitter and slightly raise the exhaust (the effects of this change are also negligible, but allow us to play more widely with the height from the ground and therefore is choice also this change).

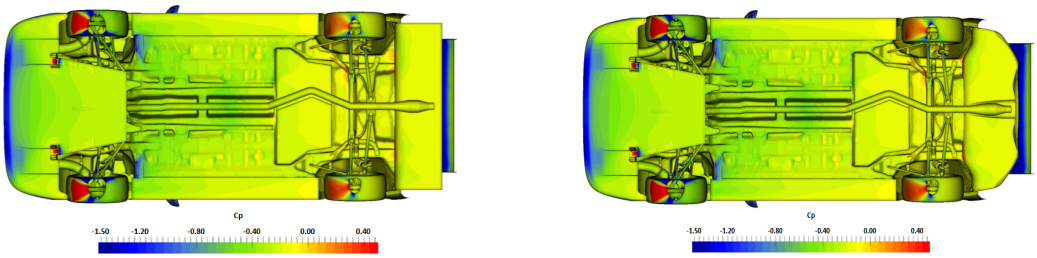

Figure 3.55: C_P maps

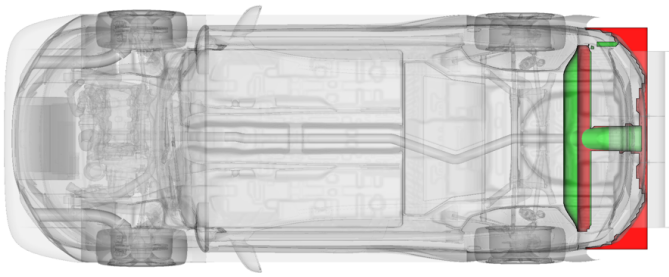

Figure 3.56: Change made on diffuser: RED = old, GREEN = new

3.3.5 Inclined rear diffuser modification

The aerodynamic efficiency must also follow the vehicle dynamics and the rider's feeling. In this case the aerodynamic performance has improved but increasing the downforce in the rear, the car rises to the front and you lose grip in the wheels where there is traction. So it is clear that in this case the increase in downforce has no benefits in performance and causes an imbalance of the load. This problem could be solved by further increasing the downforce at the front, thus recovering the traction in the tires that would adhere to the ground.

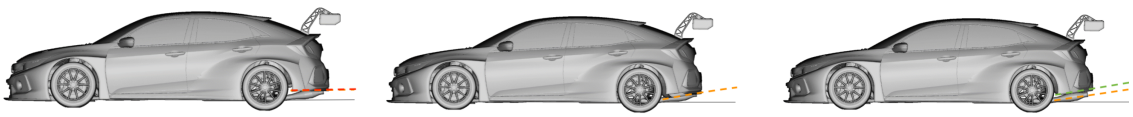

(a) First configuration (b) Second configuration (c) Third configuration

Figure 3.57: Three different configurations for the diffuser

Analyzing in detail the configuration with the inclined splitter we can only deduce that:

- there are two large depression zones around the leading edge of the diffuser, which then generate a large downforce component

- there is some loss in downforce just ahead of the right rear wheel and relatively localised losses from the chassis. As we can see from the Figure 3.59, the flowexpanded either side of the fuel box gets squeezed between the chassis structures creating high pressure and therefore lift.

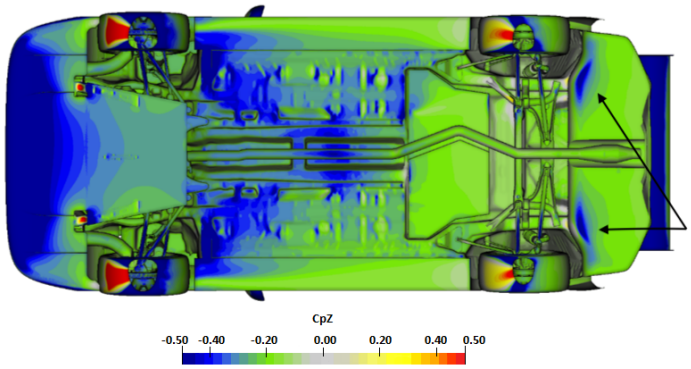

Figure 3.58: C_PT **map**

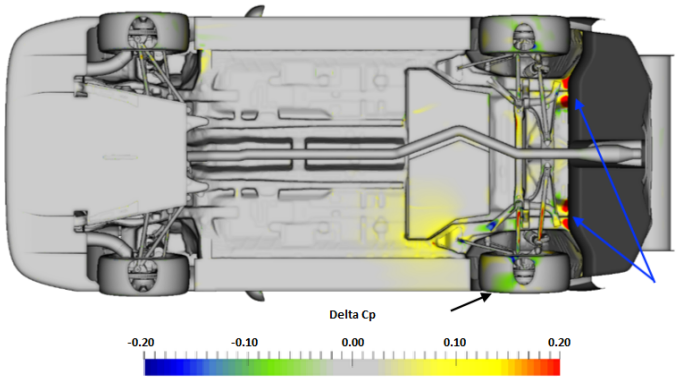

Figure 3.59: ΔC_P **map against baseline**

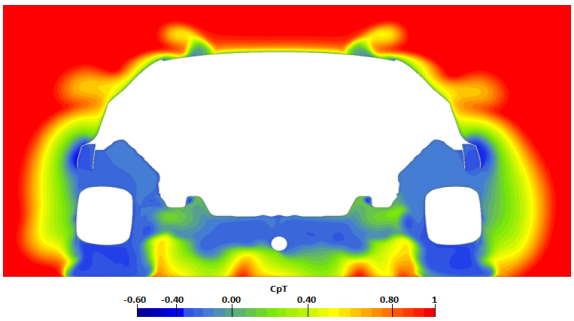

Figure 3.60: C_PT **map @** $X = 2.98\,m$

We have seen the importance of studying the flow in the underbody and the interaction of the latter with the rotary motion of the wheels. For this reason arch strakes are installed.

They slightly reduce the vehicle's resistance and help increase downforce, keeping the flow smoother and less turbulent. These bulkheads, given the low thickness, do not constitute an obstruction for the flow and allow it to be brought to the rear of the car in a more laminar manner. The wheel bulkheads that allow the rotary flow in the archway to be separated from that of the underbody assume great importance.

We see in the following figure the difference between the baseline configuration and the one with the bulkheads as indicated above:

Figure 3.61: Diffuser new configuration comparison

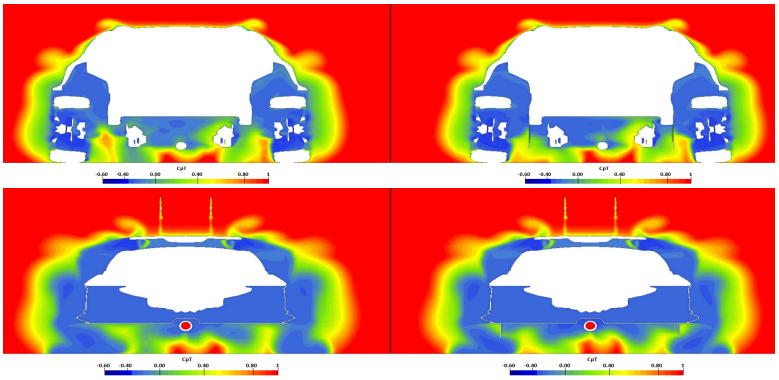

Figure 3.62: C_PT maps @ $X = 2.62$ and $X = 3.42\,m$

3.3.6 Front Archliner

We consider an archliner cover that allows to separate the flow of the engine compartment and the rotating one deriving from the front wheels. From the aerodynamic analysis it can be seen that there are considerable aerodynamic increases. There is an increase of $49\,N$ in total downforce for negligible change in drag. Furthermore, it is important to underline that a small forwards balance shift of 1.1% is also present. For these components that in some way affect the "internal" flow of the car, it is also advisable to study the variations in the flow that involves the radiators. We notice that there is a small reduction in cooling mass flows (less than 1%). A further observation that can be drawn is the majority of downforce increase from the component chassis. The weight of this component is irrelevant because of reduced thickness and of fiberglass, therefore low density.

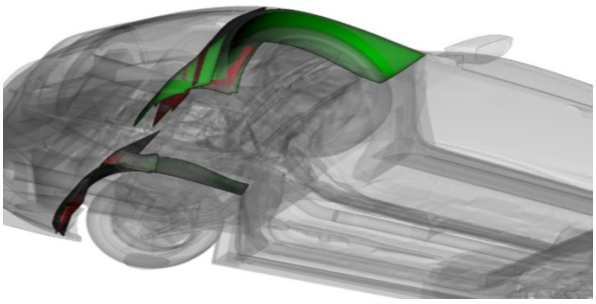

Figure 3.63: Change made on front archliner: RED = old, GREEN = new

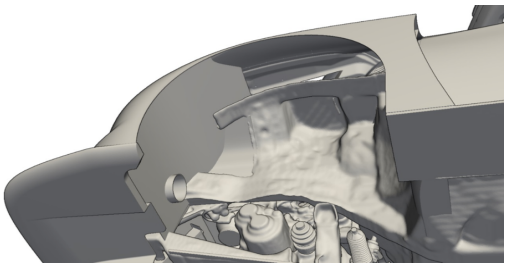

(a) 3D geometry

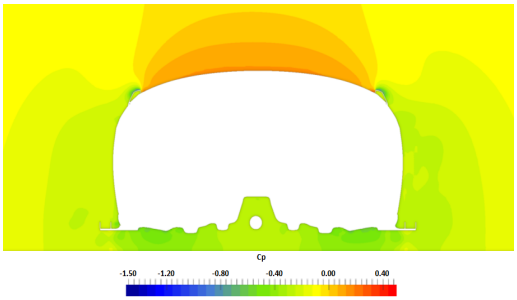

(b) C_P map @ $X = 0.50\,m$

Figure 3.64: Old configuration

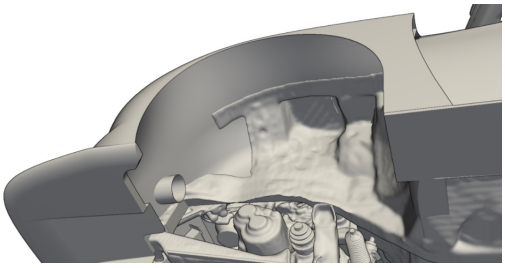

(a) 3D geometry

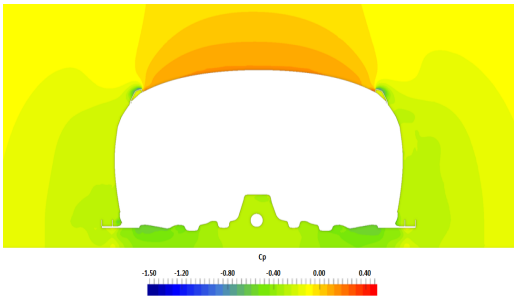

(b) C_P map @ $X = 0.50\,m$

Figure 3.65: New configuration

From CFD maps we notice that there is a greater suction pressures observed on the chassis behind the front wheels. This effect is probably due to the change in separation from the subframe, potentially due to a change in wheel arch pressures. The slightly greater separation from bottom of the back of the arch liner creates lower pressures that it helps front downforce.

3.3.7 Sill

We considered the importance of the flow below the car for the generation of the downforce, which is essential to keep the wheels attached to the asphalt. The tendency, as previously described, is to generate a flow in the underbody that moves at a greater speed than that which surrounds the car above. However, the low pressure in the throat and in the diffuser tends to draw more air from the sides. To obviate this phenomenon it is possible to use lateral bulkheads, commonly called "miniskirts" or "side skirts", able to limit air leakage, which disturbs the pressure pattern of the underbody. Consider different types of side bulkheads that somehow "seal" the flow inside the carriageway from the one outside it.

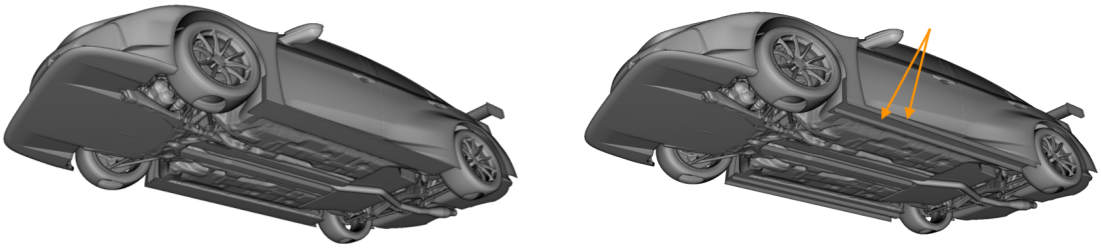

(a) Baseline configuration

(b) New configuration

Figure 3.66: Comparison between the two different configurations

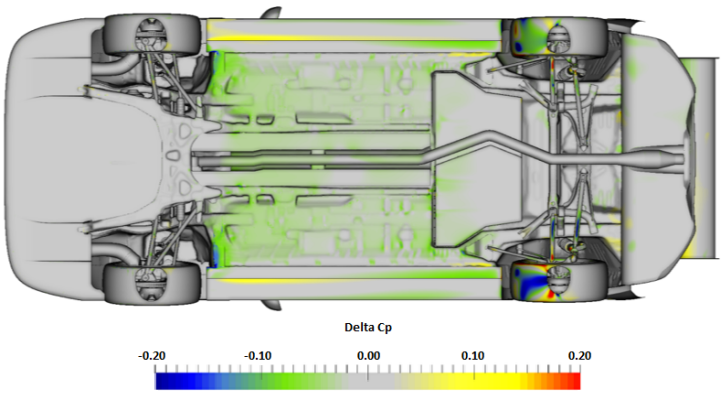

Figure 3.67: ΔC_P between the two configurations

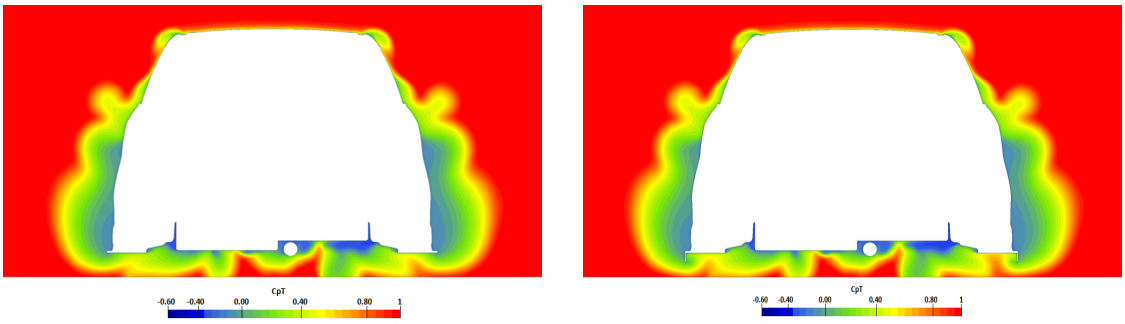

(a) Baseline configuration

(b) New configuration

Figure 3.68: Comparison between C_PT maps on section view @ $X = 2.06\,m$

From the Figure 3.67, we see the difference in the pressure coefficient respect to the baseline configuration. It is clear how the lower pressure flow is "sealed" by the external flow; this depression causes a downforce of $106N$ (6.1%) with a shifted balance of 1.6% rearwards. From the Figure 3.68, we note instead how vortices by the outboard strakes form that pull high energy flow under the sills. However, there is an even better solution that consists of lowering all the sill, so that, in addition to sealing, there is a further ground effect. This configuration allows the increase in the downforce of $156\,N$ (8.9 %), also improving the balance that is shifted 1.3 % to the rear. As we remember, since the front wheel drive tends to decrease the aerodynamic load balance at the rear in favor of the front.

To confirm this, an even more efficient solution would be the generation of a diffuser at the end of the sills, as illustrated in Figure 3.69a. This configuration, however, increases the downforce compared to the "baseline" configuration of $206\,N$ but unbalanced by a 2 % the load at the rear; the best compromise is therefore considered the previous configuration, illustrated in Figure 3.69b.

(a) Sill packer configuration

(b) Sill packer configuration + diffuser

Figure 3.69: Comparison between different sill packet configurations

3.3.8 Rear Wing Assembly

The regulation imposes multiple constraints on aerodynamics, for the reduction of costs. For example, the rear wing, has both airfoil and end plates fixed by WSC. So, given the

uniqueness of the wing for all the cars, the various teams have agreed to make it only produce by Seat so that everyone could reduce costs.

The installation of the side bulkheads help to reduce "bleeding" of air and therefore maintains the pressure difference between the two surfaces of the wing. Without the use of side bulkheads, or 'end plates', the difference in air pressure between the upper and lower surfaces of the wing pushes the air to migrate to the low pressure surface, causing a loss of downforce as well as a drag increase.

Another constraint of the regulation is the maximum height of the various components (therefore of the wing itself) which can not exceed the virtual tangent of the roof. With the modification of the rear wing fixing it was possible to obtain a more elevated wing that from the aerodynamic point of view was less efficient (less vertical load) but with a lower drag resistance. This inefficiency from the point of view of the downforce in the rear of the car allows, as already described in the case of the diffuser, to increase the downforce at the front and therefore to ensure a better grip. All these considerations should be reversed in the case of rear-wheel drive cars. We show an "illegal" example:

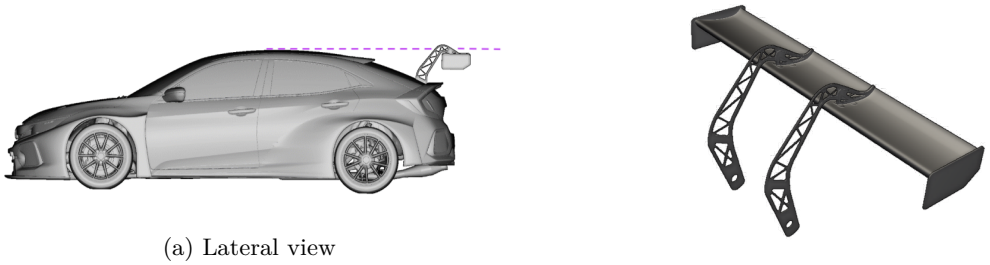

(a) Lateral view

(b) Rear wing

Figure 3.70: Upper brackets configuration

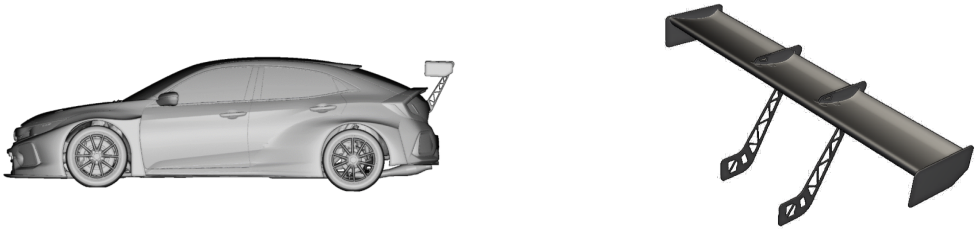

(a) Lateral view

(b) Rear wing

Figure 3.71: Lower brackets configuration

We consider different wing configurations to analyze the efficiency they can generate on the car: in addition to the different inclination of the wing, the coordinate along the x axis is also changed, moving it forward initially at $50\,mm$, following $100\,mm$.

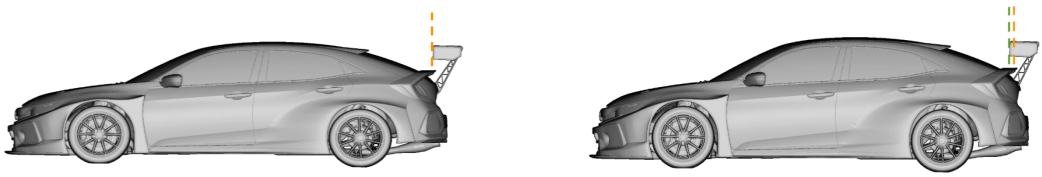

(a) Baseline rear wing (b) Forward rear wing

Figure 3.72: Comparison between the two configurations

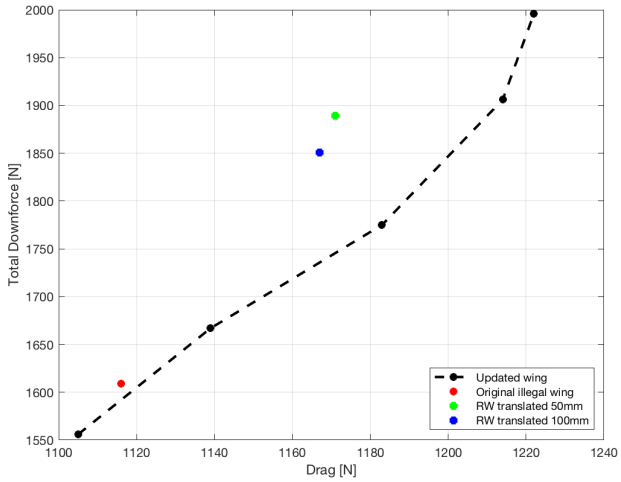

Figure 3.73: Drag & total downforce values for different configurations

RW is showing fairly linear performance through this range. It is difficult to draw any realistic conclusions from the sweep with the fluctation at the front having such a significant effect.

Comparing the downforce and balance values obtained with a translation of 50 mm we obtain:

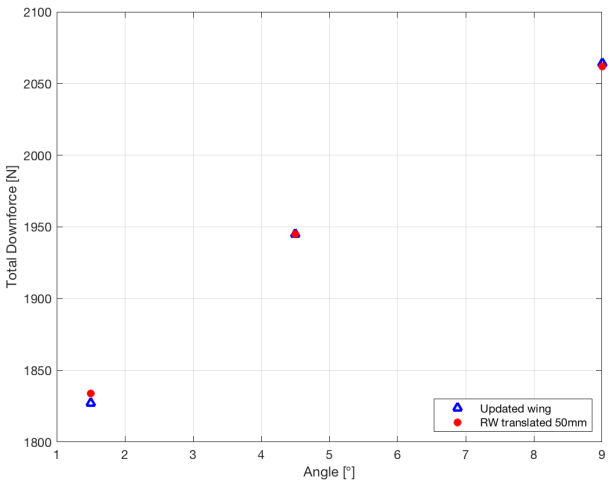

Figure 3.74: Angle & total downforce values for different configurations

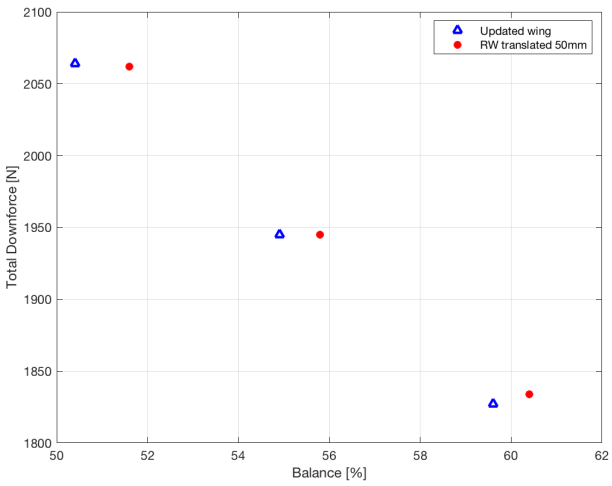

Figure 3.75: Balance & total downforce values for different configurations

The total downforce vs angle is fairly consistent between the two wing positions. The forwards wing position gives a fairly consistence balance shift of $\sim 2\%$.

Chapter 4

Aerodynamics tools and set-up

4.1 Maps

Aerodynamics is a widely used science both in the design phase, to define the car's geometry, and during the championship, where it becomes essential to set up the car, based on the circuit and the performance that we want to achieve. The aerodynamics of the car, once approved, can only be changed by the rear wing adjustment and by the rake, i.e. the difference in heights from the ground between front and rear respecting the regulation that provides for the minimum ride height of $80\,mm$ has to be respected at any time during the event (with the pressure of the tires not less than $1.5\,bars$). It can be very convenient to build maps or tools that allow you to predict the progress of the car and the performance deriving from the modification of the parameters mentioned above. Before the race we can use the data to determine the set up of the car. For the construction of these tools and graphs we used data obtained from the CFD simulations realized by the TotalSim company. Although there is only a more or less accurate simulation, it is essential to understand the trend of some parameters (including the aerodynamic coefficients) due to the variation of the rear wing or the rake and the behavior that the car demonstrates following these changes. Together with the fluid-dynamic maps of the car, which allowed us to define the final geometry of the car, TotalSim provided us with a database containing all the data of the simulations related to the final configuration. It is possible to perform a post-processing analysis of these data by building simple and intuitive graphs that allow us to make the most of them.

***NB**: As mentioned in Chapter 3.2, also in this first part of Chapter 4, all the results and considerations made are based on numerical data and on the maps provided by TotalSim Ltd. So I can not guarantee the correctness of the data supplied to me. My analysis and comments are closely related to these data.*

We consider for the moment the variation of ride height.

4.1.1 Aeromaps

Using the database, importing the experimental data, obtained with three different configurations of the rear wing into the MatLab software, we used the function "meshgrid"

to generate the mesh and "griddata" to interpolate the scattered data in order to produce gridded data. In this way, the mesh assumes certain values in each node and can be graphed using isocurves. The number of map level lines (N) has been defined equal to 25, allowing to display 25 different colors that can be associated to a given value. For the graph $C_{Z,REAR}$ we considered a value of levels equal to $5 * N$ because the values are concentrated on a reduced interval and, therefore, we considered necessary to introduce a more dense discretization to perceive these slight differences. A visualization of 2D maps was preferred because they are more usable compared to a 3D visualization.

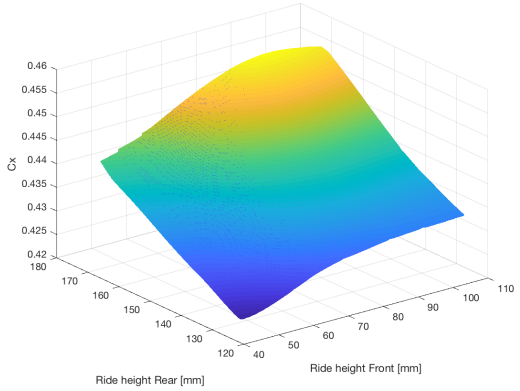

(a) Rear wing angle = 0°

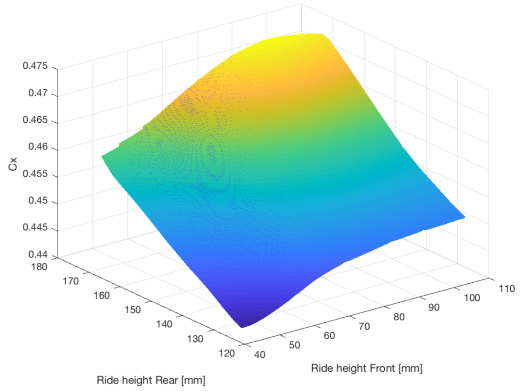

(b) Rear wing angle = 4.5°

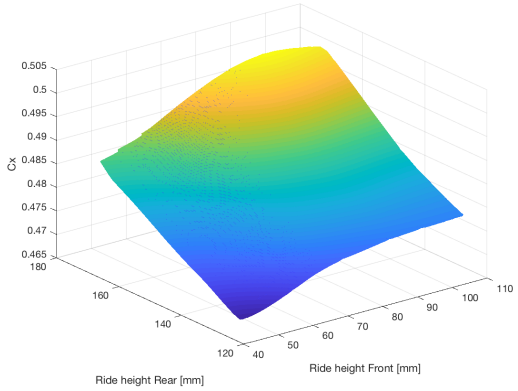

(c) Rear wing angle = 9°

Figure 4.1: Drag coefficient 3D plot for different adjustment of the rear wing

NB: *for the estimation of power, the drag coefficient C_X was increased by 8% based on empirical experience.*

Following are the graphs obtained, grouped according to the different angle of the rear wing (0°, 4.5°, 9°). For each rear wing configuration we will find, in order:

- a graph showing the total coefficient of friction C_X,
- a graph showing the front lift coefficient $C_{Z,FRONT}$,

- a graph showing the rear lift coefficient $C_{Z,REAR}$,
- a graph relating to the ratio between the front lift coefficient and the total one $C_{Z,RIP}\%$,
- a graph relating to the total lift coefficient C_Z,

The trend of the maps relative to the aerodynamic coefficients is easily predictable.

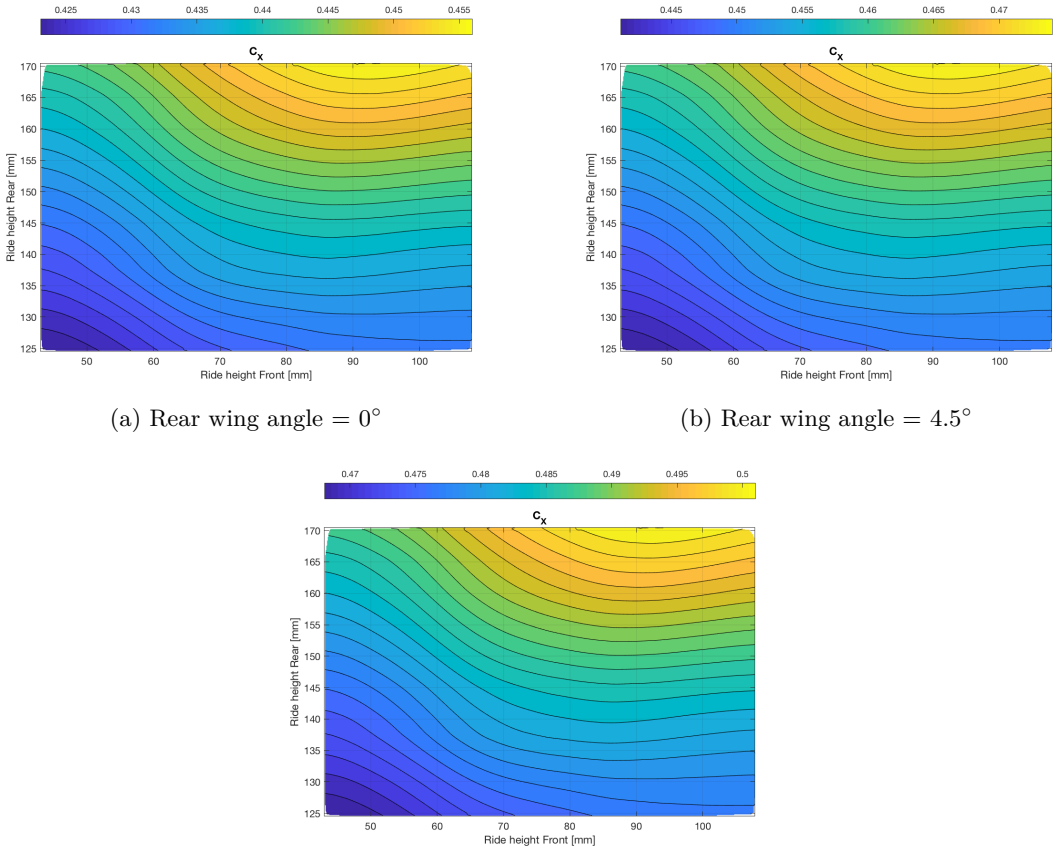

(a) Rear wing angle = 0°

(b) Rear wing angle = 4.5°

(c) Rear wing angle = 9°

Figure 4.2: Drag coefficient map for different adjustment of the rear wing

Regarding the drag coefficient we can make the following observations:

- variations of ride height affect the front surface of the car that interacts with the flow in addition to the flow that flows under the car
- increasing both the ride height to the maximum value the drag is not at the apex this because the front surface is not the maximum surface

- the maximum drag coefficient is achieved when I have a noticeable difference between front and rear and takes place at about a rear ride height of $170\,mm$ and at a front ride height between $85 - 100\,mm$.

- we get the minor drag coefficient when both heights are reduced with the least difference between them

For the lift coefficient, it is very important to analyze the force that is exerted in the front of the car and in the rear, the ratio that identifies this distribution is called aerobalance and will be dealt with later. The main contribution of the downforce is given on the front by the splitter and on the rear by the rear wing. The first one is greatly affected by the height of the car from the ground and the vertical force that it exerts decreases abruptly as the front ride height increases; raising the rear the splitter is more inclined and is more suited to its function. The rear wing instead suffers much less the heights of the car and the map is spread between values very close to each other between 0.18 and 0.32.

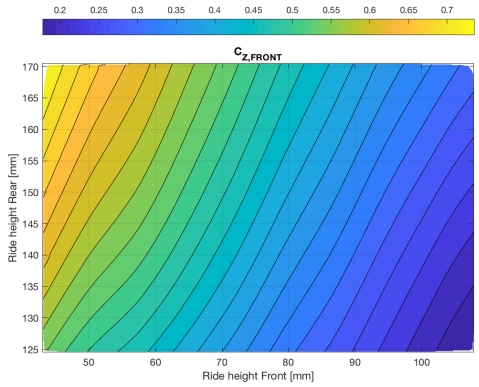

(a) Rear wing angle = 0°

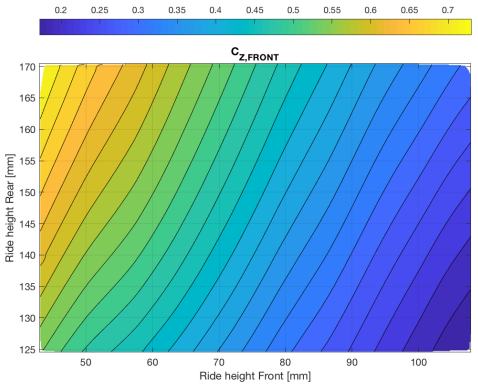

(b) Rear wing angle = 4.5°

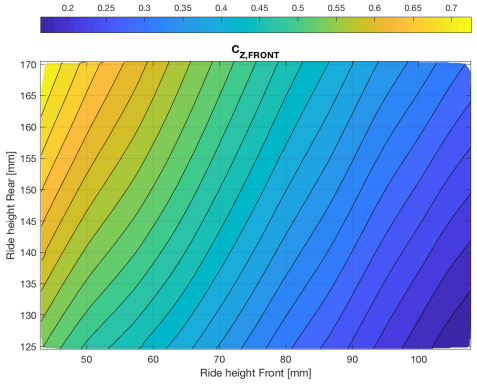

(c) Rear wing angle = 9°

Figure 4.3: Front lift coefficient map for different adjustment of the rear wing

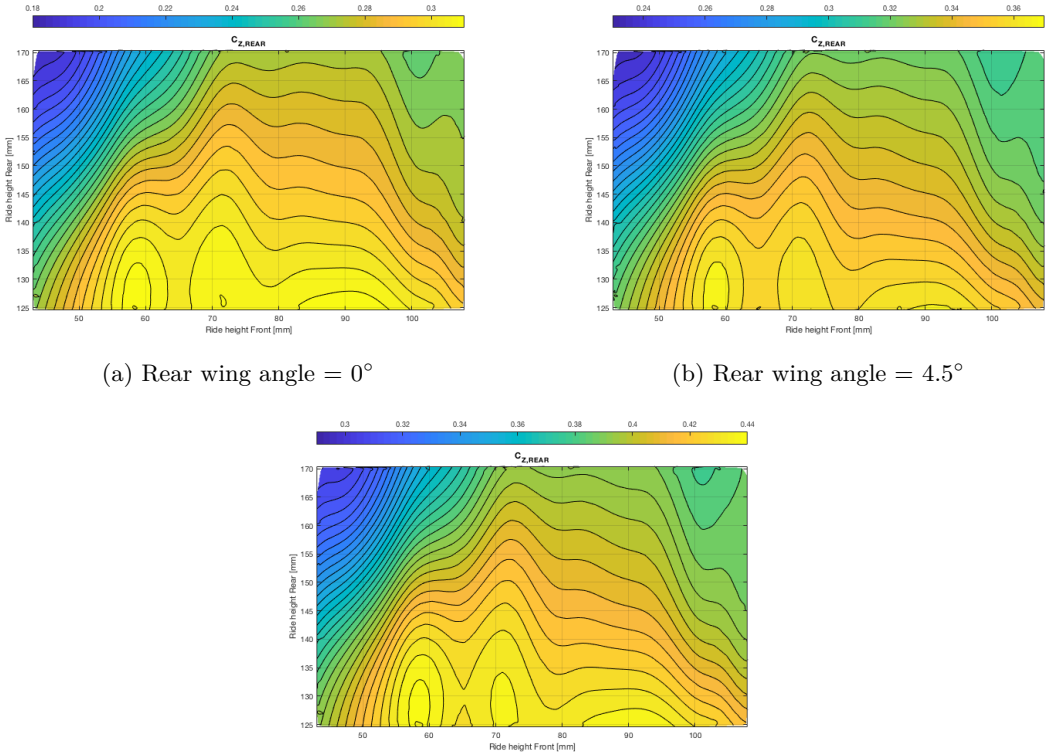

(a) Rear wing angle = 0°

(b) Rear wing angle = 4.5°

(c) Rear wing angle = 9°

Figure 4.4: Rear lift coefficient map for different adjustment of the rear wing

4.1.2 Aerobalance

The aerobalance is defined as a state of equilibrium between the downforce on the front wheels and the downforce on the rear wheels. The aerobalance can also be defined as the Center of Pressure (CoP). As such it's analogous to being the aerodynamic equivalent of Longitudinal Centre of Gravity.

This setting parameter allows the aerodynamic loads to be distributed along the longitudinal axis of the vehicle, modifying the car's behavior on the track: too much pressure at the front causes oversteer, too much at the back understeer.

The downforce is produced largely by the front splitter (fixed) and rear wing (adjustable) so we can alter the cars Centre of Pressure (the aerobalance) mainly by varying the pitch of the car and changing the inclination of the rear wing. But to win the races, the most important thing is to have the overall balance so the driver can feel very comfortable in a manoeuvrable car. Typically the CoP position closely matches that the CoG.

In low to mid speed turns the car needs a slight rear bias to the CoP, this prevents the car suffering corner entry oversteer. Where the car wants to spin as it approaches the apex. Too much front wing in these corners will make the car too pointy and hinder laptimes. In faster turns the front wing can lead the car. The drivers turn in gentler in to fast turns, which creates less lateral acceleration at the rear axle. So it's rare for the

rear to step out on turn-in in to fast corners. Thus, at higher speeds you can have a CoP biased towards neutral or the front.

In the following maps we consider the change in downforce distribution linked to the pitch angle, that is to the adjustment made by varying the height of the front and rear axle.

The behavior of the aerobalance as the ride height changes is very intuitive. By decreasing the front ride height or raising the rear ride height the balance will move to the front, increasing the coefficient $C_{z,rip}$. On the contrary, the trend will be opposite with the shift of the aerodynamic load moved towards the rear. Being a front-wheel drive car, a pressure center located near the engine is preferred.

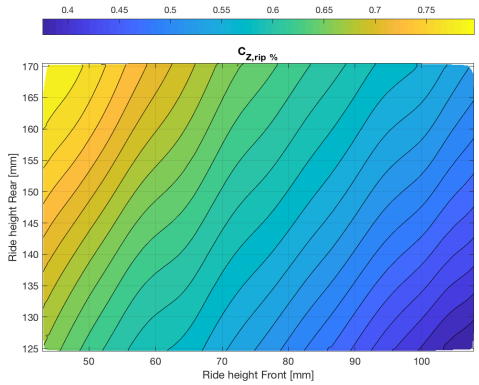

(a) Rear wing angle = 0°

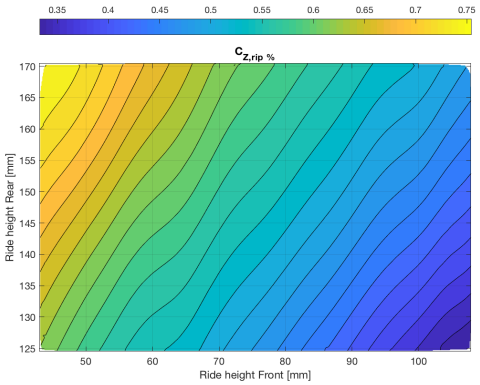

(b) Rear wing angle = 4.5°

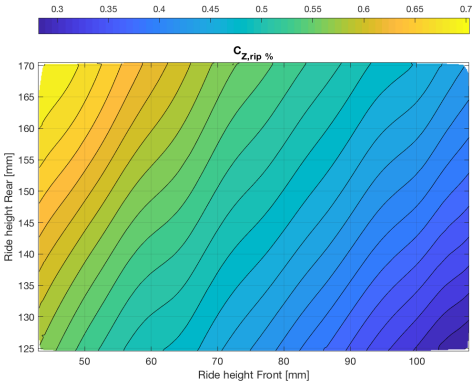

(c) Rear wing angle = 9°

Figure 4.5: Aerobalance map for different adjustment of the rear wing

We now evaluate the variation of the inclination of the rear wing.

4.1.3 Rear Wing set-up

As mentioned before, in addition to the variation of the rake of the car, a fundamental device that contributes to the realization of the optimal set-up is the rear wing. We report

the geometry of the wing.

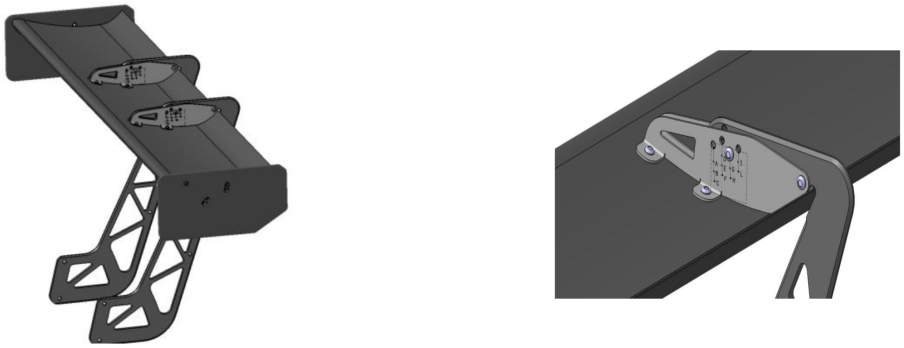

Figure 4.6: Rear wing adjustment geometry

It is possible to adjust the inclination of the wing in the different positions, shown in the figure, through the coincidence of the letters between plate and pylon. The plate is fixed to the wing.

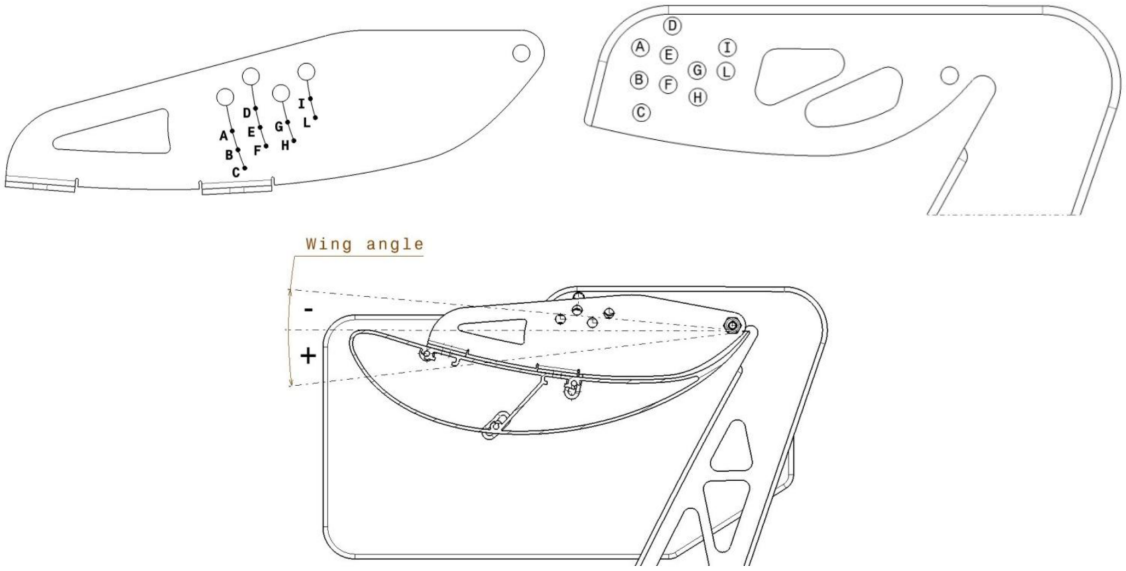

Figure 4.7: Rear wing adjustment scheme

We report the correspondence between letters and inclination of the wing. The letters are used because, in addition to being more intuitive, the value of the degrees risks mess and create misunderstanding with the angle of the car, due to the rake.

Table 4.1: Rear wing setup

Wing Letter	Wing Angle
A	−3°
B	3°
C	9°
D	−4.5°
E	1.5°
F	7.5°
G	0°
H	6°
I	−1.5°
L	4.5°

By reporting on the graphs the values obtained by TotalSim, we can obtain:

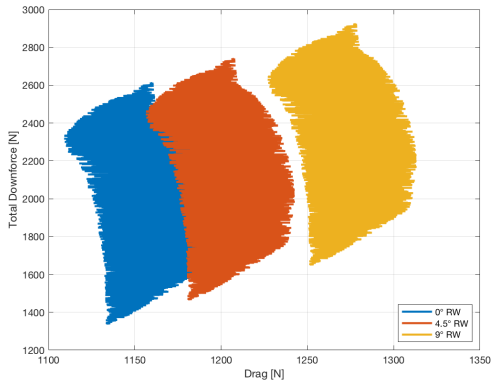

(a) Drag - Total downforce map

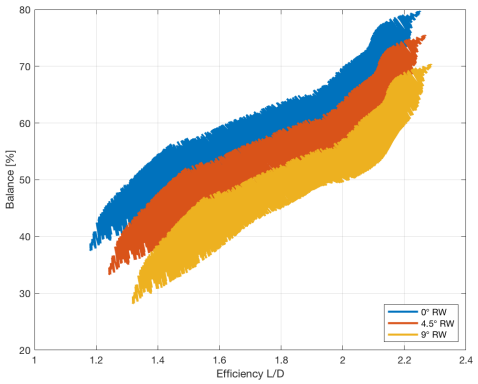

(b) Balance - Efficiency map

Figure 4.8: Characteristic maps for rear wing configurations

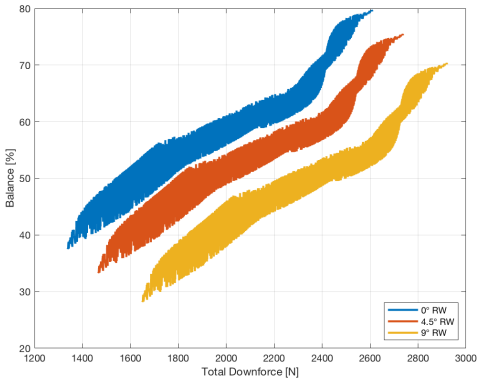

(a) Total downforce - Balance map

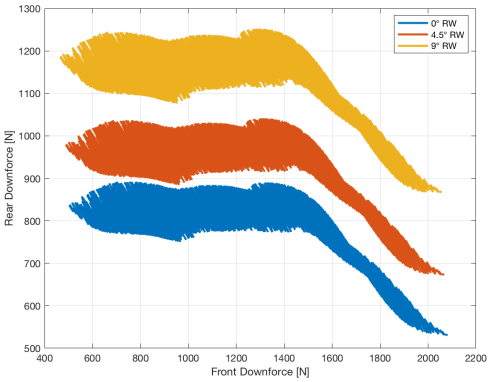

(b) Front downforce - Rear downforce map

Figure 4.9: Characteristic maps for rear wing configurations

Through a MatLab script it is possible to set values that delimit the ride height and the balance. Then comes a data reduction in which the values that do not respect these three ranges, imposed by the user, are excluded. Assigned the maximum and minimum values within which we can vary the set-up, it is clear the performance values to which we can aspire and the area within which it is possible to play through the adjustment of the aerodynamic devices.

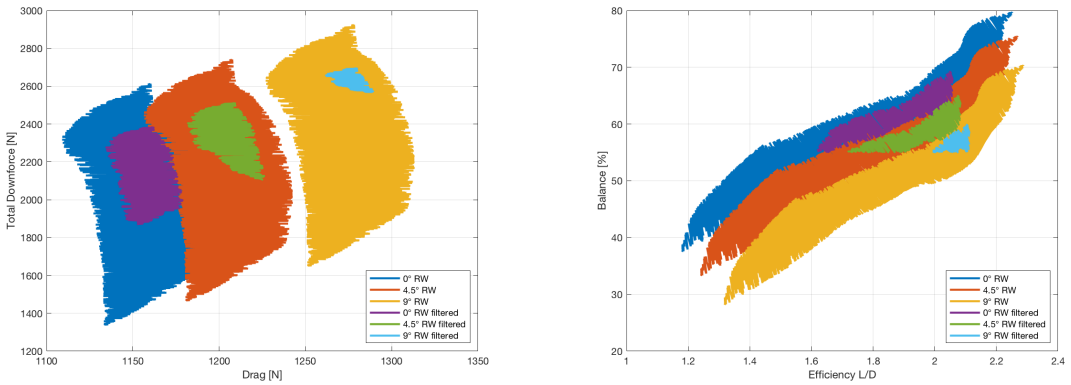

(a) Drag - Total downforce map

(b) Balance - Efficiency map

Figure 4.10: Filtered areas in characteristic maps

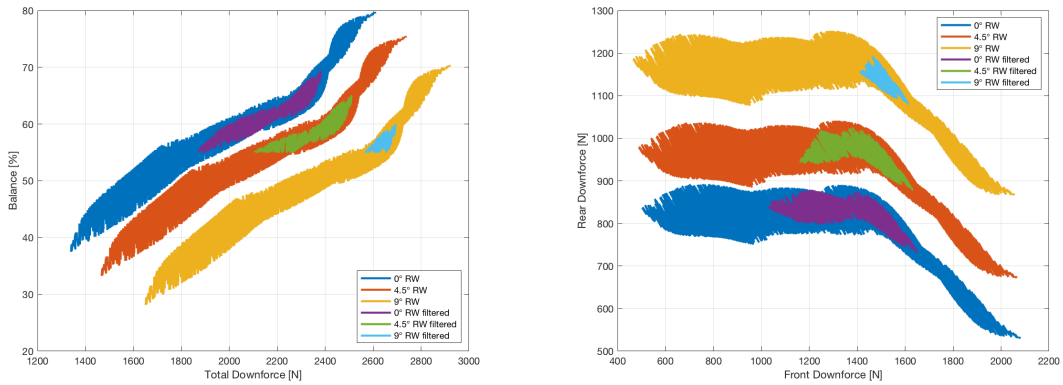

(a) Total downforce - Balance map

(b) Front downforce - Rear downforce map

Figure 4.11: Filtered areas in characteristic maps

The data available to optimize costs are only for the slope values of 0°, 4.5° and 9°; however, if the data are regressed it is possible to extrapolate the intermediate inclinations, noting how the evolution of the aerodynamic parameters when the rear wing position changes is almost linear.

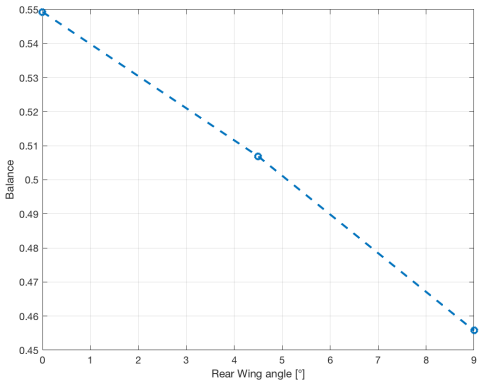

(a) Balance trend

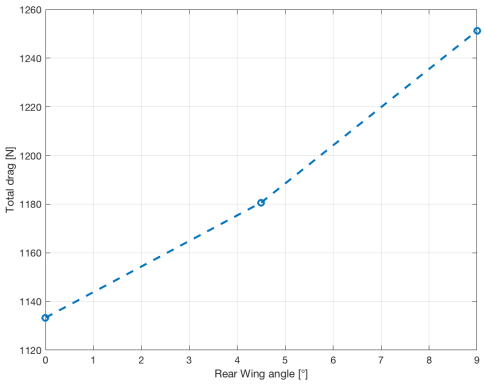

(b) Total drag trend

Figure 4.12: Rear wing adjustment trend

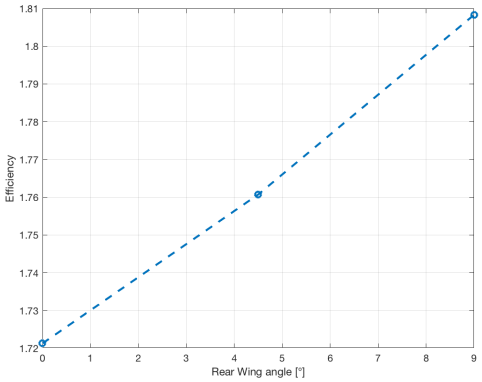

(a) Efficiency trend

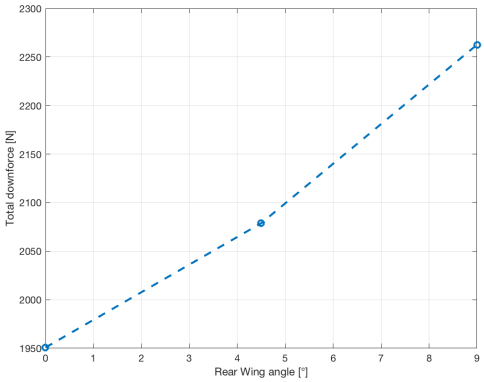

(b) Total downforce trend

Figure 4.13: Rear wing adjustment trend

This linear trend allows to easily predict and extrapolate the values of downforce and drag as the ride heights vary. Through the function given by the regression line it is possible to obtain aerodynamic maps for any value of inclination of the wing. For example, we show the maps for a value of 6°.

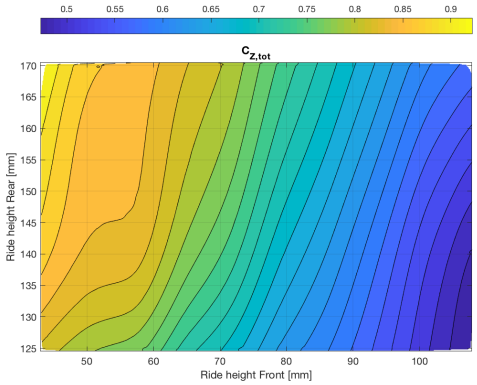

(a) Downforce coefficient for a rear wing angle = 6°

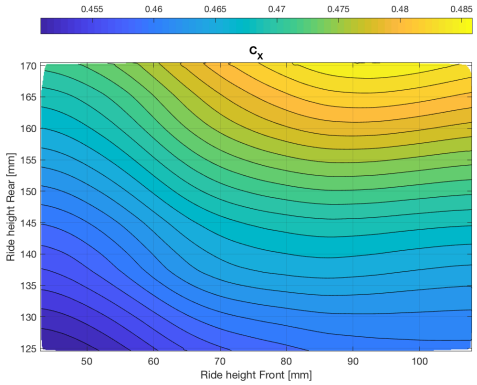

(b) Drag coefficient for a rear wing angle = 6°

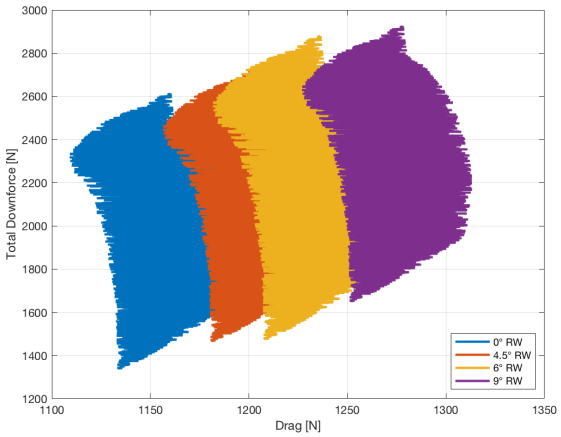

(c) Drag - Total downforce map

Figure 4.14: Data obtained with interpolation of experimental data

All the previous analyzes, with the relative approximations and taking into account the accuracy of the results studied, are appropriate in motorsport and in this championship because, as we have repeated, it is interesting to study a qualitative and indicative trend of the analyzed parameters.

4.1.4 Powermaps

Similarly to what has been seen for the aeromappe concerning the pressure coefficients, it can also be done for the power required by the car to overcome the resistance coefficient.

Importing the experimental data, obtained with three different configurations of the rear wing into the MatLab software, we calculated the power from the drag coefficient C_X at a speed of 255 km/h (70.83 m/s). Following are the graphs obtained, grouped according to the different angle of the rear wing (0°, 4.5°, 9°). For each rear wing configuration we will find, in order:

- a graph showing the power spent in CV,
- a graph showing the power spent in HP,
- a graph showing the power spent in $Watt$,

As we note, the power has the same trend as the drag coefficient. It is precisely calculated in Watt starting from this coefficient through the formula:

$$P_W = 1.08\, C_x \cdot v^3 \cdot (\frac{1}{2} S \cdot \rho) \tag{4.1}$$

Where with the 1.08 coefficient is considered the increase of the 8% of drag coefficient due to empirical evaluations. Through some coefficients it is possible to transform the power into horses (defined in two different ways: "European" CV and "British" HP), a unit much more used in the motorsport field.

$$P_{CV} = 0.00136 \cdot P_W \qquad P_{HP} = 0.00134 \cdot P_W \tag{4.2}$$

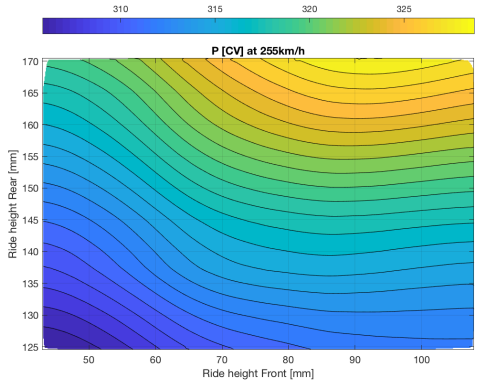

(a) Rear wing angle = 0°

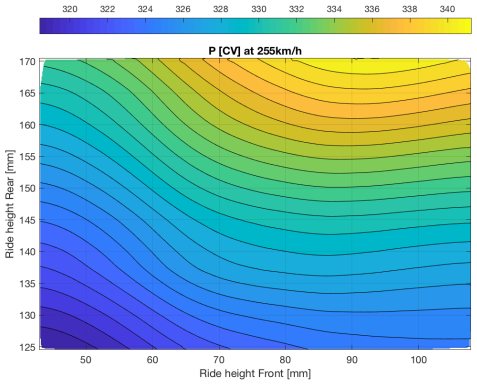

(b) Rear wing angle = 4.5°

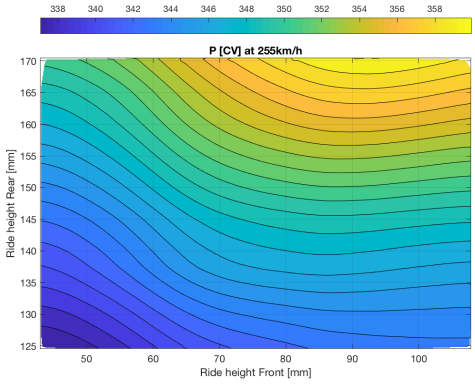

(c) Rear wing angle = 9°

Figure 4.15: Power map [CV] for different adjustment of the rear wing

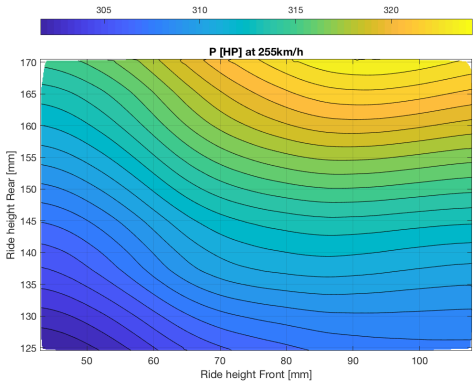

(a) Rear wing angle = 0°

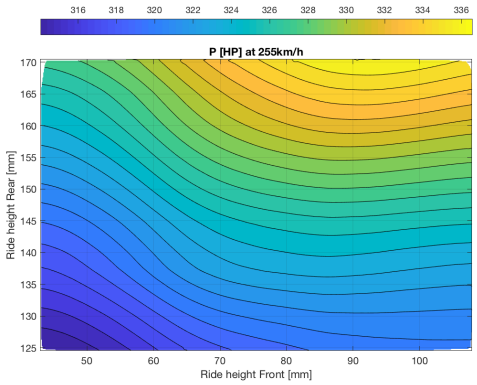

(b) Rear wing angle = 4.5°

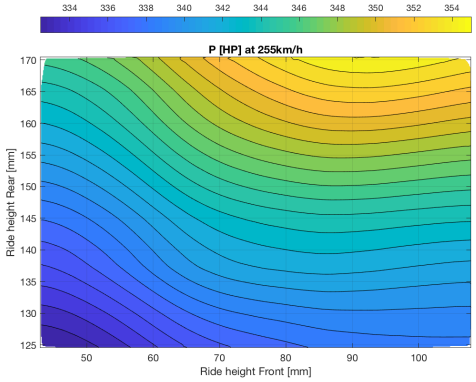

(c) Rear wing angle = 9°

Figure 4.16: Power map [HP] for different adjustment of the rear wing

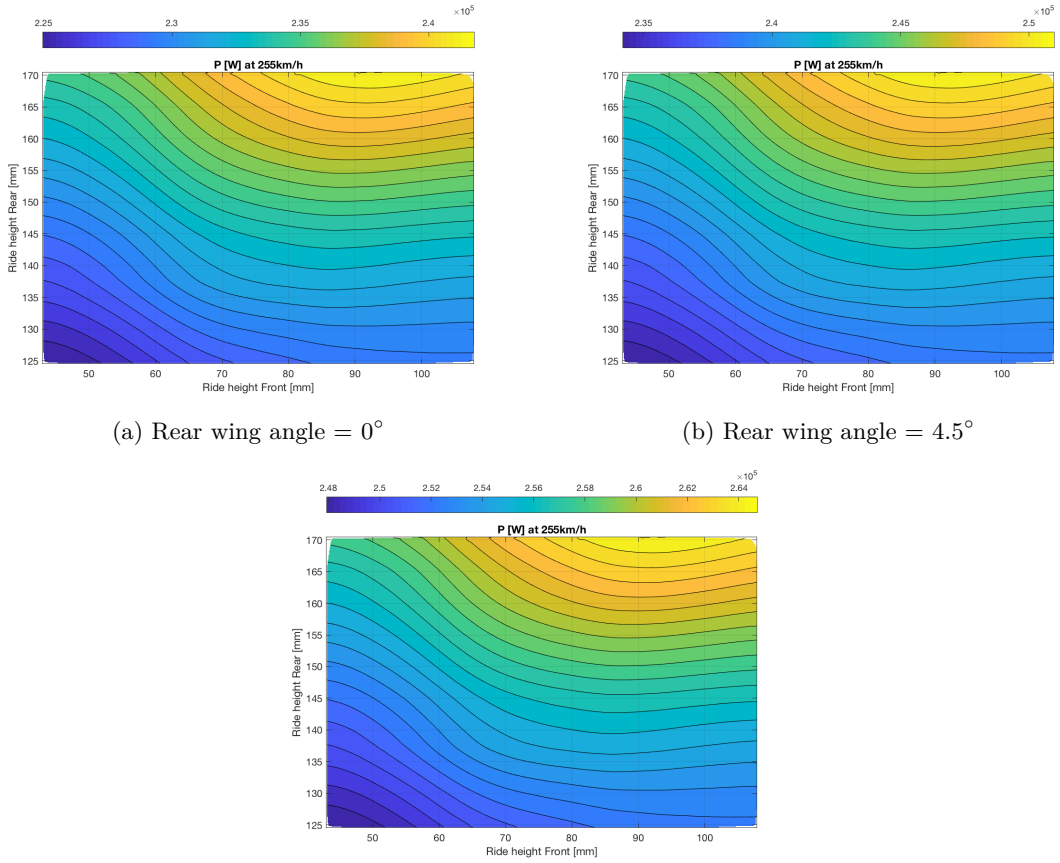

(a) Rear wing angle = 0°

(b) Rear wing angle = 4.5°

(c) Rear wing angle = 9°

Figure 4.17: Power map [W] for different adjustment of the rear wing

4.2 LapSim

4.2.1 Introduction to software

LapSim is a software developed by Bosch that allows you to simulate the time-lapse of a car with the ability to manage many parameters and to consider the conditions that most resemble the real model of the car. It is a very widespread software and used in motorsport as it's a fast, comprehensive and easy simulation package for racing activities. Before testing the modification of some parameters on the track, it is useful to check their impact through this software in order to analyze the importance of this change with regard to lap time. This parameter is in fact the most important in the world of motorsport; the races are won running faster than the others and only the one with the best times arrives victorious at the finish line.

The software, as in general each simulation software in each field, will have its order of accuracy and lap times, although similar will not be those obtained during the competition especially considering an "impossible" factor to be simulated that is the capacity of

the driver and his feeling; however, an indication of the improvement or deterioration of performance and an indication of how great is the consistency of these trends, is essential to analyze the direction in which to act. The importance of analyzing lap time before the competition makes it possible to obtain advantages in many ways: as described above (Chapter 1.1.1) the free tests, carried out the day before the competitions, last only 30 minutes and, therefore, it is necessary to have clear ideas on what test and setup on the car to optimize the time allowed and intelligently evaluate the most appropriate changes to be made to better deal with the race the following day.

By concentrating ideas in certain directions, based on the results obtained from the software, we can save both in terms of costs and in terms of time. As for the CFD, or for any simulation software, understand before experimenting in the field in which direction to move, it saves the money of fuel, track hire, transport, technicians and of course the time to conduct the tests. The speed and the ability to conduct such simulations comfortably seated in the office are the main features of this instrument. Whenever you want to conduct the experimental study on a new setup of the car, or on a new circuit, you need to modify the car in the workshop and take it to the appropriate circuit to test it. The numerical investigation only requires the realization of a new model which, for how many parameters we want to modify, will require extremely shorter time than those of the experimental investigation.

This allows a better understanding of the phenomenon under study and offers the designer an effective tool for finding better design choices. LapSim or similar software now appears to have become a mature and increasingly indispensable tool for the development of tests that are able to compete on the market in terms of quality.

LapSim is divided into two macro-tools:

LapSim Chassis

It's analysis tool as well as a vehicle simulation program. By further processing the on-car recorded data, using the simulation models, a much more profound analysis of the vehicle behavior can be gained. The visualization of the vehicle behavior creates a much easier and better understanding of the influence of several vehicle parameters on the performance.

It's possible to set masses parameters as weight distribution and mass moment of inertia, lengths parameters as wheelbase, track width and center of gravity, aerodynamics parameters as drag, lift, influence of wings, splitter, diffusor and aerodynamic maps; it's also possible to adjust brakes, springs, shocks, suspension, tires (Pacejka model), steering, differential and gearbox settings.

LapSim Engine

It supplies an easy to use engine simulation package capable of generating a torque/power and a corresponding ignition curves out of the main parameters of an engine. The model is able to simulate any 4-stroke spark ignition race engine currently seen on the market, with or without air restrictor(s). To summarize, the engine software is aiming for 95%

because avoids a vast number of variables in order to define every engine detail, in order to improve usability as well as computational performance.

It's possible to set the engine curves (power, torque, rev limiter), poppet valves, camshafts, intake dynamics (pressure in cylinder, airflows over valves, spring mass system), ignition and many other settings. It's also possible to consider an hybrid model.

Circuit

To obtain an accurate simulation it is very important to consider also the characteristics of the circuit. In addition to the GPS map, aspects such as the grip (which allows you to describe some external environmental conditions) and the slopes of the circuit are also fundamental.

So we can add banking, grip of the track, globally as well as specific areas of the track, we can set driving line of the track, specifying the position of identified corners with their minimum radius points, we can specify height points to the track layout and add wind influences to the vehicle.

With these settings we can analyze lateral acceleration of the vehicle will lead to addition vertical load on the tires due to banking and additional longitudinal resistance due to height differences, compare lines of the several individual laps and consider how wind speed influences the aerodynamic forces of the vehicle.

4.2.2 Data Analysis

- Post processing of the on-car recorded data with simulation models. Calculating vehicle handling state, aerodynamics, differential function, etc.
- Determination of tire parameters out of on-car recorded data. Possibility to analyze tire performance over the laps.
- Direct comparison between several outings and/or simulation model.
- 3D Animation of vehicle behavior for a better and more thorough understanding.
- By comparing recorded data with simulation data a validation possibility of vehicle parameters and vehicle functioning is made.
- LapSim software adds all vehicle parameters to WinDarab Files and creates automatic database. [**14**]

We discuss about the results obtained with the simulation done with the LapSim (Bosch) software. For each racetrack of the anticipated WTCR calendar (Chapter 1.1.1) and also for every other race circuit of which data was available at the moment of this writing, multiple simulation run have been carried out. Some of them are used to compare chassis items effects on laptime (max power, weight), while most of the runs are to identify sensitivity per each race track to drag and downforce. Complicate items have to be taken into more sophisticated softwares, but simpler considerations are easily taken from here.

All the tracks are shown and described very briefly in the appendix in order to have a visual impression of the characteristics of the tracks. This allows us to better understand the influence that the changes made on the car have on the laptime.

Base setup

The base setup that has been used as a reference is synthetized in the next tables shown in Figure 4.18. Of course this software uses a simplified model, but this allows us to perform quick and decently accurate simulations that are more then enough for what we are analyzing here.

Chassis		
Total weight	[kg]	1305
Weight Distribution	[%]	62.5
Wheelbase	[mm]	2700
Front track	[mm]	1715
Rear track	[mm]	1670
C.o.g. height	[mm]	473
Front Ride Height	[mm]	83
Rear Ride Height	[mm]	149
Front Motion Ratio	[-]	0.9
Rear Motion Ratio	[-]	1.0
Front main spring stiffness	[N/mm]	80
Rear main spring stiffness	[N/mm]	70
Front ARB stiffness @ ground	[N/mm]	70
Rear ARB stiffness @ ground	[N/mm]	30
Front tyre grip	[-]	1.5
Rear tyre grip	[-]	1.5

Aerodynamics		
Frontal aerea	[m^2]	2.35
Cx	[-]	0.409
Czf	[-]	0.453
Czr	[-]	0.296

Engine	
Speed [rpm]	Torque [Nm]
7000	354.7
6500	380.2
6000	409.7
5500	413.9
5000	414.6
4500	415.2
4000	412.5
3500	419.1
3000	411.9

Drivetrain	
I gear	12 / 28
II gear	13 / 23
III gear	16 / 23
IV gear	21 / 25
V gear	22 / 23
VI gear	26 / 24
F.D.	414.6

Figure 4.18: Base setup parameters

Starting from the base model, various parameters have been modified.

Center of gravity

The performances deriving from the lowering of the center of gravity are exalted in the circuits with frequent curves both slow and fast. Indeed, this effect makes the car more stable during braking and cornering due to greater grip. It's therefore interesting when the lateral accelerations g are involved.

				24mm C.o.G less (5%)
km	Circuit	Δtime [s]	Ranked	Δtime avg [s/km]
2971	Marrakech	0,01	Vila Real	-0,040
4381	Hungaroring	-0,11	Suzuka	-0,036
25378	Nurburgring	-0,48	Slovakiaring	-0,032
4307	Zandvoort	-0,05	Shanghai	-0,030
4775	Vila Real	-0,19	Chang	-0,029
4806	Termas de Rio Hondo	-0,12	Barcellona	-0,028
4023	Ningbo	-0,09	Losail	-0,026
5807	Suzuka	-0,21	Paul Richard	-0,026
6120	Macau	-0,15	Macau	-0,025
5793	Monza	-0,08	Termas de Rio Hondo	-0,025
4005	Valencia	-0,10	Hungaroring	-0,025
5344	Aragon	-0,10	Valencia	-0,025
4655	Barcellona	-0,13	Ningbo	-0,022
5922	Slovakiaring	-0,19	Aragon	-0,019
3841	Paul Ricard	-0,10	Nurburgring	-0,019
4603	Shanghai	-0,14	Monza	-0,014
5380	Losail	-0,14	Zandvoort	-0,012
4554	Chang	-0,13	Marrakech	0,003

Figure 4.19: Δ time for every circuit due to CoG variation

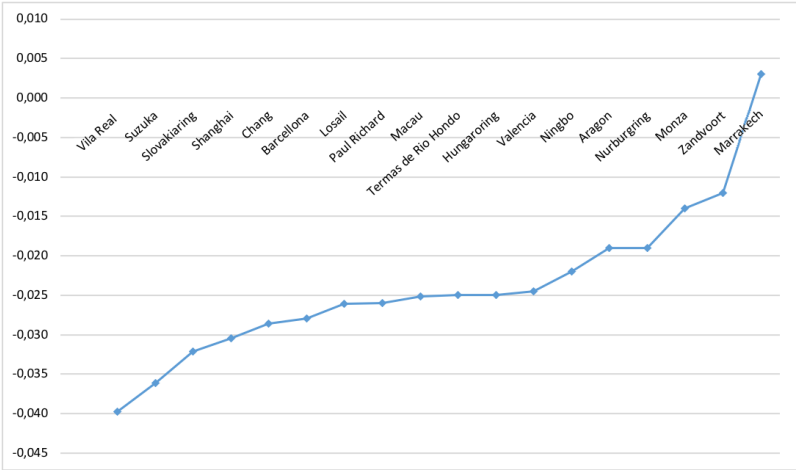

Figure 4.20: Total Δ time for every circuit due to CoG variation

In circuits like Monza, very fast with long straights and in street-circuits like Marrakesh in which there are close variants and sudden changes of direction, the time in which the car is subjected to lateral accelerations is reduced and the influence on lap time when changing the height of the center of gravity becomes more negligible.

In the Marrakesh circuit, the increase in lap time is probably a spurious effect. If the distribution of the brakes is mainly shifted to the front, lowering the center of gravity involves shifting the weight towards the rear of the car, reducing the efficiency of the braking and thus causing a loss of lap time. The presence of frequent braking therefore contrasts the positive effect due to the decrease of 5% of the height of the C.o.G.

In order to compare the circuits, the variations on the lap time is averaged on the length of the circuit in such a way that the values represented are the Δt lost or earned each kilometer. Considering the length of the Nurburgring circuit of about $25\,km$, we can

clearly see how each small change to km is multiplied, making the effect of the modification much more significant.

10 hp less

It is important to analyze how much the power of the engine influences a track, to understand on which aspects it is better to concentrate to prepare a race weekend. From the baseline of 353 hp, we went down to 343 hp that in these days appeared to be another feasible option to run in the championship.

				10hp less (2.8%)
km	Circuit	Δtime [s]	Ranked	Δtime avg [s/km]
2971	Marrakech	0,29	Ningbo	0,060
4381	Hungaroring	0,34	Shanghai	0,072
25378	Nurburgring	2,14	Barcellona	0,075
4307	Zandvoort	0,33	Zandvoort	0,077
4775	Vila Real	0,39	Chang	0,077
4806	Termas de Rio Hondo	0,39	Valencia	0,077
4023	Ningbo	0,24	Hungaroring	0,078
5807	Suzuka	0,52	Losail	0,078
6120	Macau	0,56	Paul Ricard	0,081
5793	Monza	0,65	Termas de Rio Hondo	0,081
4005	Valencia	0,31	Vila Real	0,082
5344	Aragon	0,48	Slovakiaring	0,083
4655	Barcellona	0,35	Nurburgring	0,084
5922	Slovakiaring	0,49	Suzuka	0,090
3841	Paul Ricard	0,31	Aragon	0,090
4603	Shanghai	0,33	Macau	0,092
5380	Losail	0,42	Marrakech	0,098
4554	Chang	0,35	Monza	0,112

Figure 4.21: Δ time for every circuit due to HP variation

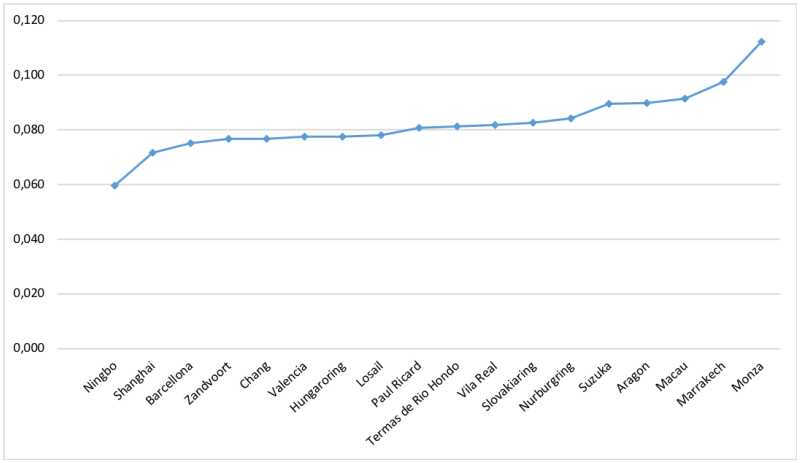

Figure 4.22: Total Δ time for every circuit due to HP variation

As we expected engine is fundamental in Monza, but it is good to know that two race tracks that share similar aero characteristics (as we will see), like Ningbo and Marrakech, have such a different sensitivity to power.

There are circuits called "traction limited" instead of "power limited" where the limit of travel is given by the grip of the wheels on the asphalt and not by the HP; therefore in these last circuits the power reduction has a reduced influence compared to circuits characterized by long straights in which the motor takes on a fundamental aspect.

5 % less weight

This will be the most used table since weight is one of the most used tool for the organizator to balance performance. From here it is quite clear that $10\,kg$ weight very differently from Ningbo to Monza.

The influence of the weight is particularly evident in circuits in which there are frequent restarts from a standstill and where very exploits the acceleration phase. This is the characteristic of slow circuits like Ningbo and Marrakech. Another circuit in which the inertia due to the weight of the car is decisive for the lap time is Zandvoort in which there are uphill sections runs at low speeds.

				5% less weight (-65kg)		
km	Circuit	Δtime [s]	Ranked	Δtime avg [s/km]		[s]
2971	Marrakech	-0,70	Ningbo	-0,239	each 10kg	-0,148
4381	Hungaroring	-0,92	Marrakech	-0,236		-0,108
25378	Nurburgring	-4,49	Zandvoort	-0,232		-0,154
4307	Zandvoort	-1,00	Paul Ricard	-0,219		-0,129
4775	Vila Real	-1,00	Valencia	-0,212		-0,131
4806	Termas de Rio Hondo	-0,99	Hungaroring	-0,210		-0,142
4023	Ningbo	-0,96	Vila Real	-0,209		-0,154
5807	Suzuka	-1,12	Macau	-0,208		-0,195
6120	Macau	-1,27	Termas de Rio Hondo	-0,206		-0,152
5793	Monza 6th long	-1,05	Barcellona	-0,204		-0,146
4005	Valencia	-0,85	Shanghai	-0,200		-0,142
5344	Aragon	-1,02	Chang	-0,193		-0,135
4655	Barcellona	-0,95	Suzuka	-0,193		-0,172
5922	Slovakiaring	-1,13	Losail	-0,191		-0,158
3841	Paul Ricard	-0,84	Aragon	-0,191		-0,157
4603	Shanghai	-0,92	Slovakiaring	-0,191		-0,174
5380	Losail	-1,03	Monza	-0,181		-0,162
4554	Chang	-0,88	Nurburgring	-0,177		-0,691

Figure 4.23: Δ time for every circuit due to weight variation

As we showed in the previous tables, we reported the value representing the Δt lost or earned each kilometer.

A column relating to the Δt in seconds each $10\,kg$ is shown to the right, considering the length of the circuit, so that the effect of weight loss is immediately evident.

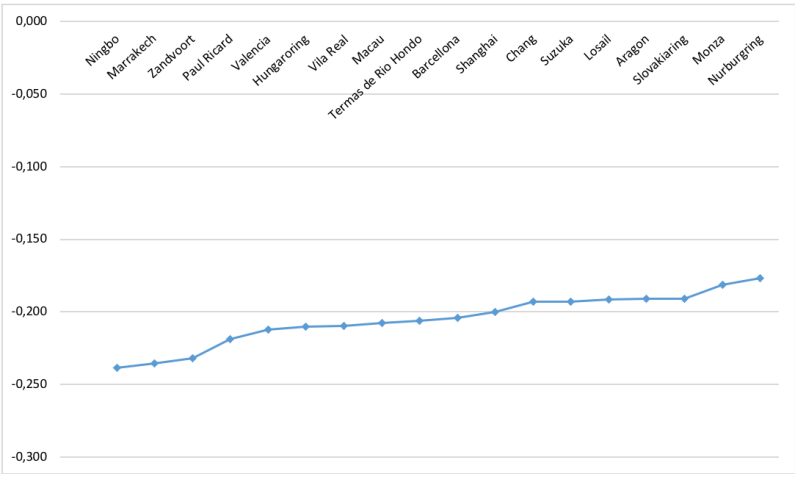

Figure 4.24: Total Δ time for every circuit due to weight variation

The power and weight tables helps us understand, and possibly counteract, the effect of the balance of performance.

Aerodynamics relative efficiency

One of the longest part of this simulation job is to obtain the relative efficiency value. We consider a basic setup characterized by the following aerodynamic parameters:

Table 4.2: Characteristic parameters of the basic configuration

C_x	0.350
$C_{z-TOTAL}$	-0.750
$C_{z-FRONT}$	0.454
C_{z-REAR}	0.269

in which we considered an aerodynamic load distributed at 60.5% in favor of the front of the car. This configuration allows to define a basic efficiency equal to the ratio of the aerodynamic coefficients:

$$E = \frac{L}{D} = \frac{-C_z}{C_x} = 2.143 \tag{4.3}$$

From this configuration, we have slightly changed the downforce in order to simulate different car set-ups and understand their influence on the track in terms of laptime. Despite varying the downforce the resistance of the car is also changed, it was decided to fix the value of the coefficient C_x in order to analyze only the effect of a parameter.

Table 4.3: Analyzed cases

Parameter	Event 1	Event 2	Event 3	Event 4	Event 5	Event 6	Event 7
C_x	0,3500	0,3500	0,3500	0,3500	0,3500	0,3500	0,3500
ΔC_x	-0,06	-0,06	-0,06	-0,06	-0,06	-0,06	-0,06
$C_{z-TOTAL}$	-0,3900	-0,4500	-0,5100	-0,5700	-0,6300	-0,6900	-0,7500
ΔC_z	0,36	0,30	0,24	0,18	0,12	0,06	0,00
$C_{z-FRONT}$	-0.236	-0,272	-0,309	-0,345	-0,381	-0,417	-0,454
C_{z-REAR}	-0,154	-0,178	-0,201	-0,225	-0,249	-0,273	-0,296
ΔE	-6	-5	-4	-3	-2	-1	0

where the term ΔE represents the relative efficiency that was calculated as a ratio:

$$\Delta E = \frac{-\Delta C_z}{\Delta C_x} \tag{4.4}$$

$$\Delta E_{track} = \Delta E_1 + (\Delta E_2 - \Delta E_1) * \frac{\Delta Laptime_1}{\Delta Laptime_1 + \Delta Laptime_2} \tag{4.5}$$

where the subscripts in the equation correspond to the value of two cases chosen as desired from the previous ones. The value of the relative efficiency of the circuit remains almost unchanged regardless of the cases considered; it is for this reason that this parameter characterizes the aerodynamic efficiency of the circuit and can be used as an indicative value of the type of circuit we are considering.

The terms $\Delta Laptime$ are calculated by making the difference between the laptime of the case considered as "*standard*" and the laptime of the analyzed case; therefore:

$$\Delta Laptime_1 = Laptime_{standard} - Laptime_1 \tag{4.6}$$

The lower this relative efficiency ΔE_{track} the more a track is rated to be a “Drag” circuit, which is a circuit where reducing drag is of the utmost importance. Monza will be the reference here. Values closest to zero on the other hand resemble circuit where downforce has to be put as priority. Circuits like Losail and Hungaroring are characterized by long, high-speed curves where the downforce is very important.

km	Circuit	Efficiency	Ranked	Relative Efficiency	
				Efficiency	
2971	Marrakech	-1,38	Monza	-5,17	
4381	Hungaroring	-1,23	Macau	-3,05	Low Drag
25378	Nurburgring	-2,34	Nurburgring	-2,34	
4307	Zandvoort	-1,42	Shanghai	-2,26	
4775	Vila Real	-1,04	Termas de Rio Hondo	-2,17	
4806	Termas de Rio Hondo	-2,17	Suzuka	-2,09	
4023	Ningbo	-1,27	Chang	-2,00	
5807	Suzuka	-2,09	Aragon	-1,92	
6120	Macau	-3,05	Slovakiaring	-1,84	
5793	Monza	-5,17	Paul Ricard	-1,83	
4005	Valencia	-1,60	Valencia	-1,60	
5344	Aragon	-1,92	Barcellona	-1,55	High Downforce
4655	Barcellona	-1,55	Zandvoort	-1,42	
5922	Slovakiaring	-1,84	Marrakech	-1,38	
3841	Paul Ricard	-1,83	Ningbo	-1,27	
4603	Shanghai	-2,26	Hungaroring	-1,23	
5380	Losail	-1,22	Losail	-1,22	
4554	Chang	-2,00	Vila Real	-1,04	

Figure 4.25: Efficiency table for every circuit

This is what we used to decide the initial aero platform setup per each race track.

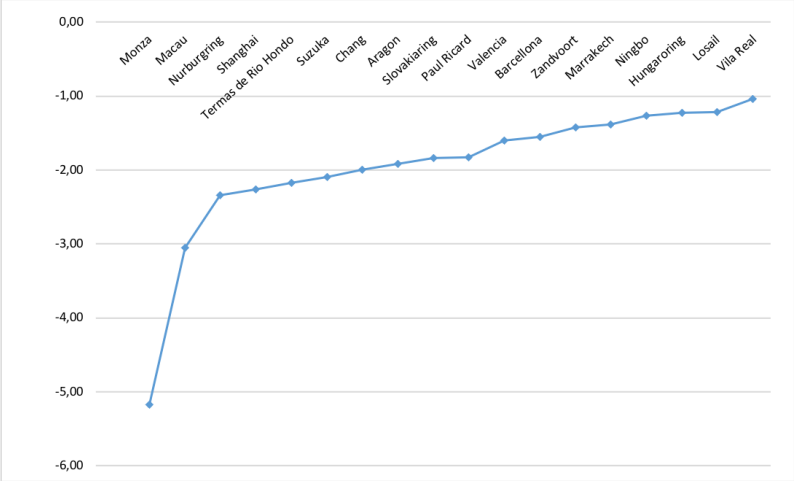

Figure 4.26: Efficiency for every circuit due to CoG variation

The relative efficiency table has to be used to decide the initial aero platform (rake and wing) setup.

4.3 Data fitting

By comparing two tracks with opposite characteristics through some graphs, it is possible to confirm what is stated in the section on relative aerodynamic efficiency and to highlight the different importance of the drag and lift coefficients in certain circuits. For a clearer view, from the table of relative efficiencies, we chose as an example a circuit called "Low Drag" (Monza), very fast in which the drag coefficient is fundamental in determining the laptime, and a circuit called "High Downforce" (Vila Real), a very slow and urban circuit

where the lift coefficient takes on greater weight than the effect given by the drag. We compared the laptime data obtained through the LapSim software of the Monza and Vila Real circuits initially based on the variation of the drag and following on the variation of the downforce.

For the drag coefficient we get:

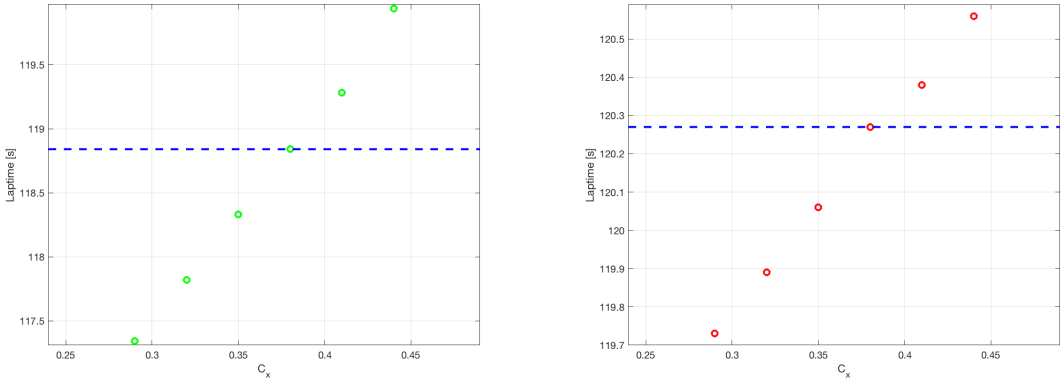

(a) Monza circuit

(b) Vila Real circuit

Figure 4.27: Influence of C_x on laptime

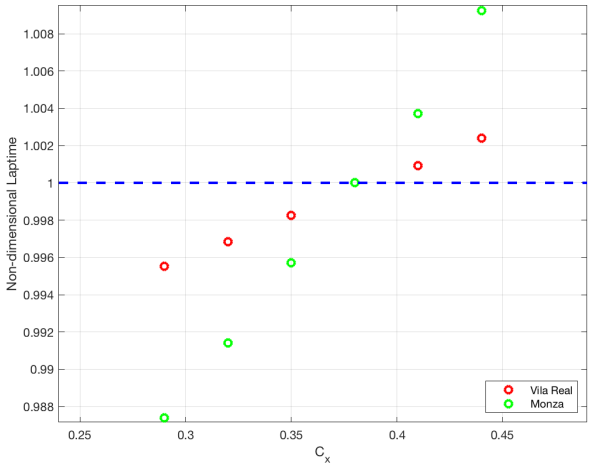

Figure 4.28: Comparison between influence of C_x on laptime

The sensitivity to the drag coefficient is clearly visible from the slope that the virtual line, joining the point values of laptime obtained through LapSim, assumes. The line referred to the Vila Real circuit is much less inclinated and so the variation in drag coefficient does not greatly affect the performance of the car, which, in this range, can gain at most a few tenths of a second per lap. Another influence is that the resistance has

on the Monza circuit, where the order of magnitude of the $\Delta time$ also reaches the order of the second in the range considered.

Similarly, for the lift coefficient I have:

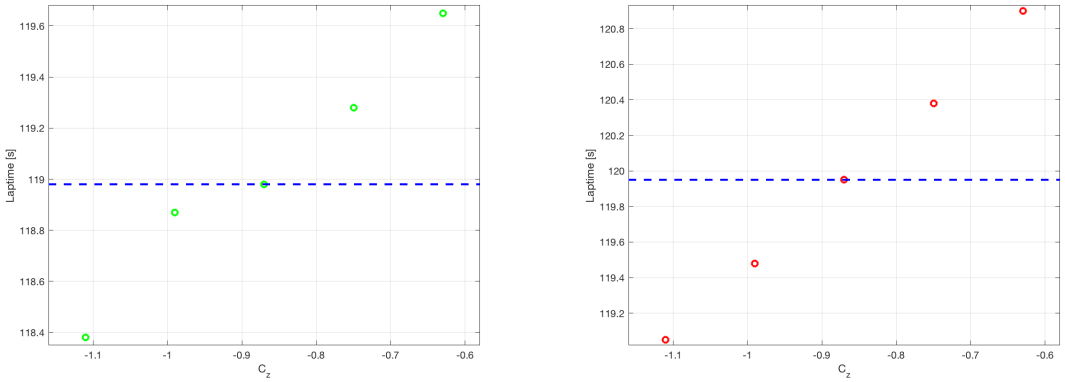

(a) Monza circuit (b) Vila Real circuit

Figure 4.29: Influence of C_z on laptime

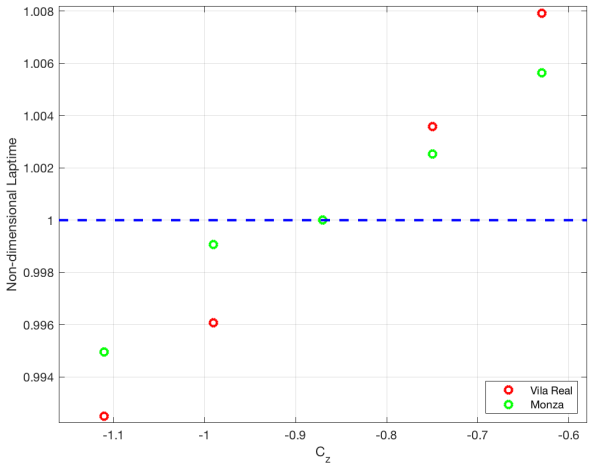

Figure 4.30: Comparison between influence of C_z on laptime

The sensitivity of the lift coefficient of the two tracks assumes an inverse trend with respect to the resistance coefficient. Monza is less dependent on the setup related to the creation of downforce on the car.

4.3.1 Maps fitting

Analyzing the values of the coefficient of lift and resistance obtained for the previous observations it is possible to build aerodynamic maps through the MatLab software that

allow to deduce the laptime indicatively, knowing the aerodynamic characteristics of the car. Interpolating the data obtained "experimentally" with LapSim and predicting the trend in the points included between these data we obtain the following graph:

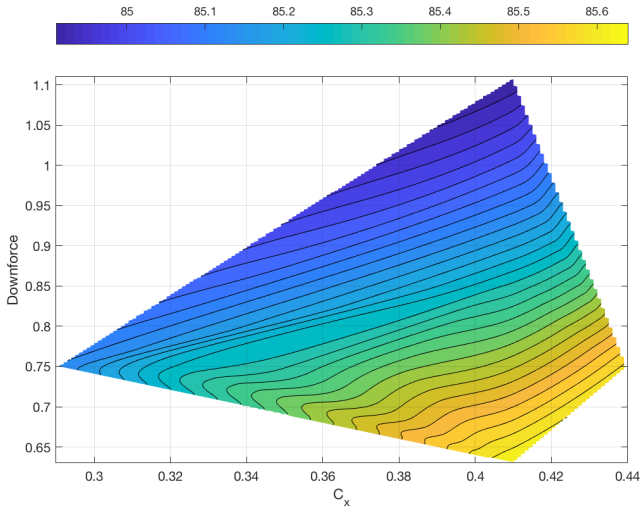

Figure 4.31: Laptime map in Marrakech

Which three-dimensionally corresponds to:

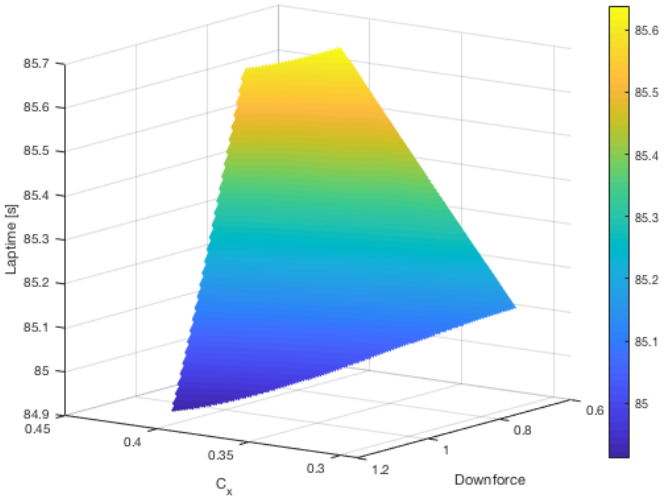

Figure 4.32: Laptime 3D map in Marrakech

Through the fitting MatLab tool it is possible to determine the equation of the plane that best approximates the data, in this way it is possible to extend the domain of the aerodynamic coefficients also to regions where there was not the presence of experimental

points. However, this fit must be used with caution, since although accuracy is good around the known data, this does not necessarily mean it is far away. For each track it is therefore possible to determine an equation of a plane that binds the drag coefficient, the downforce and the laptime. For example, we report the maps of the Marrakech circuit in Morocco and the Nurburgring in Germany.

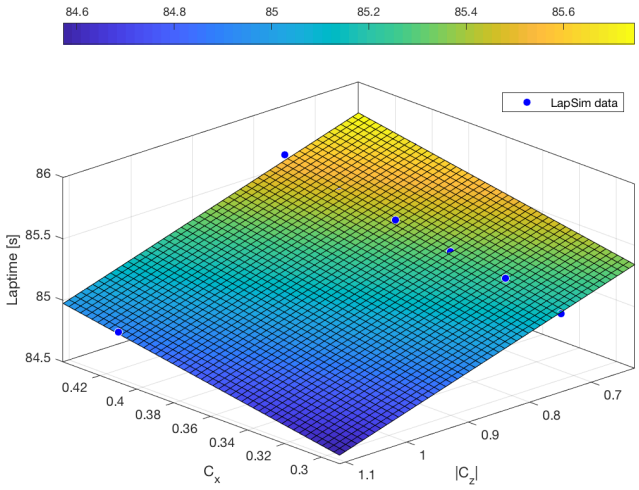

Figure 4.33: Fit-plane for Marrakech circuit

Where the general is model:

$$f(x, y) = a * y + b * x + c \tag{4.7}$$

Table 4.4: Characteristic parameters of equation model

Coefficients	
a	-1.608
b	2.685
c	85.58

Goodness of fit	
SSE	0.005386
R-square	0.9888

where SSE is "Sum of Squares Due to Error". This statistic measures the total deviation of the response values from the fit to the response values. It is also called the summed square of residuals. This is compared to the total sum of squares (SST), which measures how much variation there is in the observed data, and to the residual sum of squares (SSR), which measures the variation in the modelling errors.

$$SSE = \sum_{i=1}^{n} (y_i - \hat{y}_i)^2 \tag{4.8}$$

where $\hat{y}_i$ are the predicted values using the predicted coefficients and y_i is the i^{th} value of the variable to be predicted.

A value closer to 0 indicates that the model has a smaller random error component, and that the fit will be more useful for prediction.

R-Square statistic measures how successful the fit is in explaining the variation of the data. Put another way, R-square is the square of the correlation between the response values and the predicted response values. It is also called the square of the multiple correlation coefficient and the coefficient of multiple determination.

R-square is defined as the ratio of the sum of squares of the regression (SSR) and the total sum of squares (SST). SSR is defined as

$$SSR = \sum_{i=1}^{n} (\hat{y}_i - \bar{y})^2 \tag{4.9}$$

where $\bar{y}$ is the mean value.

SST is also called the sum of squares about the mean, and is defined as

$$SST = \sum_{i=1}^{n} (y_i - \bar{y})^2 \tag{4.10}$$

where $SST = SSR + SSE$.

$$\sum_{i=1}^{n} (y_i - \bar{y})^2 = \sum_{i=1}^{n} (\hat{y}_i - \bar{y})^2 + \sum_{i=1}^{n} (y_i - \hat{y}_i)^2 \tag{4.11}$$

Given these definitions, R-square is expressed as

$$Rsquare = \frac{SSR}{SST} = 1 - \frac{SSE}{SST} \tag{4.12}$$

R-square can take on any value between 0 and 1, with a value closer to 1 indicating that a greater proportion of variance is accounted for by the model. For example, an R-square value of 0.8234 means that the fit explains 82.34% of the total variation in the data about the average.

If you increase the number of fitted coefficients in your model, R-square will increase although the fit may not improve in a practical sense. To avoid this situation, you should use the degrees of freedom adjusted R-square statistic described below.

Note that it is possible to get a negative R-square for equations that do not contain a constant term. Because R-square is defined as the proportion of variance explained by the fit, if the fit is actually worse than just fitting a horizontal line then R-square is negative. In this case, R-square cannot be interpreted as the square of a correlation. Such situations indicate that a constant term should be added to the model.

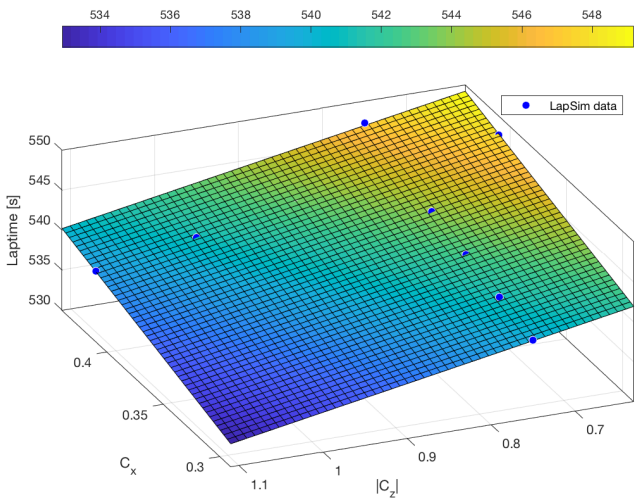

Figure 4.34: Fit-plane for Nurburgring circuit

Table 4.5: Characteristic parameters of equation model

Coefficients	
a	-18.71
b	48.6
c	539.6

Goodness of fit	
SSE	0.1815
R-square	0.9978

Then each circuit will have its equation of the plane that characterizes it.

To demonstrate the accuracy of the MatLab fitting respect to the LapSim data, we have reported on a graph the residuals between "experimental" points and projection of these points in the equation of the plane. The error, as we note, is very limited (less than 0.1% for both the circuits).

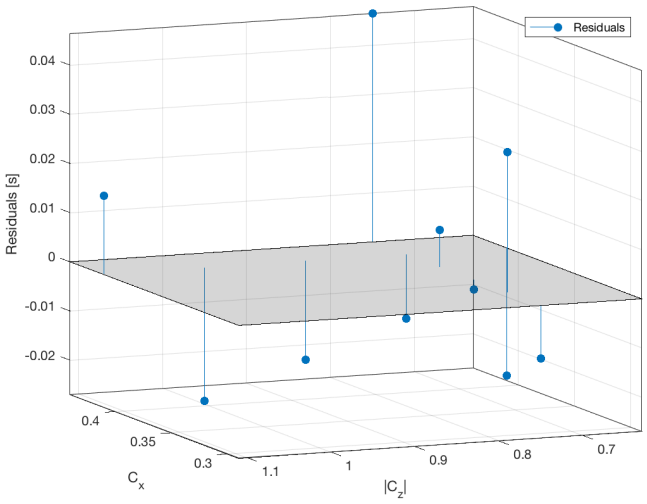

Figure 4.35: Residuals due to fit in Marrakech circuit

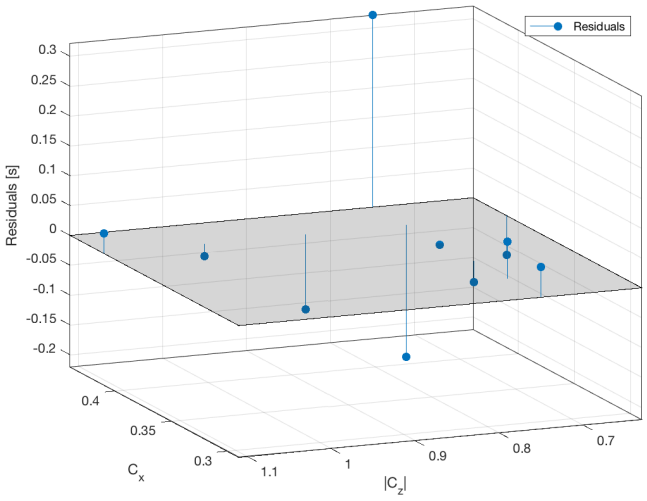

Figure 4.36: Residual due to fit in Nurburgring circuit

An important observation is that even the "experimental" points of LapSim are still simulation points made by software in the PC and therefore they have an error too with respect to the reality of the facts; even if the errors between the two software are very small, this may not be the case with the data collected on the track. However, these tools are very effective not so much for the value of the data itself as for having a qualitative trend; Motorsport is not an exact science and it all depends on thousands of parameters, but knowing qualitatively the influences and the possibility of improving performance through variations of downforce and drag is certainly a useful information to better face the races.

4.4 Rear wing airfoil CFD

As we saw in the *Chapter 1.3* the rear wing is regulated by WSC and is produced by a single company for all cars with TCR specifics. The wing is called "at constant airfoil" characterized by identical profiles in each section.

By executing a cross section of the rear wing, we obtain the wing airfoil.

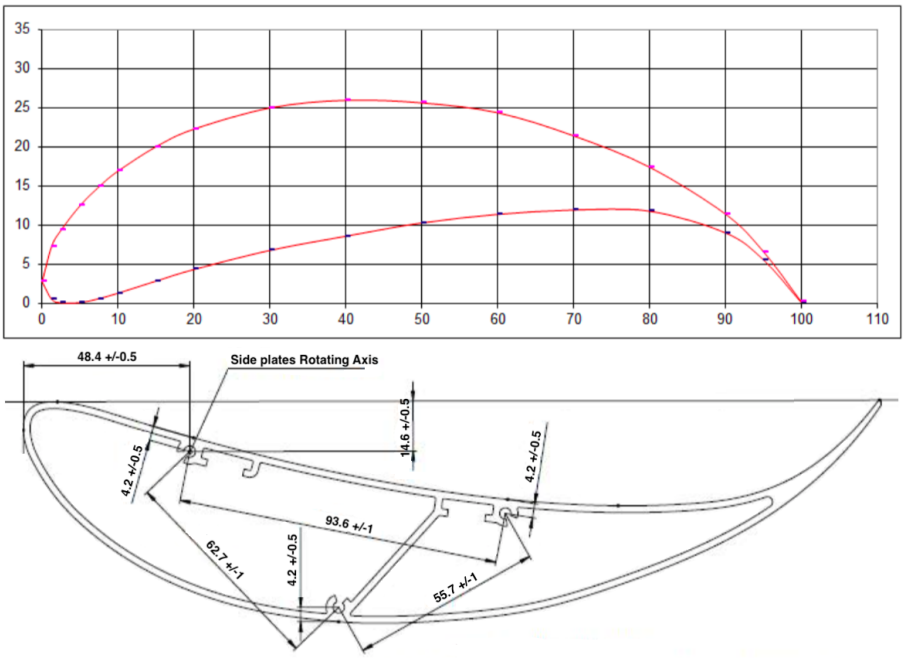

Figure 4.37: Geometry of the airfoil

Seeking the most appropriate aerodynamic characteristics for the racing car wings, a series of rather special wing sections was calculated by the Enrico Benzing. These sections, with «Be» designation, as we will see in the numbering system, were calculated following a different method than the NACA (National Advisory Committee for Aeronautics) one.

The Benzing profiles have features similar to all profiles: the leading edge is rounded, while the trailing edge is pointed. In fact, the leading edge has the task of separating the invested fluid, one upper and one lower, into two portions. On it the stagnation point is formed, that is the point in which the fluid stops. The trailing edge or escape edge instead has the task of uniting these two separate flows. However they are characterized by large buckets and smaller thicknesses unlike NACA profiles.

For simplicity of classification, the numbering system of these sections (see graph below) refers to the main parameters of the relative maximum thickness Sr (first two digits, in % chord C) and its chordwise position m (third digit, in tenths of C). After the dash, the same data are found for the relative maximum camber fr (fourth and fifth digits, in % C) and its position m in abscissa (last digit, in tenths of C).

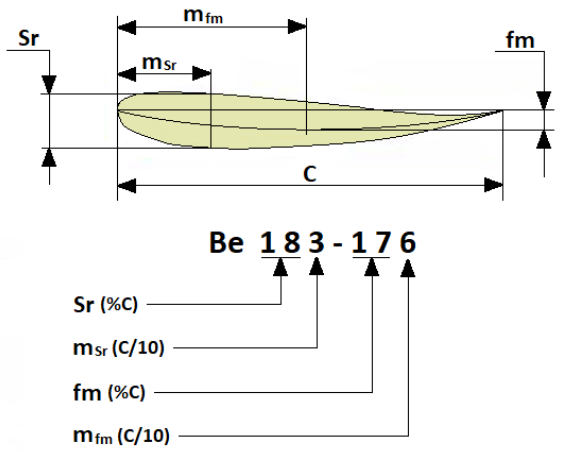

Figure 4.38: Convention of the airfoil

Where:

- C = Chord
- Sr = Maximum relative thickness
- fm = Maximum relative arrow
- m_{Sr} = Position of Sr
- m_{fm} = Position of fm

4.4.1 Analysis of stall

In fluid dynamics, a stall is a condition that entail a reduction in the lift coefficient generated by a foil as angle of attack increases. The angle at which this occurs is called the *critical angle of attack*: it is dependent upon the fluid, the airfoil section or profile of the wing, its planform, its aspect ratio, the Reynolds number and other factors, but is typically in the range of 8 to 20 degrees relative to the incoming wind ("relative wind") for most subsonic airfoils. The critical angle of attack is the angle of attack on the lift coefficient (for aviation) or downforce coefficient (for motorsport) versus angle-of-attack curve at which the maximum coefficient occurs.

Flow separation begins to occur at small angles of attack while attached flow over the wing is still dominant. As angle of attack increases, the separated regions on the top of the wing increase in size and hinder the wing's ability to create lift. When the critical angle of attack of the foil is exceeded, separated flow is so dominant that additional increases in angle of attack produce less lift and more drag.

As speed reduces, angle of attack has to increase to keep downforce constant until the critical angle is reached.

4.4.2 Technical notes

To analyze the profile we had to appeal to the CFD analysis as much simpler and faster software did not go to convergence because of the geometry of the profile that is characterized by a lot of camber and with a very variable thickness.

Software like XFOIL (an interactive program, developed by MIT, for the design and analysis of subsonic isolated airfoils) are very useful for the analysis of 4 or 5-digit NACA profiles that have a geometric shape that is very different from the rear wing profile. In the case of the profile Be 183-176 we managed to obtain valid results only up to an incidence range of $-2° < \alpha < 2°$ using a large number of iterations and a high division into profile panels.

So we had to use Star CCM+. Even the CFD analysis is affected by the particular geometry of the profile, but is much more stable, given the power of calculation. The results obtained are good overall with low residuals and so the convergence of the solution; sometimes the residuals remain high and the solution tends to oscillate.

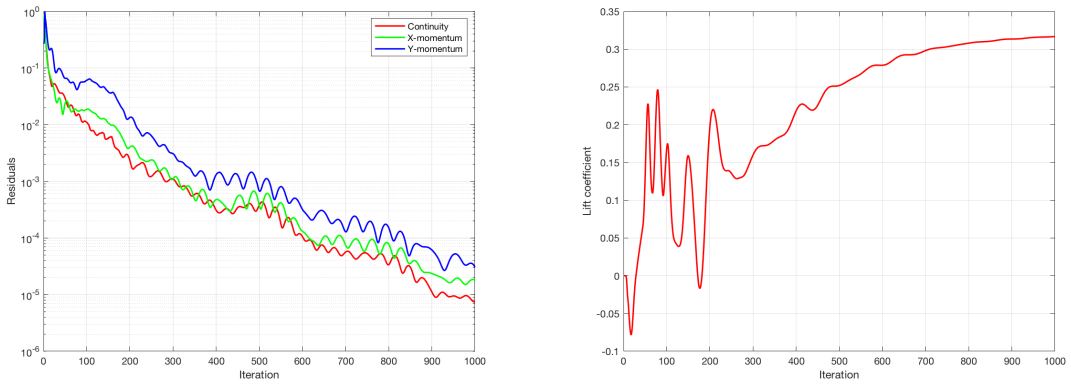

(a) Residuals monitor

(b) Lift coefficient monitor

Figure 4.39: Example of low residuals for $\alpha = 2°$

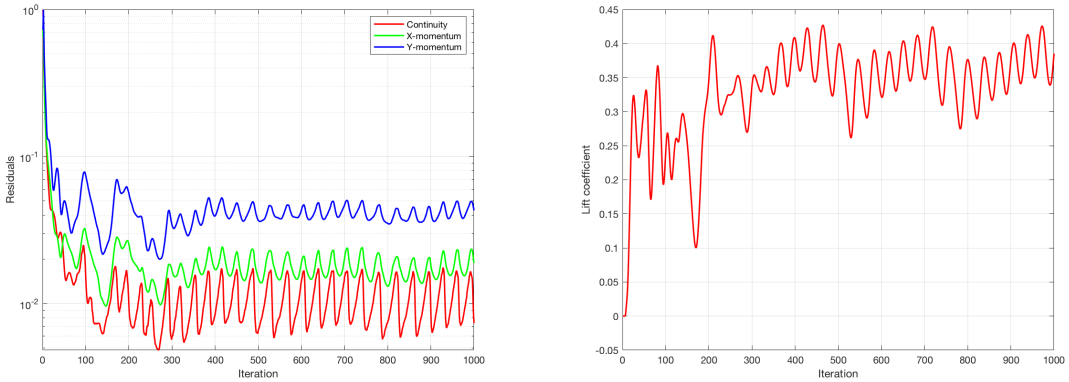

(a) Residuals monitor

(b) Lift coefficient monitor

Figure 4.40: Example of high residuals for $\alpha = 20°$

After the stall values the software becomes unstable and provides inaccurate results:

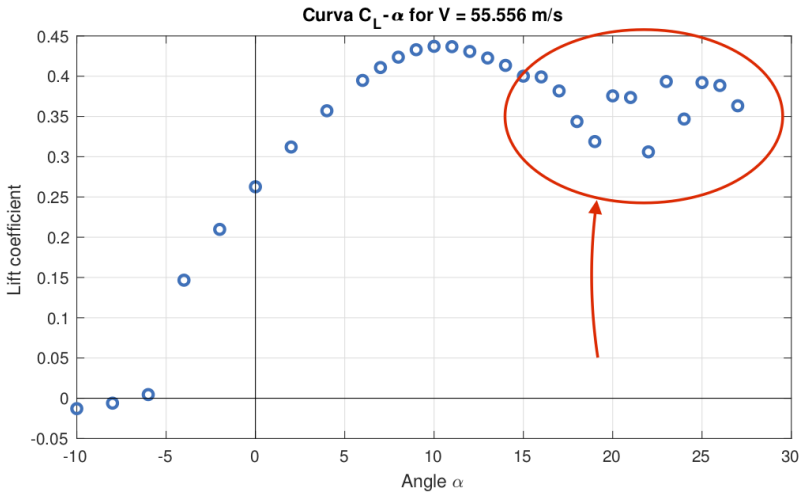

Figure 4.41: Inaccurate results

It was therefore considered appropriate to apply a data reduction to skim the resulting values.

4.4.3 Convention

Considering the wing as a whole (and not just the wing profile), the set of airflow entry points is defined as the leading edge or leading edge, ie the front line of the wing, and as a trailing edge the set of exit points, ie the back line of the wing.

Here is the inclination convention used by the *Star CCM+* software to compare it with the one used to adjust the rear wing. The convention is the same but we must pay

particular attention to the fact that in the CFD software does not change the angle of inclination of the profile, but varies the incidence of the flow with a constant angle profile equal to 0°.

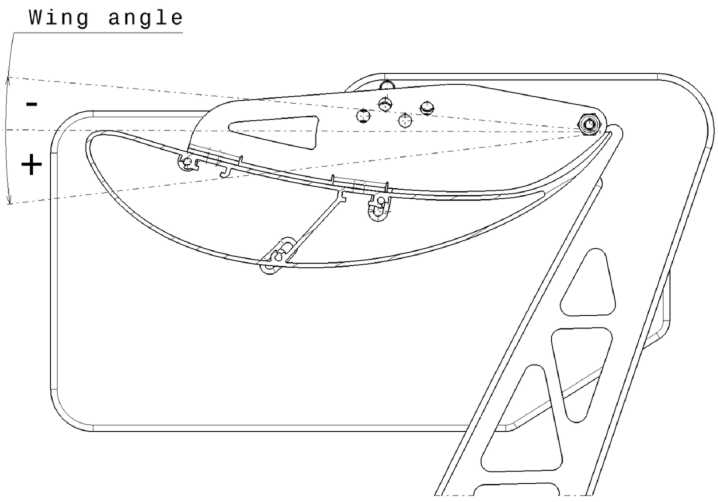

Figure 4.42: Convention rear wing

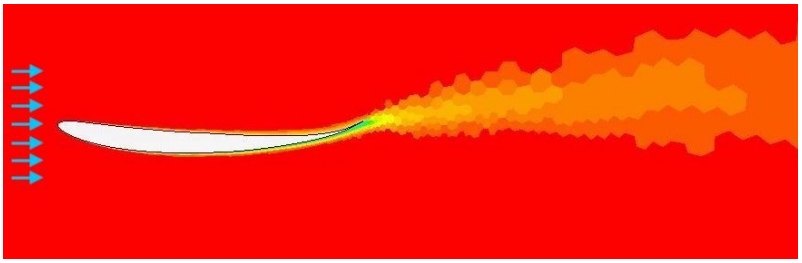

Figure 4.43: Convention Star CCM+ with $\alpha = 0°$

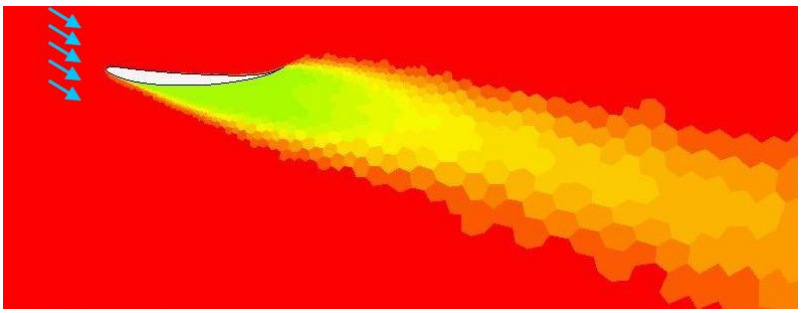

Figure 4.44: Convention Star CCM+ with $\alpha = 18°$

Another important aspect to note is that this analysis is made considering the Ground Reference System (GRS), therefore with an angle of inclination of the profile calculated

respect to the orange line in Fig. 4.45. The car has a pitch angle, due to the set up (which may reach around 2°) represented in the figure by the red line. All the values obtained will therefore have to be rescaled at this angle because the wing is adjusted through the brackets in the Car Reference System (CRS).

$$\alpha_{true}\,[^\circ] = \alpha_{obtained} + \alpha_{pitch} \tag{4.13}$$

Where $\alpha_{true} = \alpha_{GRS}$ and $\alpha_{obtained} = \alpha_{CRS}$.

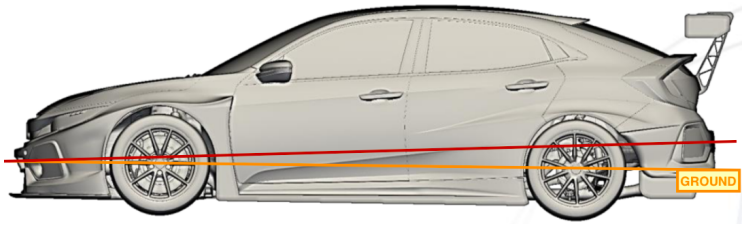

Figure 4.45: Reference systems

The values obtained from *Star CCM+* refer to the Ground Reference System, so the user must manually rescale them from the pitch angle that characterizes the car's setup using the formula above.

4.4.4 Analysis

For this simulation we considered standard ambient conditions values (temperature = $293{,}15\,K = 20°C$ and pressure = $101{,}325\,kPa = 1\,atm$). Through the ambient conditions it is possible to obtain also the density and the dynamic viscosity (with Sutherland's law) that characterizes the flow:

$$\rho = \frac{p}{R \cdot T} = \frac{101325}{287{,}05 \cdot 293{,}15} = 1{,}204 \frac{kg}{m^3} \tag{4.14}$$

$$\mu = 1{,}46 \cdot 10^{-6} \frac{T^{3/2}}{110 + T} = 1{,}817 \cdot 10^{-5} \frac{kg}{m \cdot s} \tag{4.15}$$

The Reynolds number was calculated as follows:

$$Re = \frac{\rho v L}{\mu} = \frac{1{,}225 \cdot v \cdot 0{,}25}{\mu} \tag{4.16}$$

where:

- ρ is the density of the air [kg/m3], calculated with the gas law.
- v is the speed of the fluid with respect to the object that in our case is the car speed [m/s]
- L is a characteristic linear dimension that corresponds to our chord length [m]

- μ is the dynamic viscosity of the fluid [kg/m · s], calculated with Sutherland's law

The results are reported in the tables below:

Table 4.6: Lift coefficients for Be 183-176

	C_L		
α	$v = 44.44\,m/s$	$v = 55.56\,m/s$	$v = 66.67\,m/s$
-10	-7.465e-03	-1.290e-02	-1.997e-02
-8	-3.684e-03	-6.092e-03	-1.113e-02
-6	1.666e-03	4.567e-03	8.256e-02
-5	2.983e-02	5.595e-02	9.812e-01
-4	9.101e-02	1.466e-01	2.154e-01
-2	1.329e-01	2.097e-01	3.040e-01
0	1.668e-01	2.626e-01	3.802e-01
2	1.983e-01	3.120e-01	4.514e-01
4	2.270e-01	3.570e-01	5.162e-01
6	2.513e-01	3.947e-01	5.710e-01
7	2.613e-01	4.107e-01	5.937e-01
8	2.692e-01	4.236e-01	6.111e-01
9	2.745e-01	4.328e-01	6.232e-01
10	2.768e-01	4.370e-01	6.281e-01
11	2.758e-01	4.366e-01	6.262e-01
12	2.732e-01	4.307e-01	6.214e-01
13	2.681e-01	4.225e-01	6.095e-01
14	2.617e-01	4.134e-01	5.967e-01
15	2.541e-01	4.000e-01	5.756e-01
16	2.516e-01	3.991e-01	5.642e-01
17	2.330e-01	3.816e-01	5.434e-01
19	2.110e-01	3.188e-01	4.748e-01

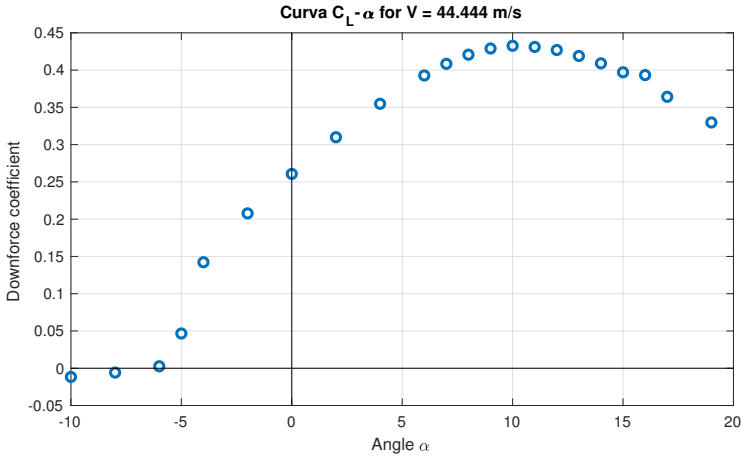

Figure 4.46: $C_L - \alpha$ **at** $V = 44.444\,m/s$

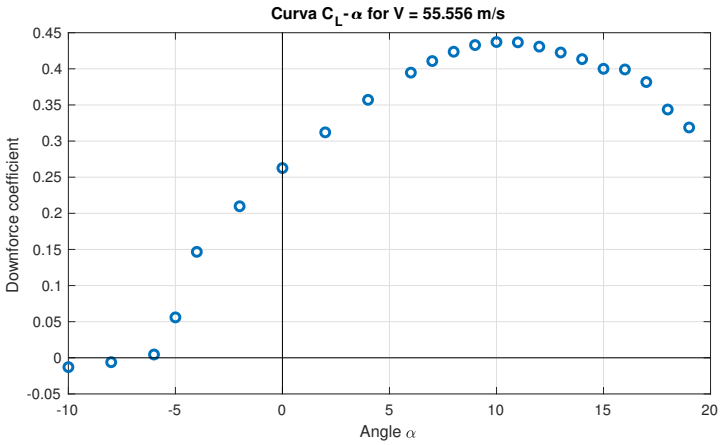

Figure 4.47: $C_L - \alpha$ **at** $V = 55.556\,m/s$

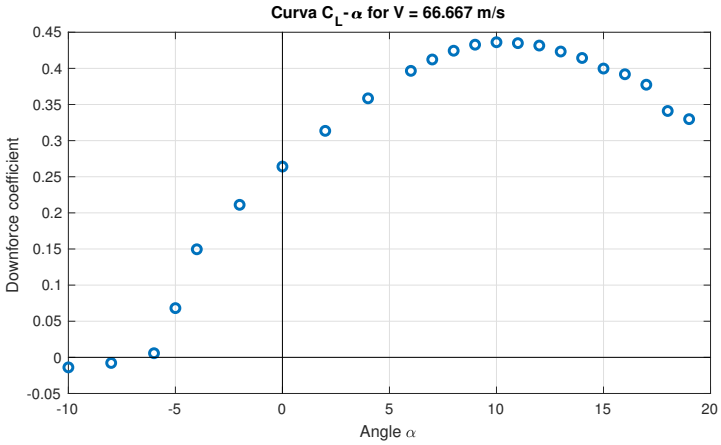

Figure 4.48: $C_L - \alpha$ **at** $V = 66.667\,m/s$

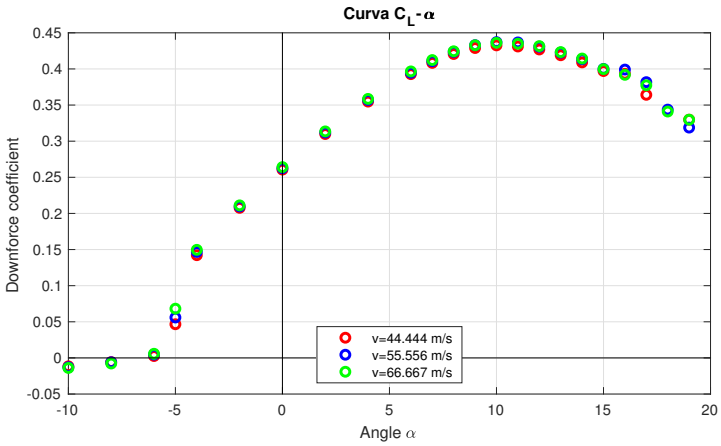

Figure 4.49: $C_L - \alpha$ **comparison**

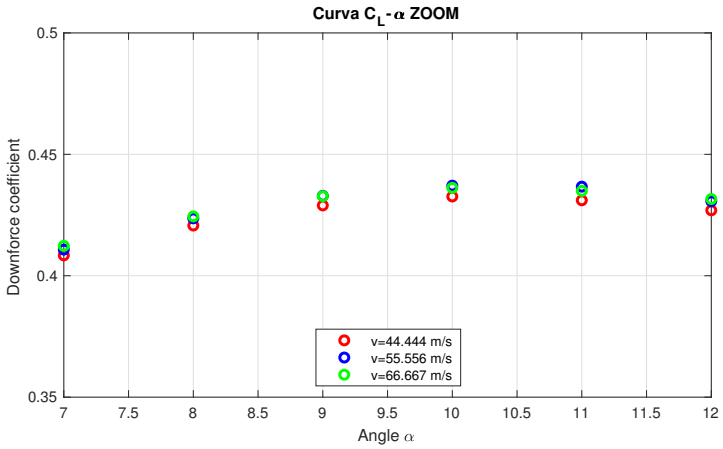

Figure 4.50: $C_L - \alpha$ **comparison (zoom)**

We notice how the graphs are superimposable, due to the Reynolds numbers very close to each other. The separation of the flow takes place on the back of the wing airfoil. The stall is recorded on the curve $c_L(\alpha)$ with the attainment of a maximum at α of about 10° and the next decreasing segment with increasing incidence.

N.B.: *In the car configuration, the stall incidence must be corrected with the flow direction. The flow follows the rear windshield and then slightly realigns to the ground direction. A flow that is not perfectly horizontal then arrives at the rear wing.*

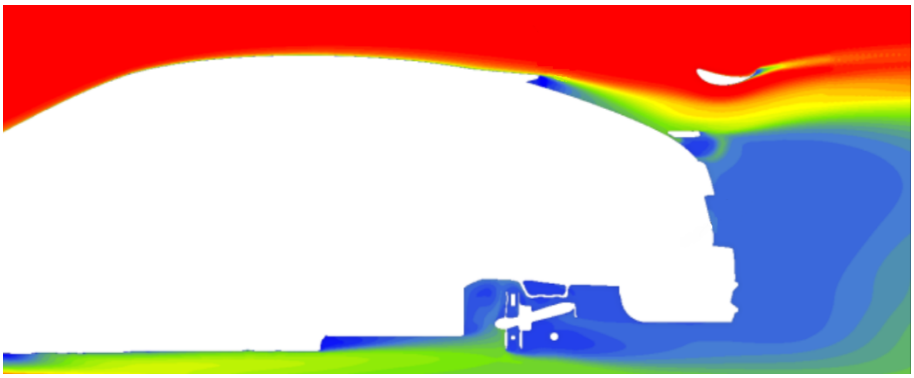

Figure 4.51: Direction of free stream

Chapter 5

Flow in wake condition

5.1 Introduction

During the season we saw how the flow of air that streams into the engine compartment is adequate if the car is subject to an undisturbed flow of air, while it is lower than expected if the car is in the wake of a other car. In some races we have therefore advised the drivers to try to avoid this situation so that the engine does not overheat and diminish its performance. To confirm this we asked TotalSim to simulate the effect of following car distance on performance using CFD software.

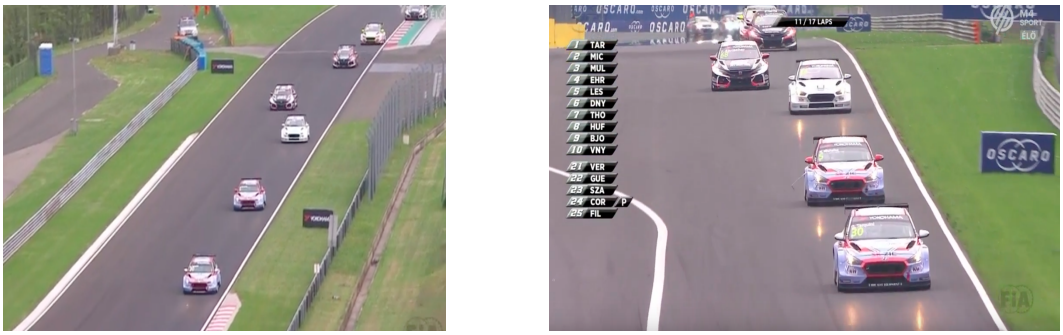

(a) Hungaroring - Street [**15**] (b) Hungaroring - Main street [**15**]

Figure 5.1: Honda Civic TCR in non slipstream condition

TotalSim moved the model created in final configuration to reproduce a mostly automated multicar setup of the following car at a specified downstream distance. Two simulations will be carried out with a following car downstream distance of 6 and 12 m, distances chosen arbitrarily but that should approximate two situations of wake that could occur on the track.

Monitoring of the radiator, intake and aerodynamic performance will be carried out and, through this analysis, we can then determine the relative performance of the following

car to the lead car. [1]

Figure 5.2: Model for CFD analysis - lateral view

Where the position of the radiators is shown behind:

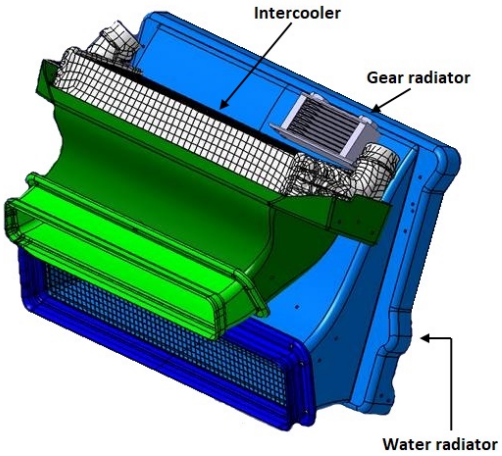

Figure 5.3: Cooling package

5.2 Phenomenology

We briefly analyze the phenomenology that describes our field of motion.
As we saw in the introduction Chapter 2, in the hypothesis of neglecting the compressibility effects of air (which are taken into consideration for air velocities above $400\,km/h$ in standard atmosphere), to neglect the energy dissipation by viscous friction and to retain the air a fluid homogeneous, we can speak about "perfect fluid", where the principle of Bernoulli is valid in its most known and used formulation.

$$p_0 = p + \frac{1}{2}\rho v^2 \tag{5.1}$$

where v is the homogeneous fluid velocity, ρ its density, p_0 the total pressure and p the static one.

[1] Because of the nature of this study there is considerable computational resource required; TotalSim estimated that $\sim$ 6000 core hours are required for each simulation.

The principle of conservation of the fluid flow rate is equivalent to affirming that the volumetric flow rate (Q), i.e. the product between the passage section (S) and the crossing speed (V), is kept constant along the air flow (called the flow tube).

$$S \cdot V = Q \tag{5.2}$$

It is sufficient to apply the previous equations in two distinct points (1 and 2) in the air flow in order to write that:

$$\frac{Q}{S_1^2} + 2\frac{P_1}{\rho} = \frac{Q}{S_2^2} + 2\frac{P_2}{\rho} \tag{5.3}$$

This equation tells us that a restriction (an S decrease) causes a decrease in the static pressure: thus we obtain an equivalent way of expressing the generation of the aerodynamic forces.

In fact, by imagining the field of motion around the vehicle as the set of "n" flow tubes, the convex surface of the car body "deforms" the field above it by reducing the passage section of the air flow, with consequent increase in flow velocity and reduction of static pressure. If this reduction takes place above the car, it will be applied a supporting force, that is facing upwards, vice versa if the convex surface is facing downwards, as in the case of the wing profiles deporting the cars, the body will be invested from a deporting force, that is towards the ground.

The Bernoulli equation assumes that there are no energy losses in the system in question: this means that it is assumed that the flow does not undergo detachment of the vein (ie the removal of the fluid vein from the surface), nor viscous effects. But when these phenomena occur, energy losses occur which lead to a simultaneous reduction of speed and static pressure, thus falling outside the Bernoulli principle.

An example is the area of strong turbulence that occurs immediately behind the car: in this area the flow has lost kinetic energy due to the positive pressure gradient and viscous effects, and a detachment of the fluid vein from the surface occurs; therefore, the air velocity in this region is low, but it is also a low pressure zone. (here therefore comes out of the Bernoulli principle).

The low pressure in this area is the main cause of the phenomenon of the wake, which allows the car that follows a few meters another car to see significantly reduced forces of aerodynamic friction and to be "sucked" forward, thus increasing its speed, with the same propulsive thrust. The phenomenon of the wake decreases in intensity as one moves away from the previous car, until it becomes null. The higher the speed at which you proceed, the more the trail behind the car will be extended and appreciable. It is also curious to know that when two vehicles move close together, one not only generates an aerodynamic advantage for what follows, but also for the front one, in a lower percentage. In fact, the presence of a vehicle in wake, helps to decrease the turbulence zone, because it acts as an extension of the body and relieves the process of detachment of the fluid vein in the rear part of the first vehicle.

It is therefore considered a car in the wake, a particularly important case in a straight line and therefore at maximum speed, in which the engine is considered to be at the

highest engine speeds subject to a lower flow. The speed, unlike the standard conditions previously discussed, is set at $55.6\,m/s$.

5.3 Analysis

What is described is also shown by the numerical results obtained: by comparing the two configurations ($6\,m$ and $12\,m$) it is possible to draw the following:

- at a lower distance both cars are more aerodynamically advantaged than $12\,m$. Decreases resistance and even downforce, which is generally sought, but which is "inconvenient" on the straight because the car must present with lower aerodynamic load to increase its speed. This reduction is not enough. Less downforce allows faster acceleration and potential top speed, unless limited by the top gear ratio and engine rev limiter.

- The loss of aerodynamic load is particularly evident in the front of the car. This phenomenon changes the pitch moment and the car is more parallel to the ground.

The problem of the lack of flow in the car is clearly visible in the following graph:

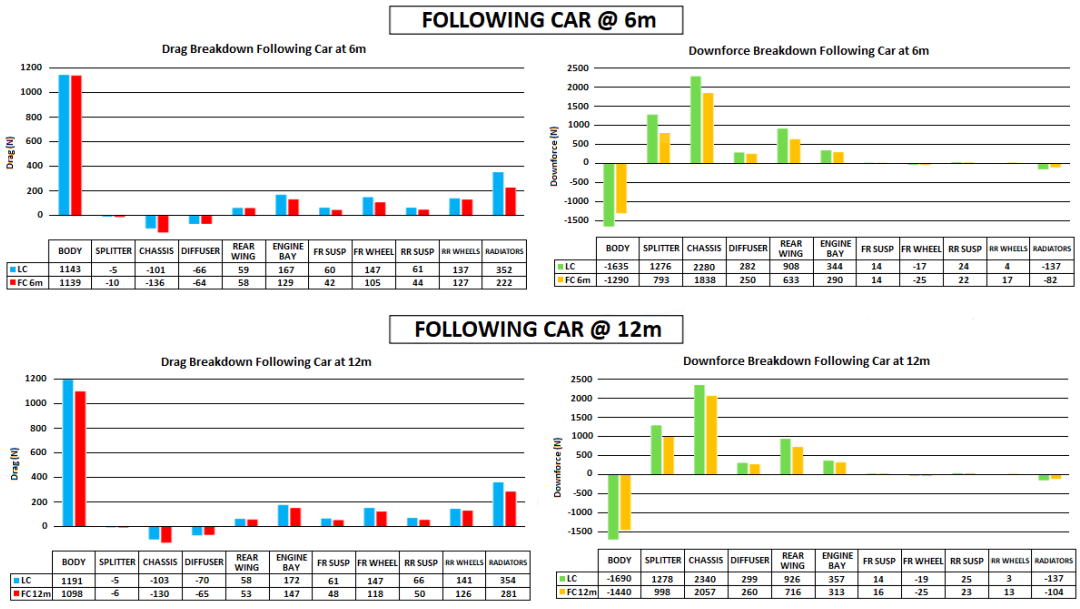

	BODY	SPLITTER	CHASSIS	DIFFUSER	REAR WING	ENGINE BAY	FR SUSP	FR WHEEL	RR SUSP	RR WHEELS	RADIATORS
LC	1143	-5	-101	-66	59	167	60	147	61	137	352
FC 6m	1139	-10	-136	-64	58	129	42	105	44	127	222

	BODY	SPLITTER	CHASSIS	DIFFUSER	REAR WING	ENGINE BAY	FR SUSP	FR WHEEL	RR SUSP	RR WHEELS	RADIATORS
LC	-1635	1276	2280	282	908	344	14	-17	24	4	-137
FC 6m	-1290	793	1838	250	633	290	14	-25	22	17	-82

	BODY	SPLITTER	CHASSIS	DIFFUSER	REAR WING	ENGINE BAY	FR SUSP	FR WHEEL	RR SUSP	RR WHEELS	RADIATORS
LC	1191	-5	-103	-70	58	172	61	147	66	141	354
FC 12m	1098	-6	-130	-65	53	147	48	118	50	126	281

	BODY	SPLITTER	CHASSIS	DIFFUSER	REAR WING	ENGINE BAY	FR SUSP	FR WHEEL	RR SUSP	RR WHEELS	RADIATORS
LC	-1690	1278	2340	299	926	357	14	-19	25	3	-137
FC 12m	-1440	998	2057	260	716	313	16	-25	23	13	-104

Figure 5.4: Drag and downforce comparison between leading car & following car at $6\,m$ and $12\,m$

The great loss of aerodynamic drag means that the radiator intercepts much less air. We see a decrease of $130\,N$ for the car placed at $6\,m$ distance and $90\,N$ for the car at $12\,m$. We confirm the general decrease in vertical aerodynamic force.

Now we consider the mass flows that intercept the water cooler, intercooler and gearbox. There is a decrease in flow and total pressure evident in both the two following cars.

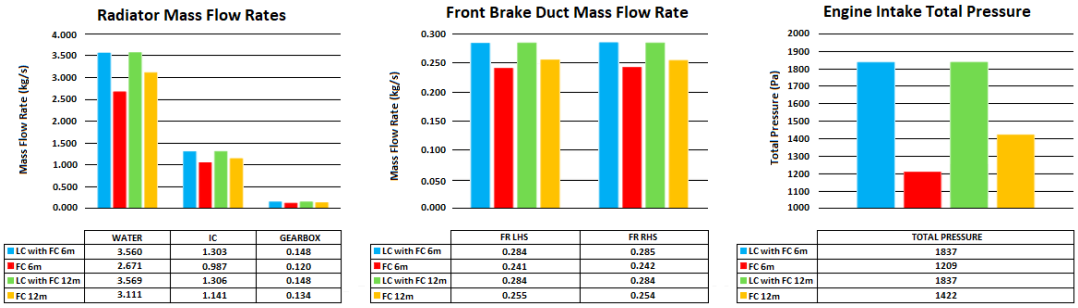

	WATER	IC	GEARBOX
LC with FC 6m	3.560	1.303	0.148
FC 6m	2.671	0.987	0.120
LC with FC 12m	3.569	1.306	0.148
FC 12m	3.111	1.141	0.134

	FR LHS	FR RHS
LC with FC 6m	0.284	0.285
FC 6m	0.241	0.242
LC with FC 12m	0.284	0.284
FC 12m	0.255	0.254

	TOTAL PRESSURE
LC with FC 6m	1837
FC 6m	1209
LC with FC 12m	1837
FC 12m	1422

Figure 5.5: Mass flow comparison between leading car & following car at $6\,m$ and $12\,m$

In the following figure we see a less stagnation on the mirrors due to the lower flow coming out of the engine compartment through the bonnet vanes. The lower stagnation is therefore particularly effective from the aerodynamic point of view but at the same time reduces the mass flows for the cooling of the components.

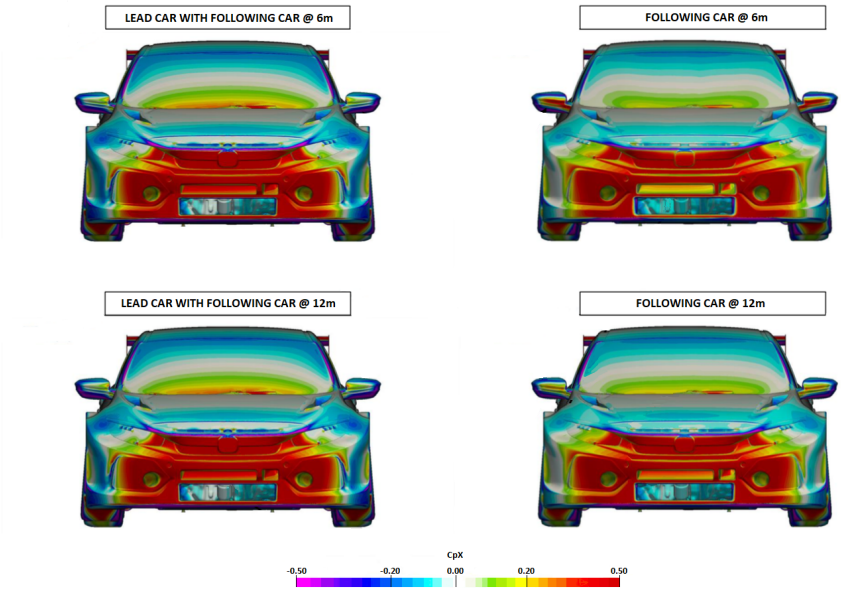

Figure 5.6: Cp_X comparison between leading car & following car at $6\,m$ and $12\,m$ (FRONT)

We describe briefly, through some comments, the main aerodynamic aspects that are highlighted in the CFD maps related to the wake. The next figure shows a general drag reduction.

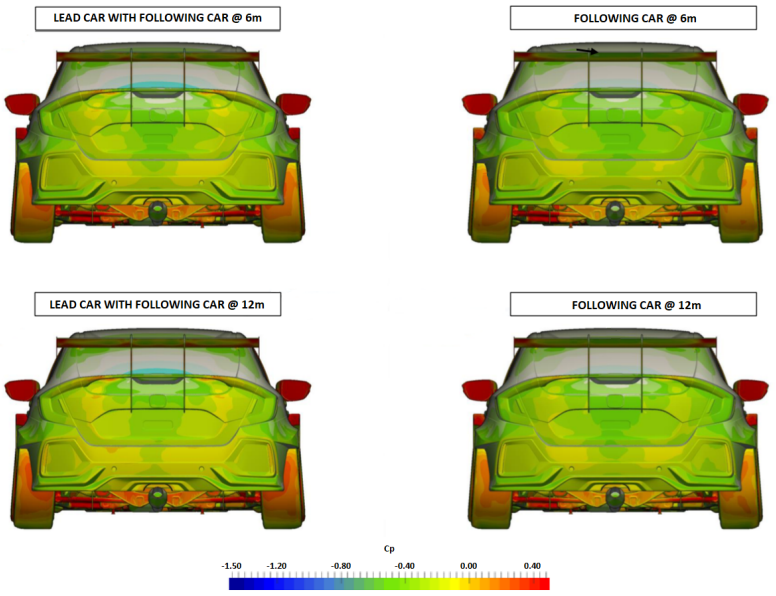

Figure 5.7: Cp_X **comparison between leading car & following car at** $6\,m$ **and** $12\,m$ **(REAR)**

We notice a less flow entering the underbody with an higher speed (colors are shifted to the light green/yellow).

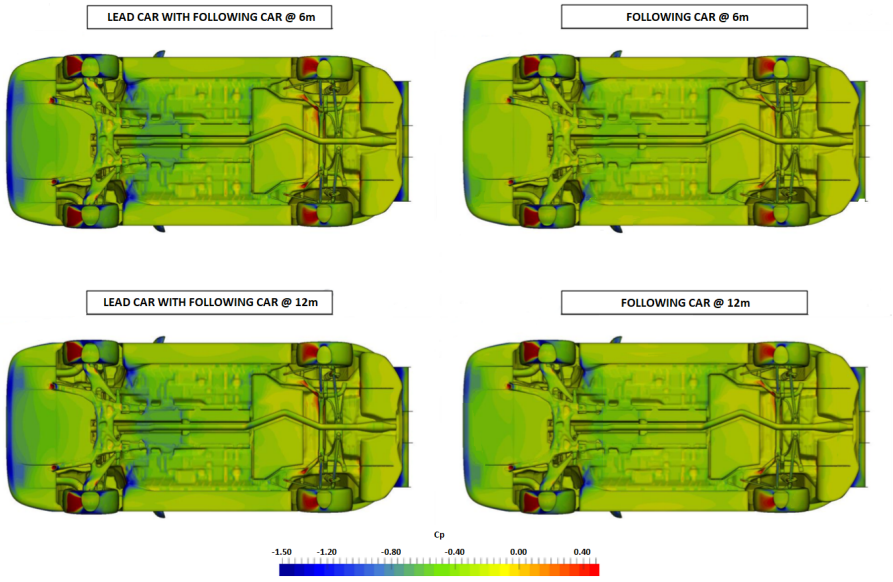

Figure 5.8: Cp comparison between leading car & following car at $6\,m$ **and** $12\,m$ **(BOTTOM)**

We analyze in detail what happens in the front bumper, because of the increase in turbulence level. Due to the wake of the lead car, lower CpT flow goes into the cooling and engine intake ducts and under the splitter. There is a separation from the outboard corner in the intake duct and an higher average CpT ahead of the following car at $12\,m$

due to the increased distance.

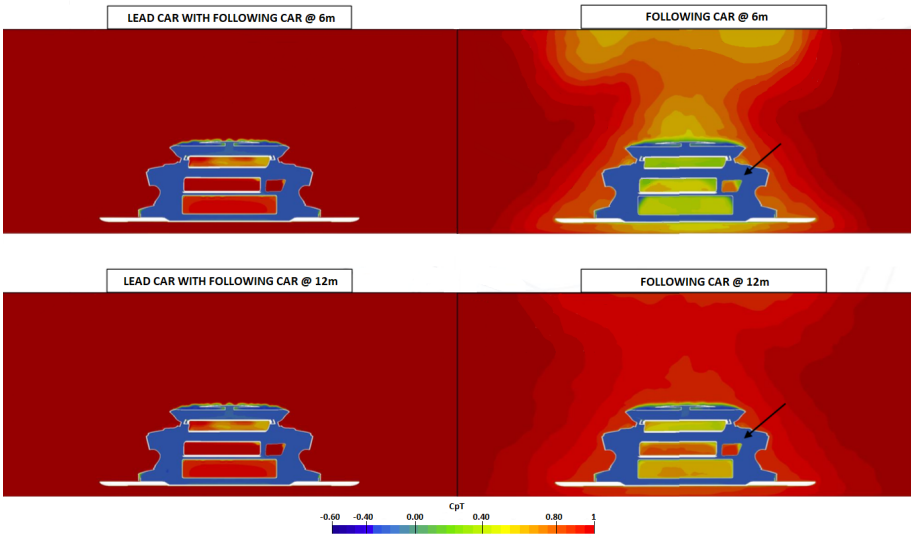

Figure 5.9: Cp_T **comparison between leading car (@** $X = -0.8$**) & following car at** $6\,m$ **(@** $X = 9.782\,m$**) and** $12\,m$ **(@** $X = 15.782\,m$**)**

We notice an increase in separation/recirculation from the top corners of the water radiator duct due to a lower CpT into the duct. Small separation in the front brake ducts is seen.

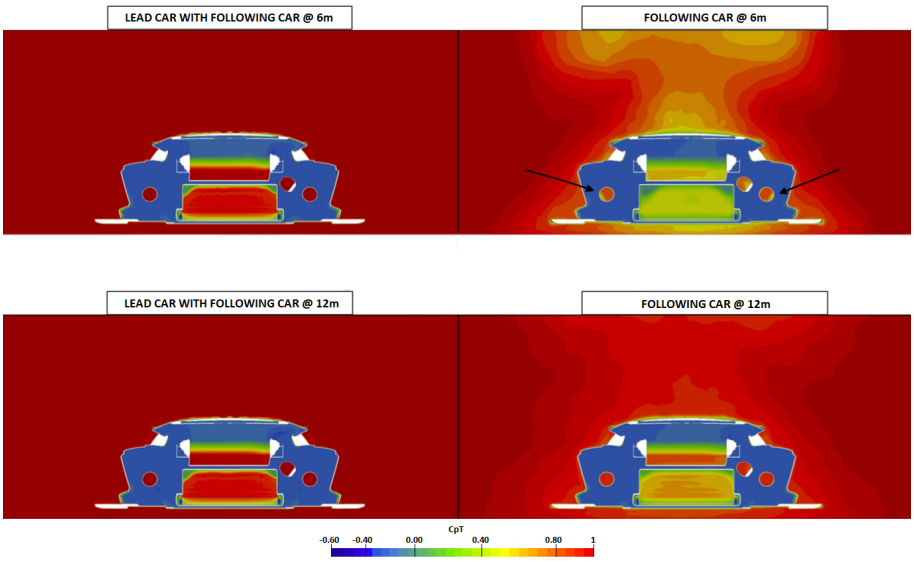

Figure 5.10: Cp_T **comparison between leading car (@** $X = -0.7$**) & following car at** $6\,m$ **(@** $X = 9.882\,m$**) and** $12\,m$ **(@** $X = 15.882\,m$**)**

We see a subtle change in wake size and shape from the lead car as the following car

distance increases. There is a separation on the underside of the rear wing of the following car near the end plates which decreases the produced downforce.

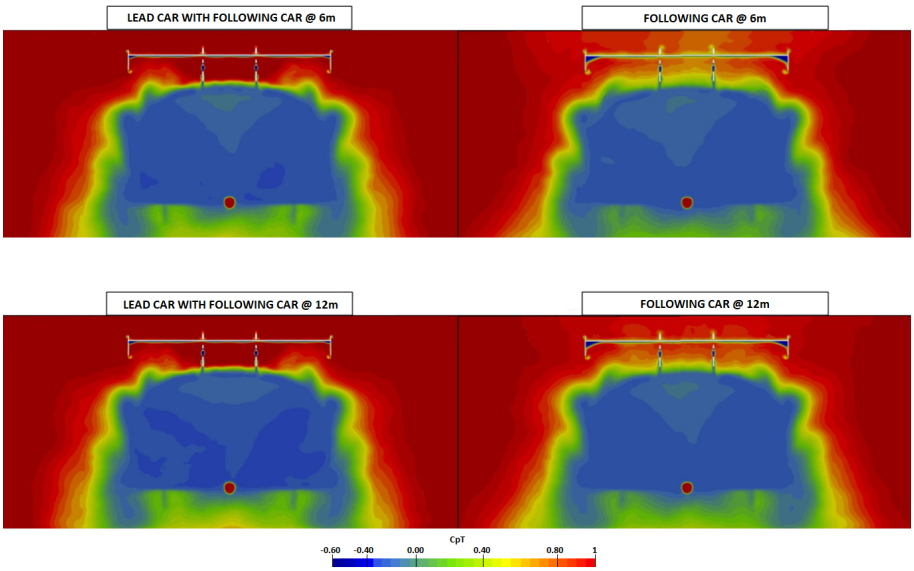

Figure 5.11: Cp_T **comparison between leading car (@** $X = 3.640$**) & following car at** $6\,m$ **(@** $X = 14.222\,m$**) and** $12\,m$ **(@** $X = 20.222\,m$**)**

Lower CpT entering the radiator ducts. Higher CpT entering the ducts with an increase in distance.

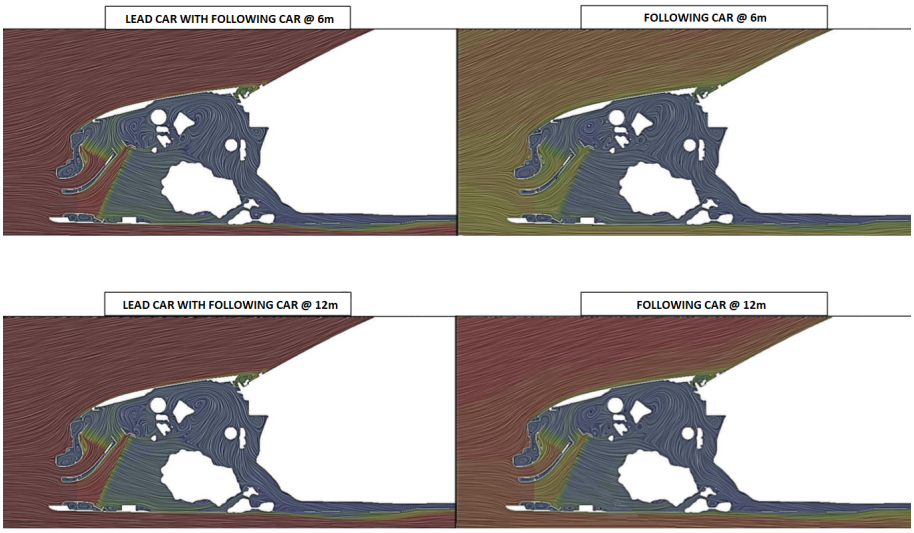

Figure 5.12: Cp_T **comparison between leading car & following car at** $6\,m$ **and** $12\,m$ **(LATERAL SECTION)**

Small separation from the front brake duct leading edge. Slightly narrower wake from the lead car with the following car at 12m.

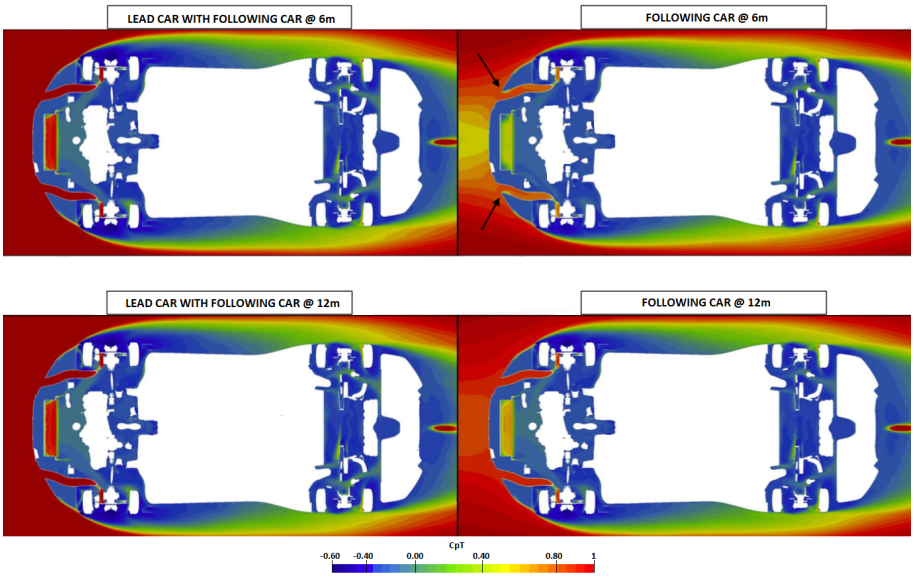

Figure 5.13: Cp_T **comparison between leading car & following car at** $6\,m$ **and** $12\,m$ **(@** $Z = 0.140\,m$**)**

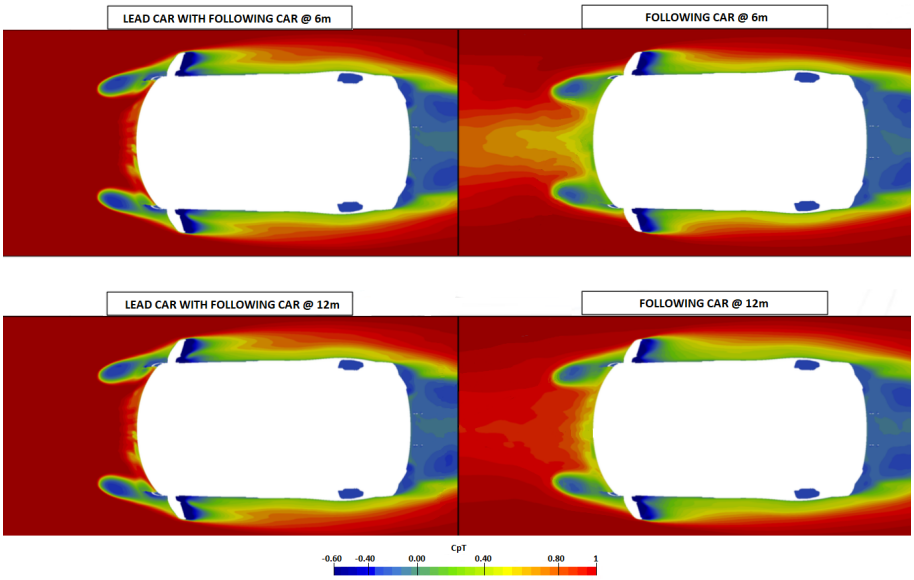

Figure 5.14: Cp_T **comparison between leading car & following car at** $6\,m$ **and** $12\,m$ **(@** $Z = 0.760\,m$**)**

In the figure above we see an increased stagnation on the wing mirror on the following cars, possible due to:

- Reduced wake from the bonnet cut-outs due to the reduced mass flow into the radiators.

- The bonnet wake is not pushed out as far, possible due to reduced stagnation on the windscreen.

Thick boundary layer from the leading edge of the engine intake duct. Addition of a large radius at the leading edge would improve the flow structure.

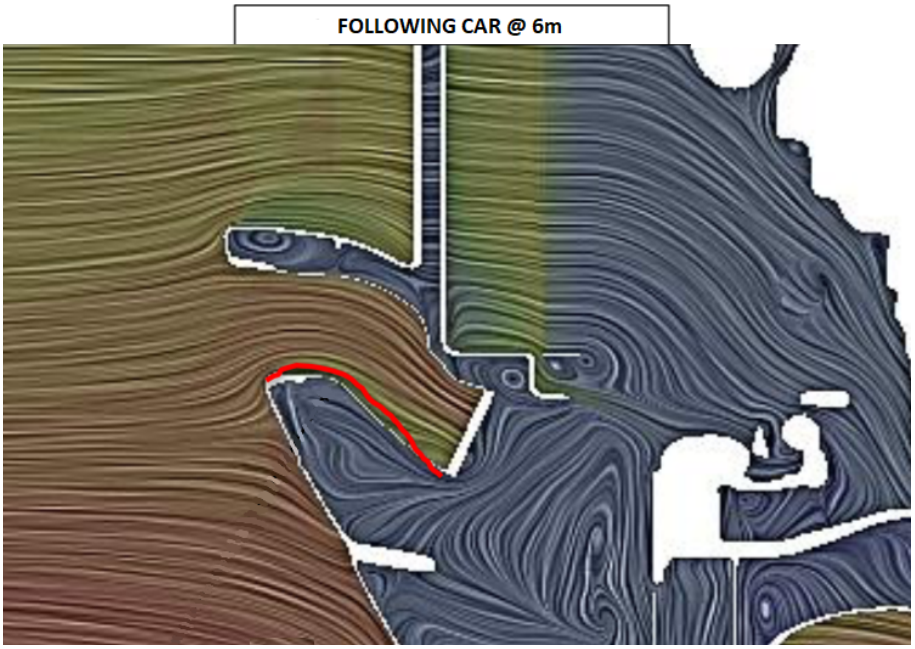

Figure 5.15: Detail of following car at $6\,m$ - Upper Section of front fender

- A following car study has been conducted in CFD using a transient DES approach for two different following car distances (6m and $12\,m$).
- Both lead cars show slightly different performance depending on the following car distance (likely due to pressure interactions).
- A $\sim 15\%$ drag reduction relative to the lead car is seen at both distances.
- Greater loss in downforce on the 6m following car by $\sim 26\%$ is observed than the loss on the $12\,m$ following car ($\sim 17\%$).
- Both following cars show a rearwards balance shift of $\sim 5\%$ and $\sim 2\%$ respectively.
- Significant reductions in mass flow rates into the radiators and front brake ducts are seen. Greater losses are observed in the 6m following car – $\sim 25\%$, $\sim 24\%$ and $\sim 19\%$ losses in the water, intercooler and gearbox radiators respectively.
- A significant loss in total pressure through the engine intake duct is seen by $\sim 34\%$ and $\sim 23\%$ respectively.

In the next chapter we will analyze a new front bumper for the next championship which, with wider openings, will increase the flow entering the engine compartment.

5.4 Solution: the new bumper

To improve the performance of the car and have a greater incoming flow in the wake condition, we thought about a possible improvement for the 2019 season that expected more openings in the front bumper (so the increase in flow in all conditions). From the figure below you can see how from the 2018 version the separations of the different bumper mouths have been eliminated, generating a single large opening and opening a crack even under the emblem (between the two lights) as in the standard cars. Recall that the increase in new openings generates an increase in drag resistance, so these openings in addition to being a regulated constraint, must also be a compromise between the functionality (ie the cooling of certain components of the car) and the loss from the point of view aerodynamic. Fixed to the bumper, in front of the openings, there are grids that protect the radiators from large debris (such as tire residues, stones ...) having a mesh $10\,mm$ x $10\,mm$ a few millimeters thick. This network must necessarily be considered in the CFD simulation since it affects the flow that enters the conveyors, modifying above all the flow rate and the total pressure. We decide to underestimate the simulation in such a way that the reality can only be better than calculated from the result of the fluid-dynamic analysis, considering a grid based on $7\,mm$ x $7\,mm$ wire mesh.

We propose two alternatives for the next season, one with two simple front openings, as described above, and the other with an inner septum in the lower opening that diverts the flow inside the turbocharger, therefore inside the engine. For the simulation we consider the engine at high revs, evaluating the car in a straight line with a speed of $55.556\,m/s = 200\,km/h$.

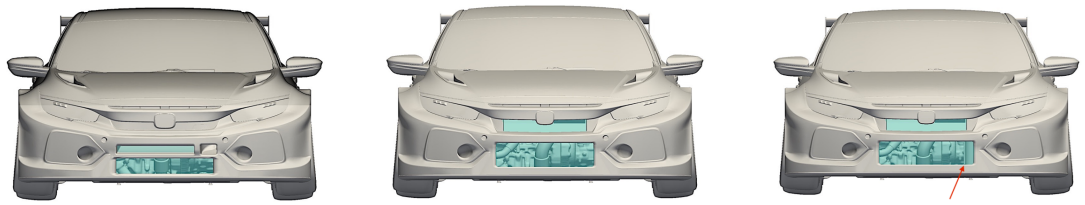

(a) Config. 1 (b) Config. 2 (c) Config. 3

Figure 5.16: Front bumper

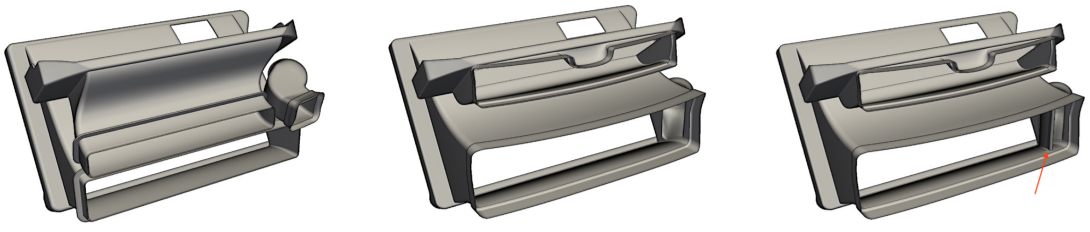

(a) Config. 1 (b) Config. 2 (c) Config. 3

Figure 5.17: Cooling duct

5.4.1 Analysis

Note that in the updated configurations the total pressure coefficient CpT is lower because the grid mesh is more dense. As you can see how the flow is able to conserve more energy by channeling the air inside the engine socket.

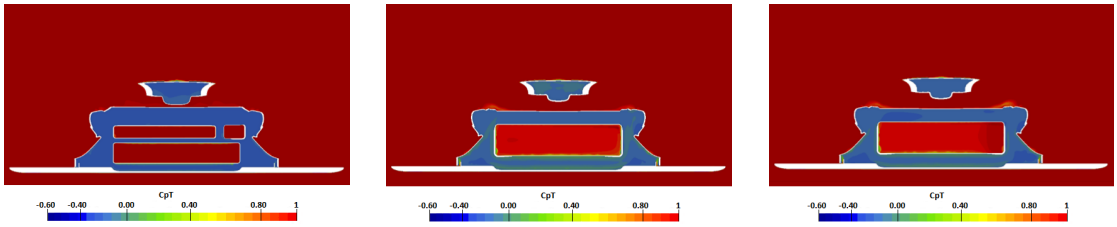

(a) Config. 1 (b) Config. 2 (c) Config. 3

Figure 5.18: C_pT **maps @** $X = -0.86\,m$

Considering sections that are more and more backward (ie towards the rear of the car) we analyze how the flow evolves in the ducts. Compared to the old bumper, the separation in the intercooler intake is smaller because the flow is not diverted as previously but thanks to the appropriate opening created it enters directly in a way that we can define as "laminar". In the lower intake, on the other hand, in the first solution there is a severe separation / recirculation seen in the engine intake duct. In the second one the addition of the intake results in increased CpT into the intake, but there is a strict separation in the water radiator duct side. This results is a recirculated flow under the gearbox radiator. In both solutions there is a separation in the lower part because, since the radiator is always placed in the same position but being the most raised opening, the angle of inclination of the flow increases with respect to the old configuration. Given the results of the analysis we thought to file as much as possible the lower thickness in a subsequent version of the bumper.

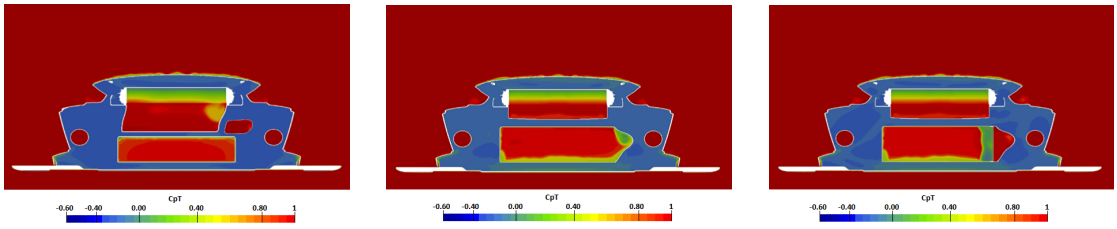

(a) Config. 1 (b) Config. 2 (c) Config. 3

Figure 5.19: C_pT **maps @** $X = -0.76\,m$

It is important to underline that in the third picture there is the problem of separation. The flow loses considerable energy because the one shown is the area behind the septum; this will be another region where it will be important to improve the geometry of the septum or conveyor to try to reduce this energy loss as much as possible.

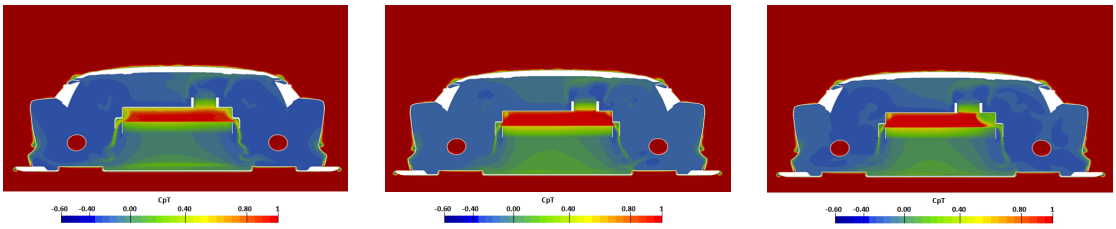

(a) Config. 1 (b) Config. 2 (c) Config. 3

Figure 5.20: C_pT **maps @** $X = -0.58\,m$

The opening under the "Honda" front emblem which allows the flow to reach the intercooler, allows the recirculation vortex to be eliminated, but in the lower part it is necessary to adjust the bumper geometry, limiting the thickness. It is not possible to play too much with this thickness because inside there is the bull bar that binds its shape.

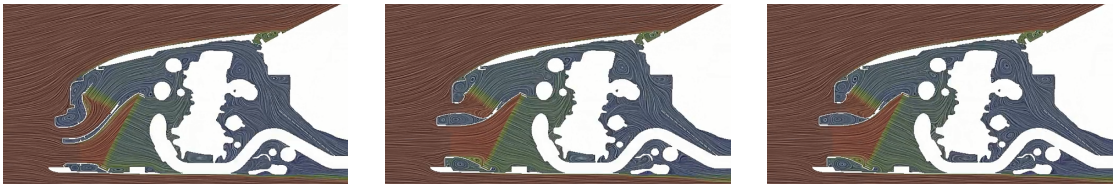

(a) Config. 1 (b) Config. 2 (c) Config. 3

Figure 5.21: C_pT **maps @** $Y = 0.00\,m$

With the fin the engine air intake is high energy, however a recirculation bubble is formed. Addition of the intake fin fix the separation on the engine intake duct. However, the inboard of intake fin separates severely harming the flow into the water radiator. A nicer profile to the leading edge, or fairing on the inside of the fin back to the duct side wall could help fix this. There are still signs of some boundary layer thickening/separation from the OB corner which could help pull the intake cooling back up to the current level.

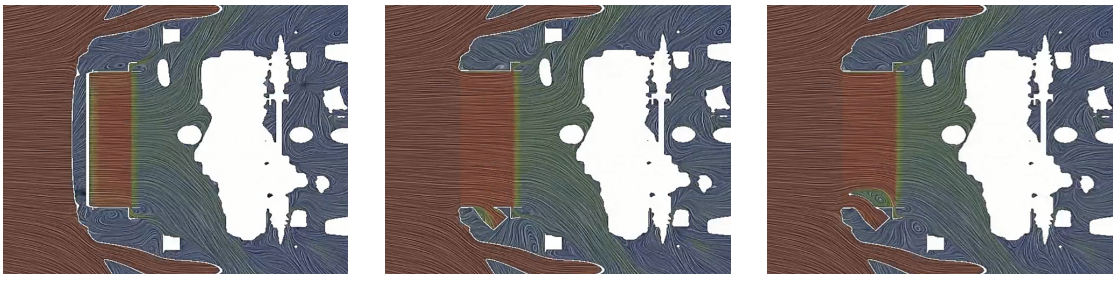

(a) Config. 1 (b) Config. 2 (c) Config. 3

Figure 5.22: C_pT **maps @** $Z = 0.12\,m$

The first configuration shows:

- An $18N$ increase in drag and $63N$ loss in downforce.

- Balance shift rearwards by $\sim 2\%$.
- Increased cooling mass flow into the water, intercooler and gearbox radiators by $\sim 15\%$, $\sim 2\%$ and $\sim 7\%$ respectively.
- Significantly decreased total pressure at the engine intake boundary face by 44%.

The configuration with intake fin shows:

- An $8N$ increase in drag and $38N$ loss in downforce.
- Balance shift rearwards by $\sim 1\%$.
- Increased cooling mass flow into the water and intercooler by $\sim$ 8% and $\sim$ 3% respectively.
- Decreased cooling mass flow into the gearbox radiator by $\sim 4\%$.
- Decreased total pressure at the engine intake boundary face by $\sim 8\%$.

Based on the aerodynamic analysis provided, it was decided to make the flow "cleaner" through the following changes:

1. Filler to IB of fin.
2. Larger radius to OB of intake.
3. Delayed expansion to lower water rad.
4. Lowered bottom duct entry surface to intercooler.

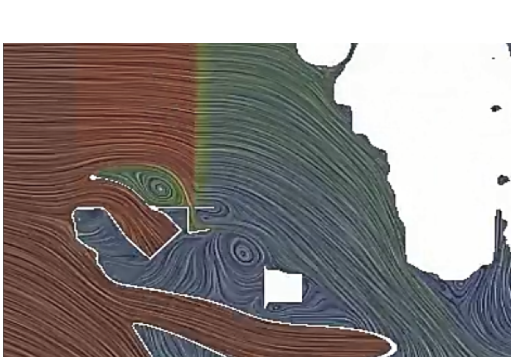

(a) Section @ $Z = 0.12\,m$

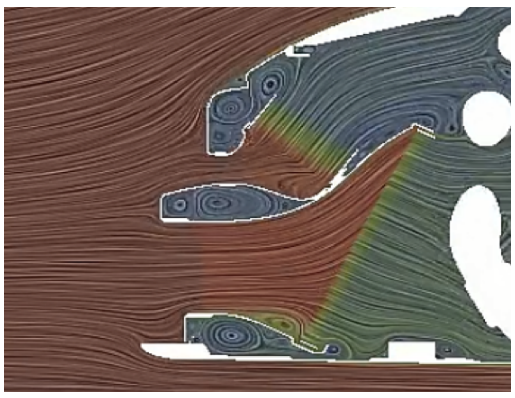

(b) Section @ $Y = 0.00\,m$

Figure 5.23: C_pT **maps**

To concretely demonstrate the value of the "numbers" provided by the CFD software, we have materially created the new front bumper, with the latest changes made after the

reading of the aerodynamic analysis which will be tested on the circuit before "series" production. Initially, the test will be dealt with by collecting the car data in standard conditions and then collecting it after the installation of the new ducts and the new bumper. 7 laps will be performed in such a way that the temperatures are brought to full capacity. Both sessions will then be accompanied by a 4 laps test in the wake thanks to another car that will precede the test car. It is important to acquire all the data of the standard car again, despite being the car that ran throughout the championship, because for a precise and accurate comparison we need the same environmental conditions and contour (same coolant, same resistances etc ...).

Chapter 6

Appendix

6.1 Race Tracks

We briefly describe the circuits mentioned earlier in *Chapter 4* so that, seeing the shape of the track, we can understand more clearly the influence that the variation of parameters such as power, weight and aerodynamics have on laptime. [**16**]

Nurburgring

Figure 6.1: Nürburgring circuit

Above all other circuits, the Nürburgring has a history and tradition which is intertwined with that of the motorsport itself. Any event here, since 1927, remains one of the greatest spectacles and challenges on the sporting calendar.

The Nürburgring is a circuit complex for motor racing that winds around the Nürburg Castle in Germany.

In the early eighties the complex underwent profound changes; today it looks like this:

- Steilstrecke, from 5.148 km (4.579 without the portion called Mercedes Arena);
- Nordschleife reduced to 20,832 km;
- Südschleife partially demolished and with some sections used for ordinary roads.

There is also a conformation (defined endurance configuration) formed by the union of the Nordschleife and the GP Strecke (excluding the area of the Mercedes Arena), 25.378 km long.

The length of the circuit means that TCR cars only do 3 laps. The straight, about 4 km, is a fundamental piece of the circuit where the full power of the engine is exploited.

Suzuka

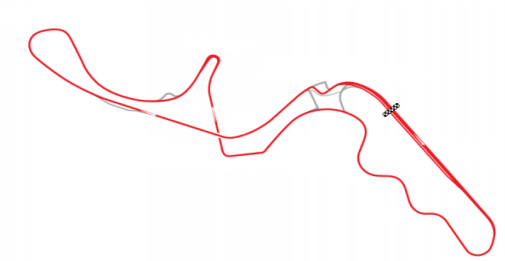

Figure 6.2: Suzuka circuit

The Honda-owned race course at Suzuka has emerged as one of the world's most demanding and rewarding motor racing circuits, packing a mix of almost every type of corner into a remarkably small space.

It is a well known circuit for hosting Formula 1; additional events today hosted at Suzuka include Super GT and Super Formula single seat series.

Vila Real

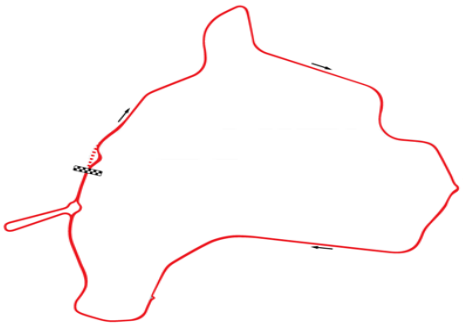

Figure 6.3: Vila-Real circuit

Vila Real is the true heart of motor racing in Portugal, with its epic street race through the hillside roads. It's a very fast circuit despite being stuck inside the city and its first run was in 1931.

Slovakiaring

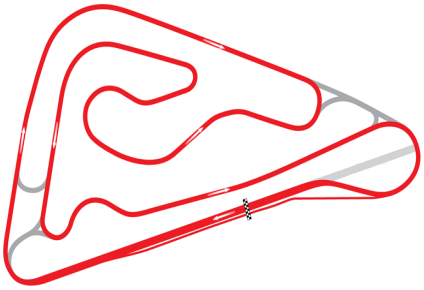

Figure 6.4: Slovakiaring circuit

Slovakia has a burgeoning car manufacturing industry, thanks to the presence of factories for Volkswagen, Peugeot-Citroen and KIA, but until recently had lacked purpose-built test and racing facilities. The Slovakiaring has emerged to meet this need and has become a popular and challenging new addition to the central European motor racing scene.

The main course is among the longest in Europe and features four artificially created elevations, which ally to the circuits high speeds. The circuit's safety measures have been installed in such a way as to enable running in both directions creating a total of 12 possible variations. During this year, the organisers of the World Touring Car Championships fill a gap in the calendar caused by the cancellation of a race in Argentina.

Macau

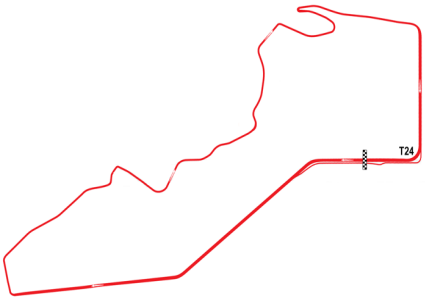

Figure 6.5: Macau circuit

Few street circuits around the world can claim a 60-year history using virtually the same layout. It's a very tight street circuit with a long main street. Characterized by a "dirty" asphalt, with a stretch in the mountains, low gears are often used and there is essentially a single stretch where drivers can overtake.

Shanghai

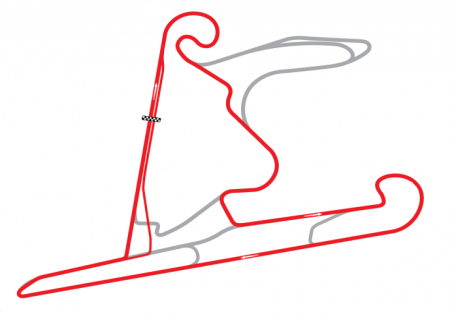

Figure 6.6: Shanghai circuit

Shanghai International Circuit is a no-expense-spared facility, conceived by the Shanghai authorities as a way to showcase the city to the world. The track layout has also been inspired by Chinese culture, with the designers claiming to have drawn inspiration from the Chinese 'shang' symbol for the overall configuration. Driver reaction has been mixed – the never-ending turn one tends to divide opinion, and much of the course is quite twisty, until you reach the 1.2 km back straight.

Losail

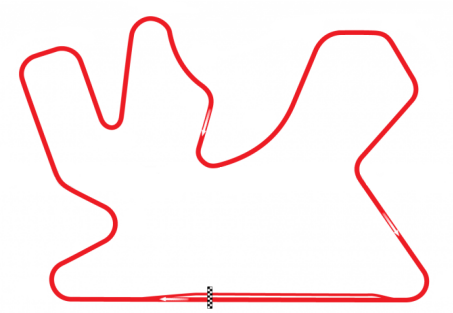

Figure 6.7: Losail circuit

Losail International Circuit was the third of the desert-based circuits that sprang up at the turn of the century and is the only motorsport facility in Qatar. Lying on the outskirts of Doha, the capital city of Qatar, it is the only circuit in the region to have both FIA and FIM homologation licenses. Designed primarily with motorcycling in mind, the track itself is a flowing layout of 5.4 km, surrounded by artificial grass designed to prevent sand from the neighbouring desert from blowing onto the circuit. The main straight is over a kilometre in length and there is a good mix of medium and high-speed corners, including a couple of quick left-handers which has proved particularly popular with the riders. In 2008, the circuit added permanent outdoor lighting for night races, creating what was at the time the largest lit venue in the world (a title later claimed by the Yas Marina circuit in Abu Dhabi).

Barcelona

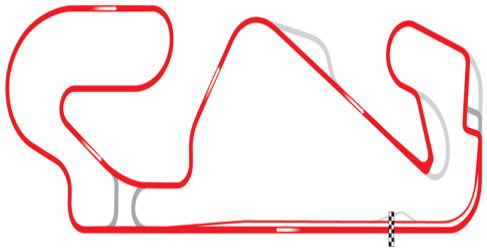

Figure 6.8: Catalunya circuit

The Circuit de Barcelona-Catalunya is one of Europe's busiest tracks, playing host to high profile rounds of Formula One, MotoGP and becoming the seasonal winter home of the F1 teams as they test their new cars and drivers. The circuit features a mix of fast and slow corners, a long straight and a variety of elevation changes. As a result, it is a popular testing venue, aided by the usual pleasant winter weather.

Chang

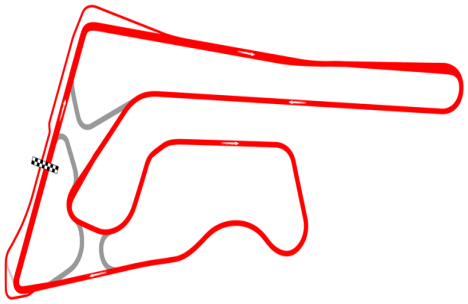

Figure 6.9: Chang circuit

The Buriram United International Circuit has exploded onto the motorsports scene, propelling Thailand onto the international stage for the first time. The circuit has been created to the highest FIA and FIM standards, potentially putting it in line to host Formula One and MotoGP races in the future. The shorter layouts have been configured with local racing championships in mind, as these typically use much lower powered near-production vehicles which would not be well suited to the long straights.

Termas de Rio Hondo

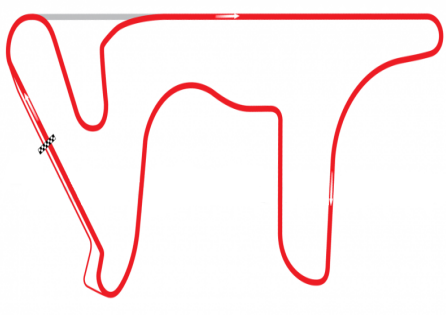

Figure 6.10: Termas De Rio Hondo circuit

The Autódromo Termas de Río Hondo is a road course located just outside the city of the same name, in the province of Santiago del Estero.

Opened in 2008, at the conclusion of the 2012 season, the circuit underwent a substantial rebuild in a bid to improve facilities and attract international motorsport. Layout changes include a new infield loop, creating a fast 180 degree first turn which slows the eventual entry onto the long straight.

Hungaroring

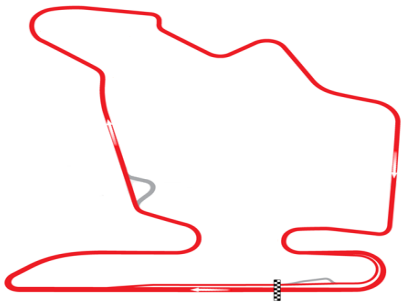

Figure 6.11: Hungaroring circuit

The Hungaroring holds the distinction of being the first venue for Formula One having hosted top level racing continuously since 1986. For the 2003 season, fundamental changes were made when the final series of bends and the pit straight were altered, in order to provide a longer pit straight. A new, tighter, first corner does offer slightly more scope for overtaking and the racing has improved somewhat. The presence of many corners makes it one of the most "downforce" circuit.

Valencia

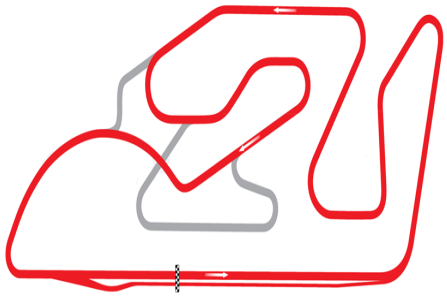

Figure 6.12: Valencia circuit

It was built in 1999 by the Government of Valencia to become the nerve centre of the local motorsport industry, forming a hub and training centre for young Spanish talent on two or four wheels.
The main Grand Prix course is just over $4\,km$ long and comprises five right handed corners, eight left handers and a $650\,m$ main straight. the curves are very narrow, almost at 90° with a big bend.

Aragon

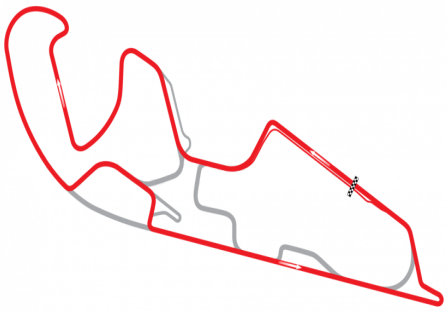

Figure 6.13: Aragon circuit

The ultra-modern Ciudad del Motor de Aragón, also known as Motorland Aragón feature a mixture of long sweeping corners and slower, tighter curves and noticeable elevation changes. The track rises from the start finish straight some $50\,m$ to its high point, before descending through a 7.2% drop at Turns 8 and 9, a corner complex which probably comes as close to reproducing the excitement of Laguna Seca's fabled Corkscrew as modern circuit design standards allow. The long back straight (more than $1\,km$) also provides a high speed challenge and, for the car-racing version, a significant overtaking spot thanks to the tight hairpin at its conclusion.

Paul Ricard

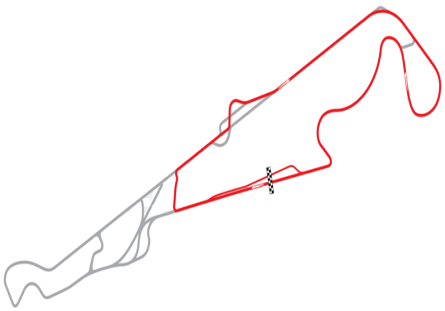

Figure 6.14: Paul Ricard circuit

The Paul Ricard circuit has, in two very different eras, claimed the title of the most modern motorsport facility in the world. Constructed by drinks magnate Paul Ricard at Le Castellet in the south of France, the circuit was the first of the modern autodromes.

In its heyday Le Castellet was considered the safest circuit in the world and became the setting for many national and international motor sports competitions. Visually, the biggest change was in the adoption of a pioneering new high-grip asphalt run-off system to replace the gravel traps of old. High-grip asphalt areas offer differing levels of abrasion, designed to slow down errant vehicles and avoid impact with the barriers. Distinguished by their bright blue and red (for ultra-high grip) colouring, the Blue Line concept has since been adopted by a number of other circuits, though not as completely as at Le Castellet.

Figure 6.15: Detail of Paul Ricard circuit

Also new was the adoption of Tec-Pro safety barriers; these offer a more scientific approach to collision control than the traditional tyre barrier and, after proving themselves at Ricard, have seen widespread adoption elsewhere. These safety innovations were recognised in 2007 when the FIA Institute for Motorsport Safety bestowed the First Center of Excellence award on the new course.

Ningbo

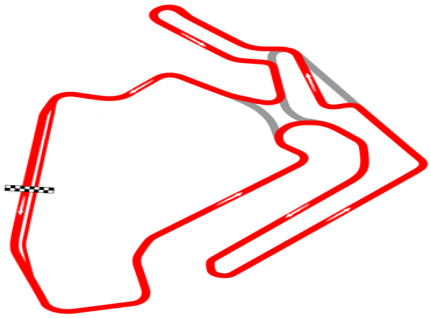

Figure 6.16: Ningbo circuit

Ningbo International Speedway (in Zhejiang province) is one of a crop of new tracks opening across China under the stewardship of auto maker Geely (owner of Volvo).

The project was officially launched on December 28, 2015 and is scheduled to be completed at the end of June 2017. The 4.015 km track has been homologated to FIA Grade 2 standards, allowing it to host all bar Formula One competition.

Monza

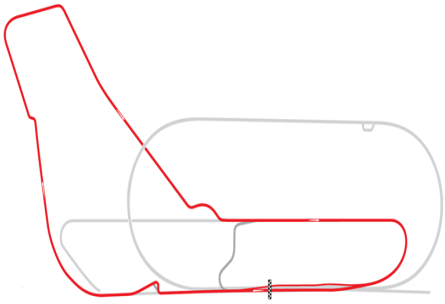

Figure 6.17: Monza circuit

Monza is a true cathedral to speed. Its history began shortly after the First World War, when the Italian motor industry was undergoing its first great ascendancy. Authorities began looking for land to create a circuit to test their cars and demonstrate to the rest of the world their superiority through sporting success.

In 1972, a chicane was introduced on the Grandstand Straight, a slightly clumsy slow-speed flick just before the entrance to the Junior circuit, along with a higher speed chicane bypassing the Vialone curve and named in memory of Alberto Ascari, who had perished at the same spot some 17 years previously. The track increased in length by 109 yards as a result.

The final changes involved a rebuilding of the first chicane in summer 2000, the new almost triangular hairpin combination providing a new overtaking point, but doing little to alleviate the traditional first lap carnage; if anything the tighter, slower combination of curves might actually have made it worse.

The presence of long and many street makes it one of the most "drag" circuit where the power of the engine emerges. Its main street allows you to reach top speed with cars of any category.

Zandvoort

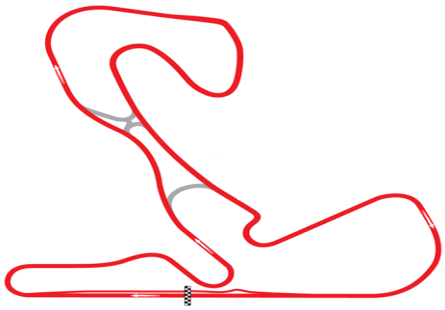

Figure 6.18: Zandvoort circuit

Zandvoort has been the centre of the Dutch racing scene and its most important circuit (at least for four-wheeled racing) since the late 1940s.

Nestling among the sand dunes the town is named after, the circuit has a lot of hills.

Marrakech

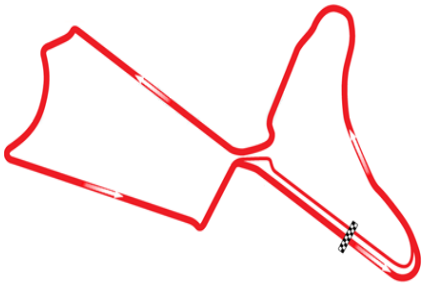

Figure 6.19: Marrakech circuit

The Circuit International Automobile Moulay El Hassan, named after the Crown Prince of Morocco, is a temporary street circuit in the Agdal district of Marrakesh.

With a series of chicane-puncuated straights joined by a large radius curve at one end and a tight hairpin at the other, it s a very narrow circuit in which the 4^{th} gear is rarely used.

6.2 Test Plan

As in the case of the bumper update described in the previous chapter, the new modifications that are carried out on the car must be tested before their use during a competition.

This experimental test (or ordinary test) consists of a procedure, designed to verify, prove or confirm a specific characteristic of a component different from the one already installed. The test typically involves the measurement of physical quantities, using sensors and measuring instruments in an environment that simulates as much as possible the conditions that this component will have to endure during its regular function. Some components require a validation that can also be obtained in the workshop, when the car is stationary, many others require a test run on the track.

A fundamental part of a test on the car or a part of it is the creation of a test plan. It consists of a document, generally executed on Microsoft Excel, which establishes all the tests to be carried out and the times in which to carry them out. In fact, the first big advantage of testing programming is that it "guides" the way to intervene during the test day.

Secondly, when viewing the documentation of a test planning it requires that the people involved have shared or at least are aware of the areas it covers and the time division of the day. It is a way to force the framing of the project and provide team members with the perimeter of the question. Thus, the authoring of the test plan really helps to define the project operating environment. Generally the problems of organizing the test day are related to time; we try to overcome this obstacle by planning every single activity and setting the times that allow us to organize them in an appropriate manner and without always having to follow the operations of the interventions. Precisely organizing test days in advance allows you to manage your time more efficiently. Through proper planning, we can achieve better results, while reducing the likelihood of ignoring important evidence or allowing ourselves to be distracted by factors of little relevance. Fixing and respecting a test plan allows us to feel less stressed as it gives us the opportunity to notice what we have done and what we still need to do.

It can happen also not to follow the test plan in a slavish way during the execution of ad hoc tests in relation perhaps of some results obtained during the experimentation of the first configurations. However, the test strategy is still an important resource to "remember" the previous project and take note of the most relevant aspects. In fact, programming allows you to define the scale of the interventions and the different tests, with the possibility/need to change the sequence on the field based on what emerges during the day.

The responsibilities of the test also include what data will be collected and how such data will be stored and reported. A result of a successful test plan should be a report on the verification of all specifications and design requirements agreed upon by all parties.

The test plan describes the following information:

- configurations to test
- number of laps to be dealt with for each configuration
- timetable considering re-entry time, assembly time, lap time
- fuel register introduced (knowing that on average the consumption is around $1\,kg/lap$)
- set tires

We illustrate an example of a Test Plan, written in the 3^{rd} August test, when the New Bumper was tested. This example is particular because the circuit was not entirely reserved for us so it was necessary to split into shifts. It was up to us for the first half hour of each hour. In addition, a compulsory lunch break was scheduled from 1:00 pm to 2:00 pm where there were no road marshals and security vehicles.

Honda Racing Team JAS

DEVELOPMENT TEST PLANNING

NEW FRONT BUMPER

civic TCR International Series

Length [m]	2650		
Reference time	01:25,0		
Driver	A. Tassi	Morning	09:00 - 13:00
Tot km	156	Afternoon	14:00 - 18:00

DAY 1 — DATE 03/08/2018

Description	#	#	Activity	Lap	T session	T work	h:mm	Tyres	Notes	Fuel
Front bumper old	1	1	Installation lap 1	1	0.01	0.00	10.00	set tyres 1		30kg
		2	Long Run 1	7	0.10	0.05	10.06			
		3	Run 1_slipstream	4	0.06	0.05	10.22		slipstream	
							10.28			
Front bumper new	2	1	Installation lap 2	1	0.01	0.00	12.00	set tyres 2		10kg
		2	Long Run 2	7	0.10	0.03	12.04			
		3	Run 2_slipstream	8	0.11	0.02	12.17		slipstream	
							12.29	end morning session		
Front bumper new + fin	3	1	Installation lap 3	1	0.01	0.00	14.00	set tyres 3		10kg
		2	Long Run 3	7	0.10	0.05	14.06			
		3	Run 3_slipstream	4	0.06	0.05	14.22		slipstream	
							14.28			
Racing radiator	4	1	Installation lap 4	1	0.01	0.00	15.20	set tyres 4		20kg
		2								
		3								
							15.22			
Racing radiator	5	1	Run 4	3	0.04	0.00	16.00	set tyres 4		
		2	Long Run 4	7	0.10	0.05	16.09			
		3					16.20		finish to change radiator	
							16.20			
Front bumper old	6	1	Installation lap 5	1	0.01	0.00	17.00	set tyres 5		
		2	Long Run 5	7	0.10	0.05	17.08			
		3					17.17			
				59			17.17	end afternoon session		

Figure 6.20: Test Plan - Cervesina 3^{rd} August

Analyzing in detail:

First column: we describe the configuration we are going to analyze.

Fourth column: note the number of turns we intend to perform; usually an installation lap is made after each modification, which consists of an OUT-IN (therefore a lap of the track without passing through the main straight), to check if all the parameters of the car are within the expected range. If the car is in good condition then proceed with the next run. In our case, to verify the efficiency of the bumper and the radiator in the presence of wake, it was necessary to bring all the parameters (in particular the temperatures) to full speed and calculated 7 laps were calculated. The last 4 laps were carried out in the wake with the use of the First Car.

Figure 6.21: Test - Run2 slipstream

Fifth column: depending on the number of laps and the average lap time, the program automatically calculates the time it takes to run each run.

Sixth column: manually enter the time that we expect to perform the work on the car when you return to the pits, which automatically turns into time in the seventh column. Between a configuration and another we had calculated a time equal to about 45 min without then expecting to enter the next round, if not for the installation lap as it happened in run 4.

Tenth column: it is essential to mark the number of kg of fuel placed in the car on one side to be aware of the weight of the car but basically not to remain in reserve.

Below we present the sheet which illustrates the set tires that will be used during the day of testing: they are illustrated schematic models of the car built through the cells of excel in which the position of the wheels is evident.

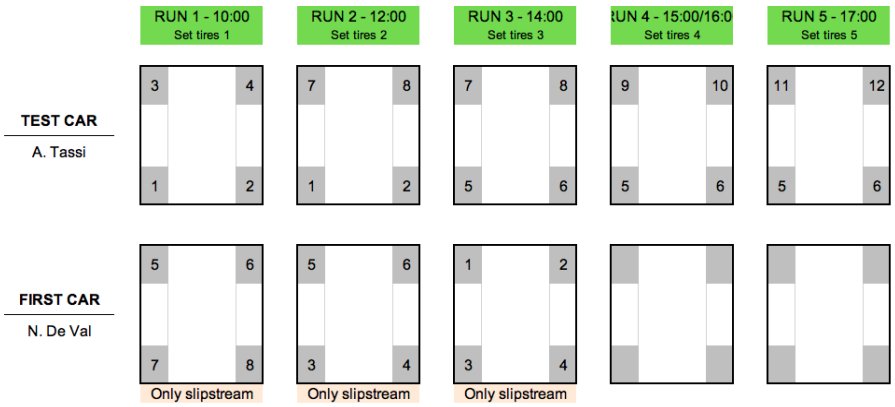

Figure 6.22: Plan of set tires

This scheme allows to assign each set to the corresponding run. It is therefore immediate to understand which tires the car must "wear". The choice of the position of the tires

depends essentially on their consumption: the rear wheels have a very low consumption compared to the front ones in which there is traction, are responsible for the steering of the car and are much more stressed even during braking due to the weight distribution. [1] On the basis of the wheels available for the test, a combination is studied that allows to obtain the conditions to be achieved. [2] In the case of the New Bumper, the aim was not to obtain the best performance in terms of lap time, but we needed a consistent and constant trend throughout the day so that the data could be compared between the different configurations.

6.3 Cooling Package H61

In this section I wanted to discuss a project that I followed within the J.A.S. Motorsport. As it is important to plan the test, it is equally important to draw up a final report in which the tests are described and highlight all the parameters and the important data obtained, accompanied by precise considerations. This work serves on the one hand to summarize and make the whole team aware of the results obtained, on the other to archive this document in such a way that it remains in the future as an acquired experience and is part of the team's background.

The goal of this task was to solve the cooling problems that $H61$ (CTCC - Chinese Tourist Car Championship) installed during the test sessions in China.

J.A.S. proposed to install the 2018 spec TCR with a complete swap of the frontal of the car. The front end of the $H61$ has been moved accordingly due the different position of the engine between the two cars, so all pipes would be easy changed and compared: then J.A.S. created the cooling package $H61\,EVO$.

[1] The wheels 5 and 6, used in the first two runs by the First Car as front wheels (subjected to great efforts), can be used as rear wheels for subsequent runs as they will suffer less stress and therefore a very reduced consumption.

[2] We see how the First Car performs a much lower number of laps than the Test Car so the consumption that is exerted on its tires is certainly lower.

Figure 6.23: New front end H61EVO

As described in the previous chapter, it is essential to test the new components that will be installed in the car; for this reason we organized a test to verify the correct operation of the new cooling package on June the 7^{th} 2018 circuit Tazio Nuvolari in Cervesina (Pavia).

To compare the two cooling packages, we decided to start with the $H61$ standard cooling package:

(a) Left side

(b) Right side

Figure 6.24: Cooling package standard H61

First runs with an ambient temperature around $23°C$. After 3 chrono laps water temperature reached already $99°C$. It's was clear that we are able to replicate the issue of Chinese tests where there is an overheating of the water that should generally reach a temperature between $85 - 90°C$. Another consideration that we could observe is that during cool down the water temperature struggle to decrease.

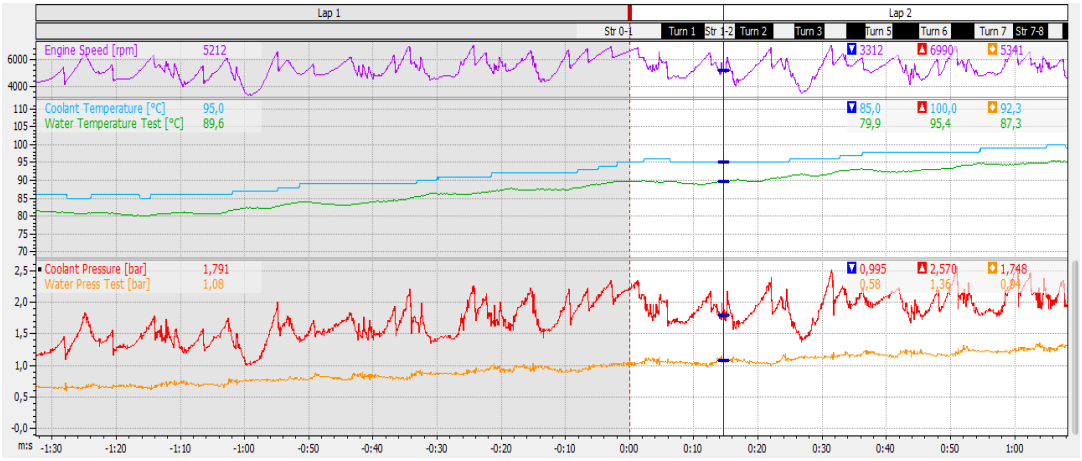

Figure 6.25: MoTec data of H61 standard configuration

The delta value between water radiator IN (sensor called: Coolant Temperature) and water radiator OUT (sensor called: Water Temperature Test) it's around $4-5°C$ which is a very low temperature delta for a cooling package.

So we decided to change then the cooling package with the new design called $H61\,EVO$.

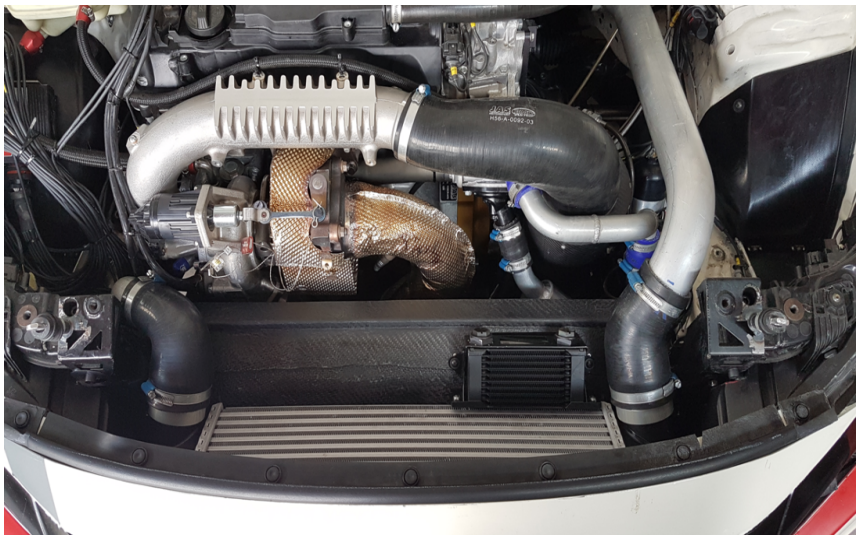

Figure 6.26: Drag and downforce breakdown in four different configurations

In this layout the water radiator has a crossflow with 20% more surface, and a volume 2,5% less. Intercooler is 1,5% less in volume compared to the standard $H61$ but leaves a lot more space for the new water radiator. A Power steering cooler has been installed in the top part of the new ducting providing a good cooling for the system knowing that it's a sensible part of the car. In the test was not connected (as the car have a EPS system) but present in order to replicate pressure wise the working condition of the duct.

At 12:40 ($28°C$) we did as schedule 8 chrono laps and it's clearly visible that the water

temperature IN-OUT of the radiator are considerably lower than with previous cooling package.

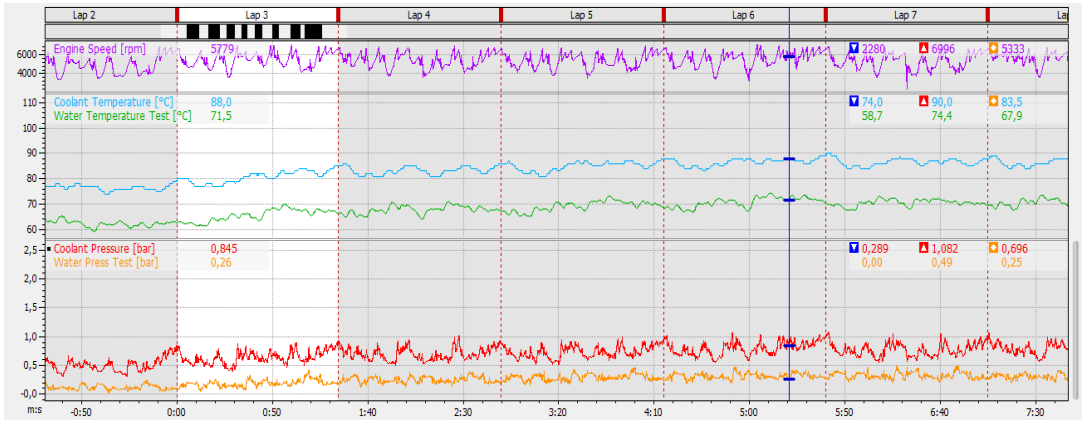

Figure 6.27: MoTec data of H61 EVO configuration

The water temperature reach a consistent operating range from lap 5 and the delta across the water radiator is around $17°C$, a good result for a well working cooling system.

Test has been performed with also some extra feature that ensure a higher safety margin on reliability wise:

- *Auxiliary Water Pump:* this item permit to circulate the water also with engine off (working together with the radiator fan)

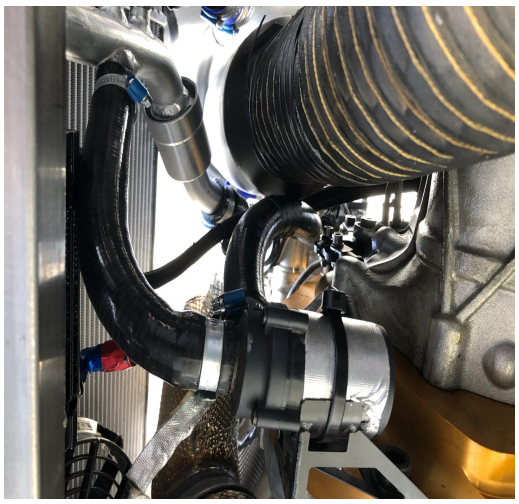

(a) Lateral view

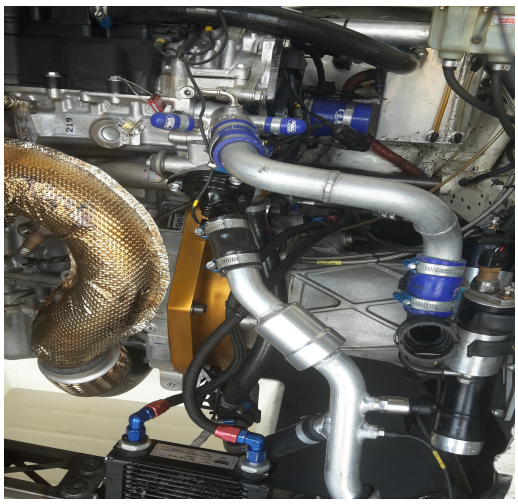

(b) Front view

Figure 6.28: Auxiliary Water Pump

- *Smaller pattern removable mesh:* During endurance races has been necessary to remove the mesh for radiator duct cleaning. Also dimension of mesh opening has

been reduced for a higher protection of the core from debrits (from $10\,x\,10\,cm$ to $7\,x\,7\,cm$ mesh) without consequences for the cooling of the car.

Figure 6.29: Bumper mesh

- *New brake cooling position:* in order to maximize opening without change too much the bumper shape, the brake cooling port has been moved outwards, with extra wall to ensure enough flow to the brake positioned on the FR arch liner:

Figure 6.30: New brake cooling position

Looking at the pressure delta between the 2 cooling package is noticeable quite a big difference in water pressure IN-OUT behavior. Seems like the $H61$ radiator has a really high Delta pressure between its ports. To be sure that there is nothing that can block the water flow the heathers have been removed but nothing has been detected.

Figure 6.31: H61 Radiator

Conclusions:
It's been proved that $H61$ cooling package is not working properly as it's should. After specific tests performed earlier this year the $K20C1$ engine require a bigger heat dissipation compared to the WTCC based $H50/H60$ engine that has a similar power. The new package for $H61$ rise up considerably the cooling performance and the extra features permit an easier life for the racing team.

Bibliography

[1] Simon McBeath. “Competition Car Aerodynamics”. 3rd Edition Paperback, Paperback, 2017.
[2] Joseph Katz. "Race Car Aerodynamics: Designing for Speed", 1995.
[3] J. D. Anderson. "Fundamental Aerodynamics". McGraw-Hill, 1984.
[4] N. F. Krasnov. "Aerodynamics". Mir Publishers Moscow, 1985.
[5] Gary A. Flandro, H. M. McMahon, R. L. Roach. "Basic Aerodynamics - Incompressible Flow", 2012.
[6] WSC Ltd. "2018 TCR Series – Sporting Regulations", 2018.
[7] WSC Ltd. "2018 TCR Series – Technical Regulations", 2018.
[8] https://www.jasmotorsport.com
[9] https://www.fiawtcr.com
[10] https://it.wikipedia.org/wiki/WTCR_2018
[11] https://de.wikipedia.org/wiki/Balance_of_Performance
[12] https://www.totalsimulation.co.uk/cfd-software/
[13] http://www.autosupermarket.it/magazine/laerodinamica-dei-veicoli
[14] http://www.bosch-motorsport.com
[15] http://europe.tcr-series.com
[16] http://racingcircuits.info